NTNU
Det skapende universitet

Kombinert Wind- og Bølgekraft

Rasmus Borenius

Marin teknikk
Innlevert: juni 2015
Hovedveileder: Dag Myrhaug, IMT
Medveileder: Professor Bernt Leira, IMT

Norges teknisk-naturvitenskapelige universitet
Institutt for marin teknikk

NTNU Trondheim
Norwegian University of Science and Technology
Department of Marine Technology – Group of Marine Structures

MASTER THESIS IN MARINE TECHNOLOGY
SPRING 2015

FOR

STUD. TECHN. RASMUS PONTUS BORENIUS

COMBINED WIND AND WAVE POWER

A design proposal of a combined wind and wave power device

Ocean wave energy as well as wind energy appear to be promising for alternative energy. The design of appropriate devices to convert energy from wind and wave is a challenge for the engineering community; in particular, to design a device that can combine wind and wave power.

The student shall:

1. Give a background of wind and wave power devices.
2. Describe successful concepts for combined wind and wave power.
3. Describe the physics and mechanisms related to how wind and wave power are converted to energy.
4. Describe available energy in wind and waves.
5. Propose a design of a combined wind and wave power device.
6. Present analysis and results of the combined wind and wave power device.

The work scope may prove to be larger than initially anticipated. Subject to approval from the supervisor, topics may be deleted from the list above or reduced in extent.

In the thesis the candidate shall present her personal contribution to the resolution of problem within the scope of the thesis work.

Theories and conclusions should be based on mathematical derivations and/or logic reasoning identifying the various steps in the deduction.

The candidate should utilize the existing possibilities for obtaining relevant literature.

The thesis should be organized in a rational manner to give a clear exposition of results, assessments, and conclusions. The text should be brief and to the point, with a clear language. Telegraphic language should be avoided.

The thesis shall contain the following elements: A text defining the scope, preface, list of contents, summary, main body of thesis, conclusions with recommendations for further work, list of symbols and acronyms, reference and (optional) appendices. All figures, tables and equations shall be numerated.

NTNU
Norges teknisk-naturvitenskapelige universitet

Fakultet for marin teknikk
Institutt for marin hydrodynamikk

The supervisor may require that the candidate, in an early stage of the work, present a written plan for the completion of the work. The plan should include a budget for the use of computer and laboratory resources that will be charged to the department. Overruns shall be reported to the supervisor.

The original contribution of the candidate and material taken from other sources shall be clearly defined. Work from other sources shall be properly referenced using an acknowledged referencing system.

The thesis shall be submitted in two copies:

- Signed by the candidate
- The text defining the scope included
- In bound volume(s)
- Drawings and/or computer prints which cannot be bound should be organized in a separate folder.

Advisors: Professor emeritus Johannes Falnes
Dr. Jørgen Hals Todalshaug, CorPower
Professor Bernt J. Leira
Professor Dag Myrhaug

Deadline: 10.06.2015

Dag Myrhaug
Supervisor

Declaration of Authorship

I, Rasmus Pontus Borenius, declare that this thesis titled, 'Compined Wave And Wind Power' and the work presented in it are my own. I confirm that:

- Where any part of this thesis has previously been submitted for a degree or any other qualification at this University or any other institution, this has been clearly stated.
- Where I have consulted the published work of others, this is always clearly attributed.
- Where I have quoted from the work of others, the source is always given. With the exception of such quotations, this thesis is entirely my own work.
- I have acknowledged all main sources of help.
- Where the thesis is based on work done by myself jointly with others, I have made clear exactly what was done by others and what I have contributed myself.

Signed: _____

Date: _____

"You see, we should utilize natural forces and thus get all our power. Sunshine is a form of energy, and the wind and tides are manifestations thereof. Do we use them? Oh no!, we burn up wood and coal, as renters we burn up the front porch for fuel. We live like squatters, not as if we owned the property."

Thomas A. Edison 1916

Abstract

In this thesis the possibility of combining wind and wave power was investigated. A literature study on different concepts of wind power, wave energy converters as well as combined wind and wave power devices has been performed. A brief introduction on the origin of wind and waves are introduced. The physics of how wind and wave power is extracted will be discussed. From the obtained knowledge, a design proposal combining the two power sources with common underwater storage tank, was elaborated and analyzed. In addition, a suitable offshore site in the North Sea with a joint distribution has been proposed. The offshore site investigated has a water depth of 29[m], an average wind power density of 872.03 $[W/m^2]$ and an average wave power density of 14.29$[kW/m]$

The analysis can be divided into three main parts. In the first part, a wind turbine blade was designed using optimal BEM (Blade Element Momentum) theory in MATLAB. The power output was then calculated for a three bladed wind turbine using the designed blade. The diameter of the turbine was set to 126 meters, which gave an average power output of 3.92MW at an operational wind speed of 10m/s and a TSR (Tip Speed Ratio) of 8. To analyse the performance of the designed wind turbine in a more realistic manner, the software ASHES was used, which resulted in a power output of 4.35MW. The average power output of the wind turbine was also calculated, using a Rayleigh distribution. This resulted in a average energy production of 3.22MWh.

The second main part of the analysis investigated the time average power output of a WEC (Wave Energy Converter) in frequency-domain for both regular and irregular sea. In this regard, the CorPower WEC was chosen. The hydrodynamic coefficients for the WEC were obtained using the software WAMIT. In addition, the WEC was equipped with a new technology called WaveSpring. To

calculate the power output for different sea state conditions, a scatter diagram of the North Sea site was used. The calculations made in MATLAB showed that the WEC is able to produce between 10-320[kWh], depending on the sea state condition. In average the WEC is able to produce 127, 61[kWh] when placed at the aforementioned offshore site. The calculations also showed that the efficiency of the device capturing wave power increased with approximately 30% for the most occurring sea states due to the WaveSpring. In addition, a model of the WEC was established in the software SIMA. However, running and analysing this model has not been a high priority in this thesis and has, therefore, not been performed.

The third main part of the analysis estimates the required size of the under water storage tanks. As expected, the WEC proved to have low energy production compared to the wind turbine. Based on this, it was decided to find out how many WECs are needed to produce the same amount of energy as one wind turbine. This resulted in 25 WECs per wind turbine. When combining the two power sources we get a total amount of 6407.21[kWh]. This resulted in a total required volume of 58901.58$[m^3]$ at a water depth of 29[m].

Since the wave power density of the offshore site is rather low, different sites have to be investigated before deciding whether the proposed system is feasible. One should also reconsider the site with regard to water depth. The volume of the under water tank decreases exponentially when entering deeper waters. The total required volume of the tank reduced to less than half when installed at for example 80[m].

Sammendrag

I denne master oppgaven ble muligheten for å kombinere vind- og bølgekraft undersøkt. Det er blitt utført et litteraturstudie på ulike konsepter av vindkraft, bølgekraft og kombinert vind- og bølgekraft. Basert på den oppnådde kunnskapen i litteraturstudiet, ble det utarbeidet og analysert et konsept som kombinerer vind- og bølgekraft. Konseptet går ut på å ta i bruk undervanns tanker som lagrer potentiel energi. Det ble også foreslått et passende område med felles distribusjon i Nordsjøen. Det undersøkte offshore området har en vanndybde på 29 [m], en gjennomsnittlig vindkraft tetthet på 872,03 $[W/m^2]$ og en gjennomsnittlig bølgekraft tetthet på 14,29 $[kW/m]$

Analysen kan deles inn i tre hoveddeler. I første del, ble et vindturbinblad designet i MATLAB ved hjelp av BEM (Blade Element Momentum) teori. Utgangseffekten ble deretter beregnet for en trebladet vindturbin sammensatt av det designede bladet. Diameteren på turbinen ble satt til 126 m, noe som ga en gjennomsnittlig effekt på 3.92MW ved en operativ vindhastighet på 10 m/s og en TSR (Tip Speed Ratio) av 8. For å analysere ytelsen til vindturbinen på en mer realistisk måte, ble programmet ASCHES brukt, noe som resulterte i en effekt på 4.35MW. Den gjennomsnittlige effekten av vindturbinen ble også beregnet ved å anvende Rayleigh-fordelingen. Dette resulterte i en gjennomsnittlig energiproduksjon på 3.22MWh per time.

Den andre hoveddelen av analysen undersøkte gjennomsnittseffekt over en tisperiode av en WEC (Wave Energy Converter) for både vanlig og uregelmessig sjø i frekvens-domene. I denne forbindelse ble det valgt å bruke modellen til CorPower. De hydrodynamiske koeffisienter for WECen ble funnet ved bruk av programmet WAMIT. I tillegg ble WECen utstyrt med en ny teknologi som kalles WaveSpring. For å beregne strømproduksjonen for forskjellige sjøtilstander, ble et

scatter-diagram av området brukt. Beregningene som ble gjort i MATLAB viste at WEC er i stand til å produsere mellom 10-320 [kWh] per time, avhengig av forholdene på. WECen er i gjennomsnitt i stand til å produsere 127,61 [kWh] per time når den plasseres på det nevnte offshore-området. Beregningene viste også at effektiviteten av å høste bølgekraft økte med ca. 30 % for de mest forekommende sjøtilstandene på grunnet av WaveSpring. I tillegg ble det laget en modell av WEC i programmet SIMA. For å avgrense omfanget til oppgaven, ble det bestemt å ikke gå videre inn i analysen av denne modellen. Dette kan være et emne for videre arbeid.

Den tredje hoveddelen av analysen anslår den nødvendige størrelsen på undervanns tankene. Som ventet, viste WECen å ha lav energiproduksjon i forhold til vindturbinen. På bakgrunn av dette ble det besluttet å finne ut hvor mange WECs som er nødvendig for å produsere den samme mengden energi som en vindmølle. Dette resulterte i 25 WECs pr vindturbin. Når man kombinerer de to kraftkildene får man en total energi pruduksjon på 6407,21 [kWh] per time. Dette resulterte i et total nødvendige volum av 58901,58 [m^3] på en på 29 [m] vanndypde.

Siden bølge energi tetthet i det undersøkte offshore-området er nokså lav, burde forskjellige områder undersøkes for å finne mest optimal plassering. Man bør også ta vanndybden i betraktning da, volumet av undervanntankene minsker raskt når en oppsøker dypere vann. For eksempel vil det totale volumet som kreves av tanken reduseres til mindre enn halvparten når tankene blir instalert på 80 meters dypde isteden.

Acknowledgements

This Master Thesis has been written during the 2015 spring semester at the Norwegian University of Science and Technology. The thesis has been submitted to partially fulfill the requirement for completing the degree of Master of Science, and has been performed at the Department of Marine Technology in Trondheim, Norway.

The motivation behind this thesis was to determine whether it is possible to combine wind and wave power with a common energy storage underwater tank. The idea arose after investigating different already existing hybrid devices and their disadvantages. The attempt of the elaborated solution is to reduce these disadvantages, such that a combination may be possible to conduct. I suggested doing an analysis of this in my master thesis in hydrodynamics and caught my supervisors interest to the subject.

To ensure the quality of this thesis many people with expertise have been asked for advice. I would , however, like to thank some of them in particular. First of all I would like to thank my supervisors Dag Myrhaug and Bernt Leira, Professors at NTNU, for their guidance and dedication throughout the work with this Master Thesis. We had many educational meetings at the institute, which kept me focused and motivated. I would also like to thank Johannes Falnes for many hours of informative conversations. I am very thankful that he gave me an impression of what he had explored during his many years of research within wave energy. I feel privileged to be able to get this kind of support. Also I would like to thank Jørgen Hals Todalshaug and Madjid Karimirad, for their prompt replies to inquiries over email.

In addition, I would like to thank my fellow students and family, who helped me to overcome obstacles from day to day, and kept my motivation going. In particular M.Sc. Eivind Finne Riley and M.Sc. Asgeir Hovdelien Midthaug were very helpful with the parts of the thesis dealing with wave power. A special thanks goes to my life partner Colleen, who had to endure my absence during this demanding year.

Trondheim, June 2015

Contents

List of Figures

List of Tables

Abbreviations

WEC	**W**ave **E**nergy **C**onverter
HAWT	**H**orizontal **A**xis **W**ind **T**urbine
TSR	**T**ip **S**peed **R**atio
FWEC	**F**loating **W**ave **E**nergy **C**onverter
OWC	**O**scillating **W**ater **C**olumn
PTO	**P**ower **T**ake **O**ff
JONSWAP	**J**oint **N**orth **S**ea **W**ave **P**roject
AoA	**A**ngle **o**f **A**ttack
RAO	**R**esponse **A**mplitude **O**perator

Symbols

v, U	wind speed	m/s
$\bar{v}$	mean wind speed	m/s
$p(v)$	Wind Weibull/Rayleigh distribution	-
a, k	Weibull distribution shape parameters	-
h	height over sea surface	m
z_0	roughness length	m
m	mass	kg
$\dot{m}$	mass flow rate	kg/s
A	swept area	m^2
ρ	density	kg/m
ν	kinematic viscosity	m^2/s
E_k	energy	J
P	power	W (J/s)
ω	angular frequency	rad/s
ω_p	peak frequency	rad/s
M, A_{33}	Added mass coefficient in heave	kg
R_r, B_{33}	Damping coefficient in heave	kg/s
S, C_{33}	Stiffness coefficient in heave	kg/s^2
$S(w), S(f)$	Wave spectrum	m^2s
X	Complex motion amplitude in heave	m
ζ_a	Wave amplitude	m
R_u, B_{PTO}	Damping from the PTO system	Ns/m
f_{PTO}	Force from the PTO system	N
F_e	Excitation force	N

H_s	Significant wave height	m
H_{m0}	Zero moment wave height	m
H	Wave height	m
k	Wave number	m^{-1}
$\bar{P}$	Time averaged power	W
W	Capture width	m
λ	Wave length	m
T	Wave period	s
T_P	Peak period	s
T_e	Wave energy period	s
T_z	Zero crossing period	s
σ	standard deviation	-
p	pressure	N/m^2
C_p	power coefficient	-
R	total radius of blade	m
F_T	thrust force	N
C_T	thrust coefficient	-
a	axial induction factor	-
a'	rotational induction factor	-
ω	rotational speed	rad/s
U	tangential velocity	rad·m/s
ϕ	flow angel	$^\circ$
θ	twist angel	$^\circ$
α	angel of attack	$^\circ$
W, U_{rel}	relative flow velocity	m/s
T	thrust force	N
M	torque force	N
F_L	lift force	N
C_L	lift coefficient	-
C_D	drag coefficient	-
C_a	axial force coefficient	-

C_r	rotational force coefficient	-
L_C	chord length	m
dr	blade element length	m
Z	blade number	-
σ	solidity factor	-
$\dot{V}$	volume flow rate	m^3/s
η	efficiency	-
$\bar{P}$	average power	W
$\hat{F}_e$	complex excitation force amplitude	m
f_e	excitation force coefficient	-
R_r	damping due to friction	kg/s
M	mass	kg
ω_0	natural angular frequency	rad/s
δ	damping coefficient	-
ϵ	random phase angel	rad
B	WEC width	m
V	Volume	m^3
C	conversion factor	-
D	tank diameter	m
L	tank length	m

Dedicated To My Brother

Chapter 1

Introduction

1.1 General Background

Natural resources are normally harnessed in such a way that a maximum output is obtained by a minimum input. Similarly, the energy resources presenting the highest energy density are, from an economical standpoint, most interesting. Oil, coal and wood are typical candidates. However, distribution, availability and pollution are decisive factors, which have to be accounted for.

According to the International Energy Outlook 2013 (EIA, 2013) the world's energy demand is expected to increase with approximately 56 percent from 2010 to 2040. This is mainly due to increased population and growing economy in developing countries.

The main energy sources we depend on today may be divided in three categories: Nuclear fuels (4.3%), Fossil fuels (86.3%) and Renewable energy(9.3%) (BP, 2014) as shown in Figure 1.1.

The share of fossil fuels is expected to remain nearly constant until 2040. From Figure 1.1 it is seen that the share of renewables has to increase by 3.8 percent until 2040, which means that the energy produced from renewables has to be doubled within the next 25 years. In addition to this challenging task, climate research has shown that the current consumption of fossil fuels has resulted in a negative impact on the environment. It should therefore play a much smaller role as a global energy resource in the future. Renewable energy is clean energy in terms

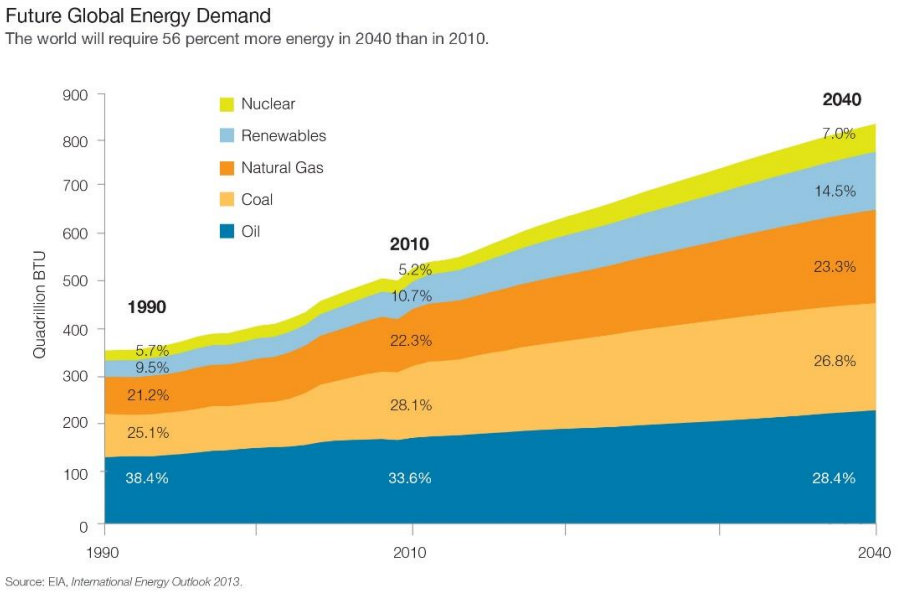

FIGURE 1.1: World consumption (EIA, 2013)

of no or little contribution to greenhouse emissions, and the access to renewable energy sources is inexhaustible. The need for research into alternative renewable energy sources has therefore become a growing issue in the recent years.

1.2 Marine Renewable Energy

Marine renewable energy resource are still in an early stage of development. Marine renewable energy will most likely play a major role in the challenging task of providing the growing population with electricity in the future. This type of energy can be divided into seven groups:

- Tidal energy
- Marine current energy
- Ocean thermal energy
- Osmotic power (Salinity gradient energy)
- Marine bio energy
- Offshore wind
- Wave Energy

In this thesis offshore wind and wave energy was investigated as a contribution to the growing power demand.

1.2.1 Offshore Wind and Wave Energy

Wind and ocean waves represent major forces of the nature. Mankind has fought against their devastating effect and tried to utilize the forces given by nature as a substitution for own muscle strain. They soon learned how to master the forces of the wind for moving vessels across the seas. People explored one another's coastlines, helped by wind. But the wind generates waves, and storms make the ocean rough and dangerous. The waves still have to be tolerated and are still challenging modern shipbuilders. Wind soon proved to be a reliable energy source and is nowadays supplying many households with electricity. It is, however, not until recently men began to wonder how to extract energy in waves for useful purposes. As of yet, wave energy is difficult to harvest in a way which makes it cost competitive. Wind energy has been one of the fastest growing renewable energy sources in recent years (Wang, 2015). It plays a vital role in combating global warming, environmental pollution and the energy crisis all over the world. Presently, offshore wind power makes up only a minor percentage of the total wind energy produced, but it has probably become the most promising renewable energy source. Wave energy, however, still remains almost unexploited and it still has not reached full industrial recognition as an energy source. No solution has yet sufficiently been proven successful. Many ideas have been supported financially without having succeeded in the end. This fact reflects of course badly on harvesting energy from waves. Regardless of this, many inventors and engineers still have hope in wave power as a renewable energy source. The energy density of ocean waves is high, compared to wind or sunshine. Wave energy may represent an interesting potential for generating energy in many developing countries with isolated coastal settlements. To absorb this energy flow has, however, proven to be more difficult than converting continuous flows of waterfalls or wind. This is because of the intensity of the energy flow waves being small in relation to the strength of the structure required to withstand the forces of the moving masses of water. This creates major challenges to survivability in extreme conditions.

1.3 Scope and Objectives of the Thesis

A combination of wind and wave power could reduce the installation and maintenance cost by occupying common infrastructures. The aim of this Master Thesis was therefore to elaborate a design proposal, which combines these two power sources and to calculate the power output of the proposed system. To realize this objective, the following sub-objectives have been defined and achieved:

- A detailed literature research, to ensure an up to date overview of technologies.
- Elaborating a concept which combines wind and wave power.
- Finding a suitable offshore site with high wind and wave energy distribution.
- Establishing an aerodynamic model of a wind turbine blade to calculate the aerodynamic loads on a horizontal axis wind turbine and the resulting power output in MATLAB.
- Testing the design blade in the software ASHES.
- Establishing a numerical model of a wave energy converter (WEC) in MATLAB. Sea state information was used to obtain numerical results for the buoy behavior, heave motion and absorbed energy.
- Calculating the total combined power of the proposed system.

In addition, a model representation of the WEC was set up in SIMA. However, due to time constrains, further analyses were not performed in this thesis.

Chapter 2

Wind Power

Wind power is one of the most environmentally friendly large-scale power sources available today. There are several hundred thousand windmills in operation around the world, many of which are used for water pumping (Manwell, 1988). Attempts to generate electricity from wind energy have been made since the end of the nineteenth century.Yet it was not up to the 1980s that the technology has matured sufficiently (Manwell, 1988). Wind energy is now one of the most cost-effective methods of electricity generation available (Quaschning, 2013). In this chapter the origin and the utilization of wind is explained.

2.1 Origin of Wind

The sun is responsible for the origin of the wind in the troposphere. The earth is constantly absorbing huge amounts of solar radiation energy. The earth has to radiate this energy back into space to not continuously get warmer. Due to the different distances that the solar radiation energy has to travel, the earths surface is heated unequally (Quaschning, 2013). This results in the poles receiving less energy than the region around the equator, which causes a gigantic energy transport from the equator to the pols. In addition the dry land heats up and cools down more quickly than the ocean. This energy transport is primarily the reason for wind to occur.

The differential heating powers lead to a global atmospheric convection system reaching from the earth's surface to the stratosphere, which acts as a virtual ceiling (Manwell et al., 2010). The rotation of the earth deflects this air current and creates relatively uniform winds, the so called trade winds. This is illustrated in Figure 2.1. Because of the earths rotation the wind is deflected to the right in the

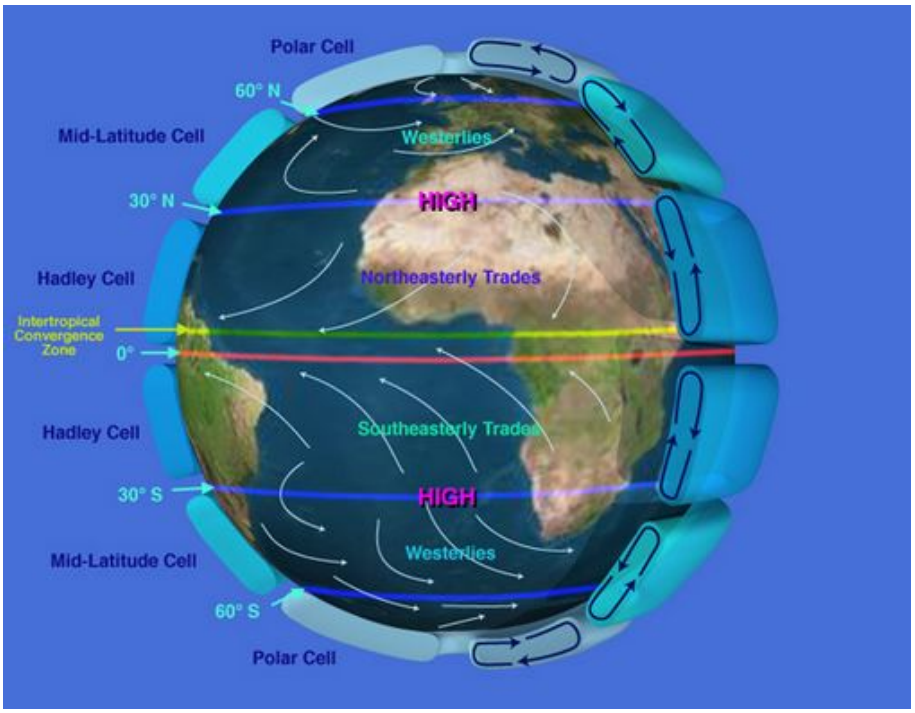

FIGURE 2.1: Global circulation of wind
(EOM, 2013)

northern hemisphere and to the left in the southern hemisphere. This is called the Coriolis effect.
Additionally to this gigantic energy transport, high and low pressure regions contribute locally to the wind generation. Yet on a much smaller scale than the trades.

All of our weather and the greenhouse effect occur in the troposphere. In Figure 2.2 the entire atmosphere is shown. It is estimated that 1-3% of the energy from the sun that hits the earth is converted into wind energy (Manwell et al., 2010). Most of this wind energy can be found at high altitudes where continuous wind speeds of over 160 km/h occur (academia, 2015).

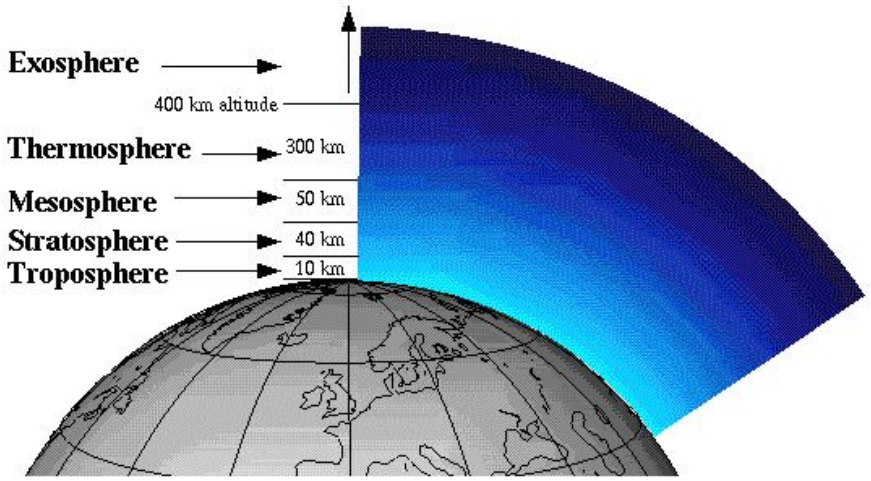

FIGURE 2.2: The Atmosphere
(theozonehole, 2015)

2.1.1 Wind Probability Distribution

To determine the wind energy for a specific site annually, it is common to use a wind probability distribution function. These distributions are either determined from comparative measurements or statistical parameters (Quaschning, 2013). Distribution of incidence of the wind speed can be presented graphically as a histogram. The wind speed histogram can also be interpolated with the use of analytic distribution functions, such as the Weibull and Rayleigh distribution functions (Quaschning, 2013). The Weibull function is described as

$$p_{Weibull}(V) = \frac{k}{a}(\frac{v}{a})^{k-1} exp[-(\frac{v}{a})^k] \tag{2.1}$$

where v is the wind speed and a and k are the parameters that determine the function shape (GreenPower, 2015). These parameters are dependent on the site one is investigating. The mean wind speed can be estimated numerically by

$$\bar{v} = a(0.568 + \frac{0.434}{k})^{\frac{1}{k}} \tag{2.2}$$

In Figure 2.3 a sample histogram of wind speeds for a random site is shown, together with a Weibull-distribution. If a and k are replaced by k=2

$$a_{k=2} = \frac{\bar{v}}{0,886} \approx \frac{2}{\sqrt{\pi}}\bar{v} \tag{2.3}$$

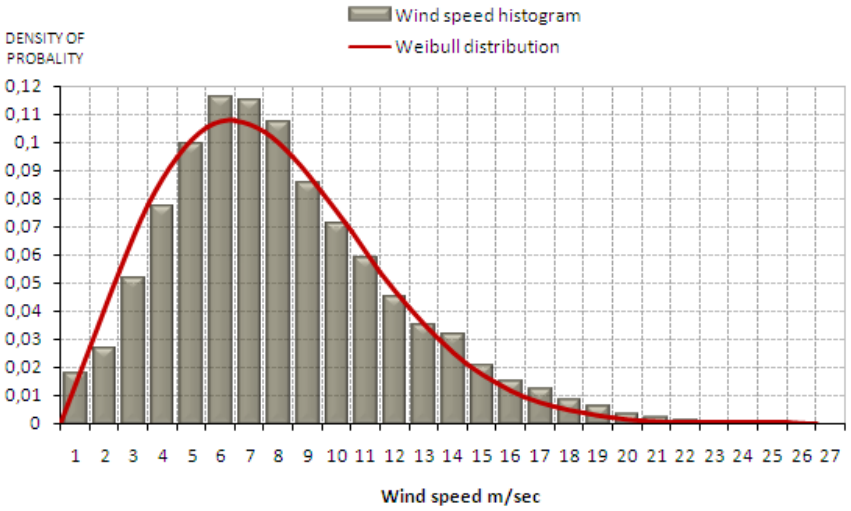

FIGURE 2.3: Wind speed histogram (GreenPower, 2015)

then the Rayleigh-distribution is obtained,

$$p_{Rayleigh}(v) = \frac{\pi}{2}\frac{v}{\bar{v}^2}exp(-\frac{\pi}{4}\frac{v^2}{\bar{v}^2}) \tag{2.4}$$

which means that the wind distribution function can be expressed by the Rayleigh-distribution for a site, by introducing the mean wind speed $\bar{v}$ (Quaschning, 2013). In Figure 2.4 the Rayleigh-distribution for varying mean wind speeds is shown. From the figure it should be noted, that the probability distribution $p(u)$ is decreasing for increasing mean wind speeds.

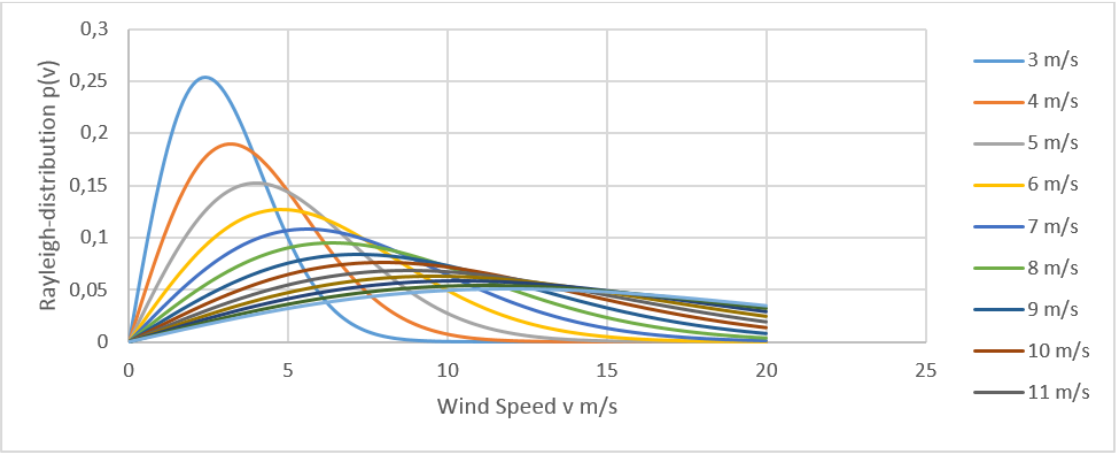

FIGURE 2.4: Rayleigh distribution for varying mean wind speeds

2.1.2 Influence of the Terrain and Altitude

For a power estimation of wind turbines, the mean wind speed at hub height is required (Quaschning, 2013). Offshore wind turbines typically have there center of rotation at 80-90 meters over the sea bed (Jonkman and Scott, 2009). The mean wind speed $\bar{v}$ is typically measured at a height of 10 meters. To determine the wind speed v at a height h_2 (e.g. at 80m), the Log wind profile can be used

$$v(h_2) = v(h_1)\frac{ln\frac{h_2-d}{z_0}}{ln\frac{h_1-d}{z_0}} \tag{2.5}$$

where $v(h_1)$ is the wind speed at height h_1, d is a parameter taking into account obstacles slowing down the wind (which can be set 0 for offshore sites) and z_0 is the roughness length (z_0 ≈0.0002 at offshore sites (Quaschning, 2013)). The roughness length determines, at which height the wind speed is slowed down to zero.

2.2 Offshore Wind Turbines

In general a wind turbine produces electricity by converting the wind's kinetic energy into electrical power by transferring it through a drive shaft to a generator in the nacelle. The nacelle and wing blades can be rotated and adjusted on the basis of wind direction and strength, for optimal use of energy (Statkraft, 2015). Figure 2.5 shows an illustration of the major components of a horizontal axis wind turbine (HAWT), being the most common modern wind turbine type.

Wind turbine rotors consist of two or three blades designed with a low area of the wind being swapped solid. This design results in a high rotational speed relative to the incoming wind compared to other turbine types (Manwell et al., 2010). In addition, it matches well with the frequency requirement of the electrical generator it is connected to, hence reducing the need for big gear boxes. It also shows superior efficiency potential compared to other wind turbine types .

Most installed wind turbines are horizontal axis wind turbines based onshore. Among the available technologies for offshore renewable energy, wind technology is the most mature(Muliawan, 2014). Approximately 2% of the global installed wind power is installed offshore in water depth of less than 20 [m] (Muliawan, 2014). The most common foundations are bottom fixed, such as mono-pile or

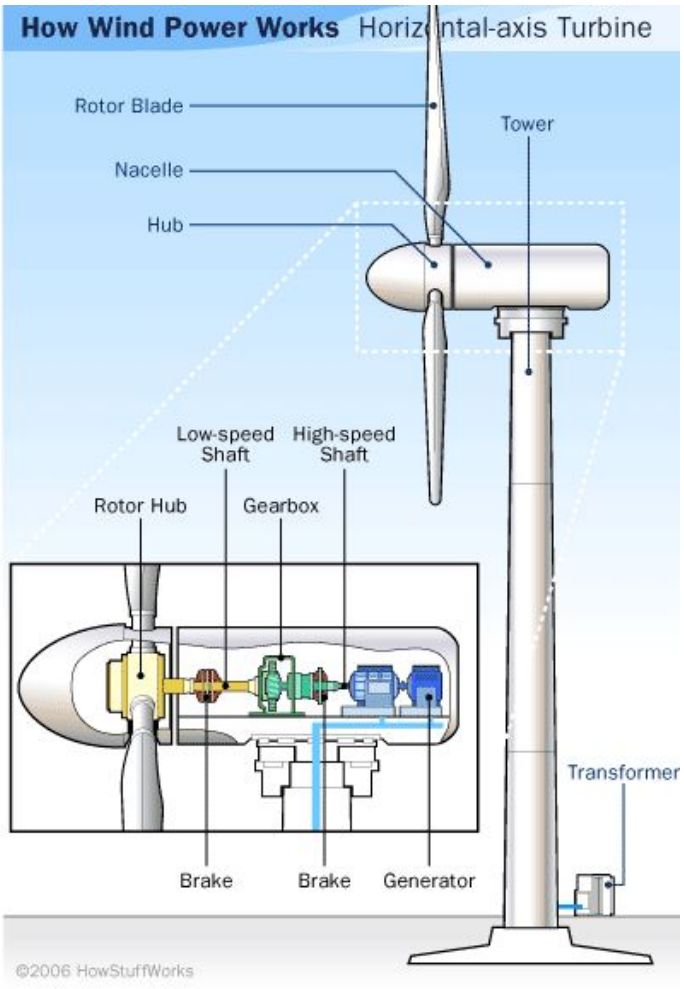

FIGURE 2.5: Horizontal axis wind turbine (Layton, 2015)

jacket foundations, which can be seen in Figure 2.6.

Due to visual pollution and noise even deeper water offshore sites are now being considered. This makes it difficult and more expensive with a bottom fixed solution. Floating wind turbines are therefore expected to be the future within offshore wind (Wang, 2015). There are, however, no commercial wind farms based on floating turbines yet. In Figure 2.7 the concepts of floating devices are presented.

FIGURE 2.6: Bottom fixed wind turbines (SINTEF, 2014)

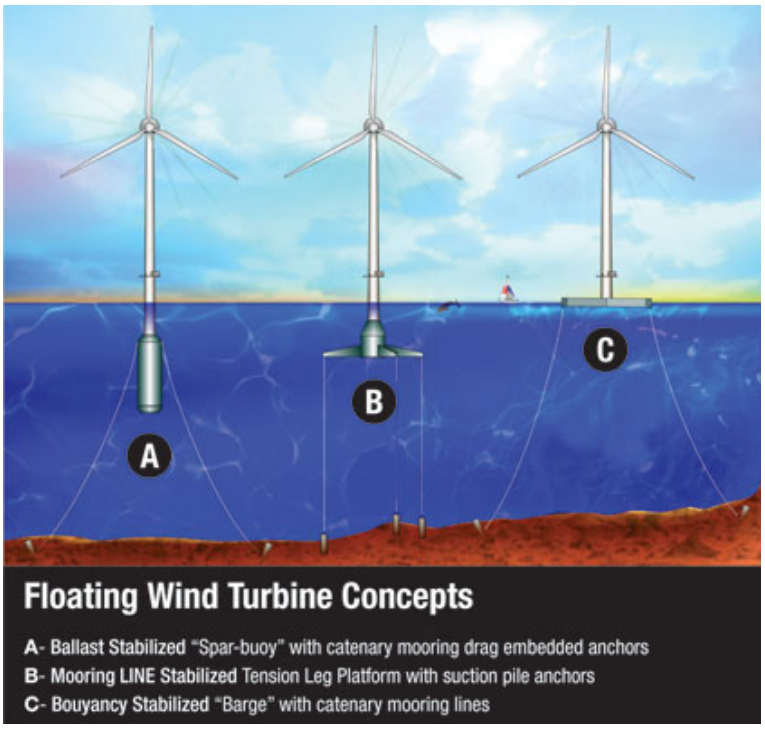

FIGURE 2.7: Floating wind turbine concepts (NREL, 2011)

2.3 Energy and Power

As mentioned, wind is driven by a pressure drop between a low and a high pressure side of a weather system. The energy in the wind is only found in the motion of the air, the kinetic energy. The contained kinetic energy in wind can be calculated in general with the following equation:

$$E = \frac{1}{2}mv^2[J] \tag{2.6}$$

where m is the mass of air in kilograms and v the velocity of the wind in meters per second $[ms^{-1}]$. We know that energy per unit of time is equal to power. Then the power in the wind, P is equal to kinetic energy in the wind per second and can be written as

$$P = \dot{E} = \frac{1}{2}\dot{m}v^2[W] \tag{2.7}$$

The mass flow of air $\dot{m}$ $[kgs^{-1}]$ can be expressed by the air flowing through an area A with a density ρ_{air} and velocity v

$$\dot{m} = \rho_{air}Av[kg\ s^{-1}] \tag{2.8}$$

Hereby we can express the power contained in the wind by

$$P = \frac{1}{2}\rho Av^3[W] \tag{2.9}$$

The main relationships, which can be seen from the formulas above, are that the power in the wind is proportional to:

- The area through which the wind is passing
- The cube of the wind velocity. The wind velocity has therefore a strong influence on power output. If the wind velocity is for example 4 ms^{-1} instead of 3 ms^{-1}, the power increases by a factor of more than two (Manwell, 1988)
- The density of air, which at sea level is 1.2256 $kg\ s^{-1}$; but average densities in cold climates may be up to 10% higher than in tropical regions (Manwell, 1988)

Chapter 3

Wave Power

In this chapter, the origin and the fundamental physics of ocean waves are presented. Aditionally, the mathematical background for the calculations made in MATLAB for irregular waves based on the potential flow theory is presented (see Appendix B.1). On this basis, an initial estimation of the potentially available energy in waves can be made.

3.1 Origin of Ocean Waves

Before continuing the discussion about ocean wave energy it is necessary to mention a few words about the physical setting. The sun and the atmosphere drive almost all dynamical processes in the ocean. As explained in Chapter 2 the imbalance in the heat exchange between the ocean and the atmosphere leads to wind. These winds then generate most of the waves due to friction on the ocean surface. There are other reasons for waves caused by for example the interaction between earth and moon, but because of lesser relevance for this thesis, it will not be considered in detail.

Most of the waves seen on the ocean surface are called ocean surface waves, or wind waves. It is common to differ them into classes like the swells and wind seas. Waves seen in the oceans are, however, often combinations of wind seas and swells. (Myrhaug, 2006) Wind seas are waves created or affected by a local wind system, while swells generally can be described as the waves seen after the wind has stopped blowing or as waves large enough to not be affected by local wind

systems. The size of the swells depend on the strength of the wind and the fetch, which is the distance over that the wind has built up the swells.

3.2 Characteristics of ocean waves

Focusing on a propagating wave or a group of waves, it can be observed how an individual wave appears in the beginning of the wave train and travels to the front of the wave train, where it dies out. What actually is seen is the difference between phase and group velocity, which means the difference between the speed that a particular phase of the wave propagates with and the speed that the wave group propagates with. However, when looking at shallow water waves this phenomenon is not as obvious. In linear wave theory the waves propagating change their wavelength, but the frequency, or the period remains constant (Myrhaug, 2006). For regular wave progressing on deep water the water particles move approximately in circular orbits. A particular water particle moves once around its circle in a time T, the period. For a stationary wave field, the following equations determine the change as the water depth changes.

$$\omega^2 = gk * tanh\ kh = constant \tag{3.1}$$

$$\frac{\delta k_y}{\delta x} - \frac{\delta k_x}{\delta y} = 0 \tag{3.2}$$

$$Ec_g b = constant; E = \frac{1}{2}\rho g \zeta_A^2 \tag{3.3}$$

The dispersion relation 3.1 describes the interrelation between the different wave parameters such as wavelength, wave height and frequency and therefore determines how the waves change as the water depth changes. With help of the dispersion relation it can be shown that the phase velocity is twice the group velocity in deep waters whereas they are identical in very shallow waters. Since the periods remain constant while the wavelengths decrease, as the wave travels into the coast, individual wave crests stack up, causing the wave heights to increase. As a result wave braking and white water may occur (Myrhaug, 2006). Focusing on a single particle in a wind wave, it will be noticed that its orbital motion changes as the water depth decreases. In deep-water waves the particles path is as mentioned circular and the orbits are closed. As depth decreases, the influences on the waves from the sea floor increases. A rule of thumb defines deep water when the water depth is greater than half the wavelength. Hence, the definition of deep water

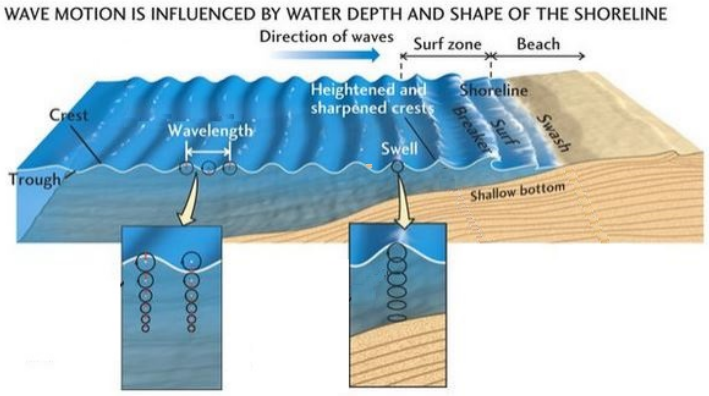

FIGURE 3.1: Wave motion (Welland, 2011)

depends on the length of the waves. In shallow water, the orbital motion becomes disturbed due to the influence of the sea floor. The particles in motion do not return to their original position and differ therefore from the properties of linear wave theory. This drift of the particle is called Stokes drift, since the Stokes wave theory is taking the nonlinear motion of the particle into account. The circular particle paths in deep waters become elliptical in shallow waters (Myrhaug, 2006). However, when looking at wave energy, the particle's path and detailed information about the waves are generally not of great concern. It can be concluded that when waves travel into the coast one need to take notice of the changing physical setting. The sea floor influences the waves, resulting in the particle paths becoming more elliptical. In shallow water, linear wave theory is no longer valid and a more complex non-linear theory is needed to describe the waves. The non-linear wave theory will not be presented here, instead it is concluded that waves loose energy as they travel into shallower water due to sea-floor interactions and that the surge component of the particle motion increases relatively.

The sea states, which usually are described by statistical parameters, are of much greater interest. A wave buoy is the most common equipment used for measuring waves, which records the elevation of the sea surface. With these recordings the power spectral density function can be established for a given data set(Myrhaug, 2006). This function is commonly referred to as the wave spectrum and it is derived by Fourier transformation of the time traces of wave elevations.

3.2.1 Wave Spectrum

A wave spectrum $S_w(\omega)$, which can be seen as a graph of how wave energy is distributed on frequencies, can be derived from wave amplitudes and vice versa (Myrhaug, 2006).

$$\zeta_a = A = \sqrt{2S_w(\omega)\Delta\omega} \tag{3.4}$$

where $\zeta_a = A$ is the amplitude of the wave component corresponding to the frequency ω for a frequency band $\Delta\omega$ and S_w is the wave spectrum. The wave spectrum used in the calculations is the JONSWAP (Joint North Sea Wave Project) spectrum. The JONSWAP spectrum is often used for design purposes in the North Sea for constructions on deep water in fully developed sea. Another, and a maybe more suitable, wave spectrum to use would have been the Torsethaugen spectrum. This spectrum takes into account low frequency waves such as swell (Myrhaug, 2007), which are of high interest when dealing with WECs. However, for simplicity the JONSWAP spectrum is used in the following.
The JONSWAP spectrum is a 5 parameter spectrum and is based on the Pierson-Moskowitz (PM) spectrum, a 1 parameter spectrum for the North-Atlantic only dependent on wind velocity (Myrhaug, 2007). The PM spectrum is defined as

$$S(\omega) = \frac{A}{\omega^5} e^{-\frac{B}{\omega^4}} \tag{3.5}$$

$$A = 0.0081g^2 \tag{3.6}$$

$$B = 0.74(\frac{g}{v_{wind}})^4 \tag{3.7}$$

Where v_{wind} is the wind velocity 19.5 [m] above MWL. In the JONSWAP spectrum the wind velocity is replaced by the peak frequency $\omega_p = \frac{2\pi}{T_p}$ and parameters A and B are redefined as

$$A = \alpha g^2 \tag{3.8}$$

$$B = \frac{5}{4}\omega_p^4 = \beta\omega_p^4 \tag{3.9}$$

$$\rightarrow \omega_p = 0.87\frac{g}{v_{wind}} \tag{3.10}$$

Where β is a form parameter. In addition the the JONSWAP spectrum is multiplied by a peak factor,

$$\gamma^{exp[-\frac{1}{2}(\frac{\omega-\omega_p}{\sigma\omega_p})^2]} \tag{3.11}$$

which varies between 1 and 7, and when $\gamma = 1$ the spectrum equals the PM spectrum. The equation for the JONSWAP spectrum is then found by combining Eq. (3.5),(3.8),(3.9) and (3.11).

$$S(\omega) = \alpha\frac{g^2}{\omega^5}e^{-\beta(\frac{\omega_p}{\omega})^4}\gamma^{exp[-\frac{1}{2}(\frac{\omega-\omega_p}{\sigma\omega_p})^2]} \tag{3.12}$$

In the calculations made in this project it was decided to reformulate this expression with respect to $f = \frac{\omega}{2\pi}$ [Hz=s^{-1}]. The spectrum can then be written as:

$$S(f) = 2\pi\alpha\frac{g^2}{(2\pi)^4 f^5}e^{-\beta(\frac{f_p}{f})^4}\gamma^{exp[-\frac{1}{2\sigma}(\frac{f}{f_p}-1)^2]} \tag{3.13}$$

Where f is the frequency and $S(f)$ is the spectral density function. In the figure below the JONSWAP spectrum and the PM spectrum can be seen. The spectral

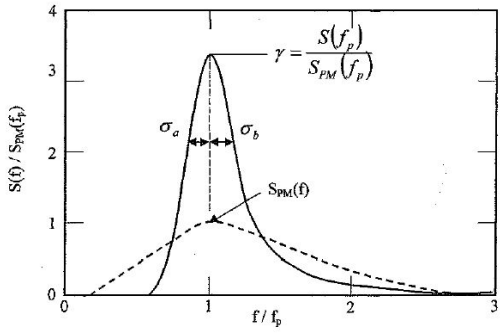

FIGURE 3.2: JONSWAP vs. PM spectrum (Myrhaug, 2007)

parameters α and σ are seen. α determines the shape of the spectrum in the high frequency part, while sigma is the standard deviation:

$$\sigma = \begin{cases} \sigma_a & for \quad \omega \leq \omega_p \\ \sigma_b & for \quad \omega > \omega_p \end{cases}$$

3.2.2 Wave Statistics

The wave spectrum holds all information needed to derive parameters such as:

- H_s, the significant wave height or H_{m0} the zero-moment wave height, which today is more common to represent a certain sea state
- $H_{1/3}$, the significant wave height defined as the mean of the one third highest waves
- T_p, the peak wave period
- T_z, the zero-crossing period
- T_e, the wave energy, which corresponds with the energy transported

H_{m0} is derived as:

$$H_{m0} = 4\sqrt{m_0} \tag{3.14}$$

where m_0 is derived through the spectral moment function:

$$m_n = \int_0^n \mathrm{f}^n S(f)\mathrm{d}f \tag{3.15}$$

The wave energy period, T_e is also derived through the spectral moments,

$$T_e(f) = \frac{m_{-1}}{m_0} \tag{3.16}$$

$$T_e(\omega) = 2\pi\frac{m_{-1}}{m_0} \tag{3.17}$$

3.2.3 Energy Density in Regular and Irregular Waves

The energy stored in waves includes the kinetic and potential energy. In regular waves, the averaged wave energy density, $\bar{E}$ (per unit surface area) is given as

$$\bar{E} = \frac{1}{2}\rho g A^2 \tag{3.18}$$

where A is the amplitude of the incident wave. The average rate of energy flux, or wave power, across a fixed control surface is product of the group velocity and the product of the energy density.

$$\frac{d\bar{E}}{dt} = V_g\bar{E} \tag{3.19}$$

where V_g is the wave group speed and is calculated

$$V_g = \frac{\omega}{2k} \tag{3.20}$$

when deep water is assumed. In Eq. 3.20 ω is the wave angular frequency and k the wave number (Eq.3.1). The wave power in deep water can then be expressed as

$$\frac{d\bar{E}}{dt} = \frac{1}{32\pi}\rho g^2 H^2 T[W/m] \tag{3.21}$$

where $H = 2A$ is the wave height of the regular wave and T the wave period.

3.2.4 Irregular Waves

Once T_e is calculated from Eq. (3.16), the energy flux per meter wavefront for irregular waves can be calculated with the following formula also only valid for deep waters (Falnes and Todalshaug, 2012).

$$\frac{d\bar{E}}{dt} = \frac{\rho g^2}{64\pi} T_e H_{m0}^2 = k T_e H_{m0}^2 [W/m] \tag{3.22}$$

However, when the 2D spectrum is used for deriving various statistical parameters, the directional information about the sea state is lost. As mentioned earlier in this chapter, ocean waves are a result of different weather systems. A swell might enter from one direction, while the wind of a local weather system might create waves from a completely other direction. The result is an irregular sea state with waves traveling in all directions.

3.3 The Wave Energy Resource

The power per meter wave front of a unidirectional sinusoidal wave is given by Eq. (3.23) (Multon, 2012).

$$P = \frac{\rho g^2}{32\pi} T H^2 [kW/m] \tag{3.23}$$

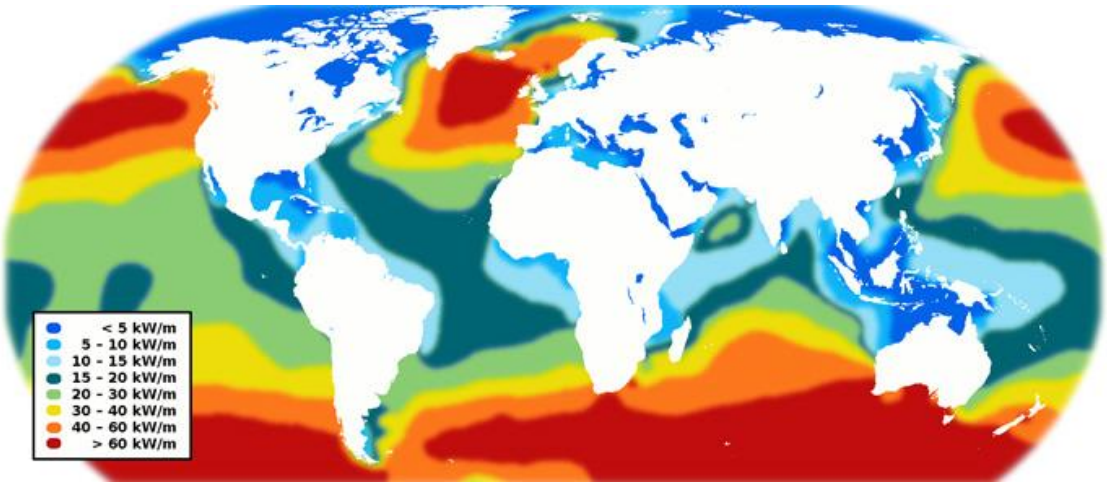

FIGURE 3.3: Global annual mean power (SWECO, 2007)

Where T is the wave period and H the wave height. This formula yields for a single sinusoidal wave, and cannot be used to predict the power from a sea state with irregular waves. A typical wave in the North Sea has a wave period of T=10 s and a wave height of H=3 m. The power per meter wave front can then be calculated as

$$P = \frac{\rho g^2}{32\pi} T H^2 = \frac{\rho g^2}{32\pi} \cdot 10s \cdot (3m)^2 = 88[kW/m] \tag{3.24}$$

In an irregular sea state with the same input parameters as for the regular wave, the power per unit meter wave front is exactly half, as seen from Eq. (3.25)

$$P = \frac{\rho g^2}{64\pi} T_e H_s^2 [kW/m] \tag{3.25}$$

Where T_e is the wave energy period, and H_s is the significant wave height(EIA, 2013). From Figure 3.3 it is seen that the average annual wave power is 40-60 kW per meter wave front along the Norwegian coast. The wave energy potential along the Norwegian Coast is according to (**?**) estimated to be 600 TWh per year, where 12-30 TWh is assumed to be exploitable.

3.4 Wave Absorption

In wave energy, the term absorption refers to the conversion of the incoming wave energy flux to mechanical power. Figure 3.4 explains the basic principle of absorption of waves (Falnes, 2005). The first curve a indicates an undisturbed incident

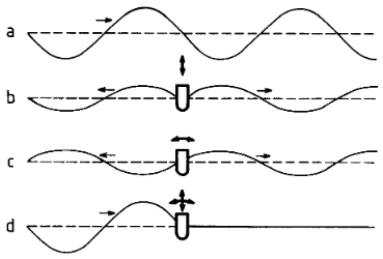

FIGURE 3.4: Absorbtion of waves (Falnes, 2005)

wave. Curve b shows the wave radiation pattern by a WEC oscillating in heave while curve c shows the wave radiation pattern by a wave energy converter oscillating in surge. The last curve d shows the resultant wave field after the superposition of all three waves a, b and c. The most important knowledge when designing a wave energy converter is easily seen through this figure. In order to absorb a wave it is necessary to generate a wave. Hence the known statement of the highly respected wave power explorers Johannes Falnes and Kjell Budal: "*To absorb a wave means to generate a wave*!" or " *To destroy a wave is to create a wave*! "(Falnes, 2005) A detailed NTNU research in the early 80s of these two explorers has shown that it is not of economic interest to build a wave power device, which is designed for more than 300kW. That brings up the question whether wave power is an alternative energy source at all. The answer Falnes and Budal came up with was that, in order to operate in a profitable manner, wave power stations have to be mass-produced.

3.4.1 The Budal Diagram

If the wave-power level is as in Eq.(3.21) and the wave length is

$$\lambda = (g/2\pi)T^2 \tag{3.26}$$

then the maximum amount of power that can possibly be extracted from the wave per unit length is the total amount of power in the wave which is given in (3.27) (Falnes, 2002).

$$P_w = \frac{\rho g^2 H^2 T^3}{64\pi^2} \tag{3.27}$$

However, in reality a lower amount will be absorbed by the WEC. This was theoretically described by Budal and Falnes. They argued that the total volume V

of the body sets limits for both the maximum excursion, velocity and excitation force in heave. They found a theoretical upper bound for the power P_a which is given in 3.28. This is illustrated in Budals diagram in Figure 3.5.

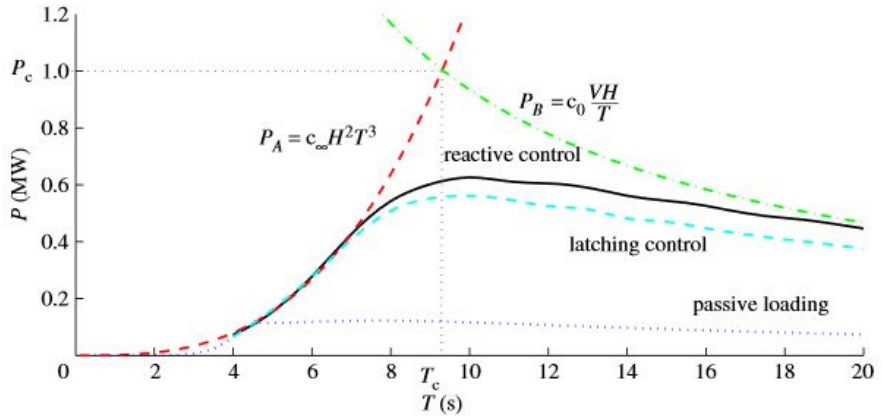

FIGURE 3.5: Budal diagram (Falnes and Todalshaug, 2012)

$$P_B = \frac{\pi \rho g H V}{4T} \rightarrow c_0 = \frac{\pi \rho g}{4} \tag{3.28}$$

From the formula it becomes apparent that the power outtake is dependent on the volume. Larger volume will shift the curve to the right. The goal is to design a WEC where the volume is as small as possible and at the same time absorbs as much as possible energy. This is done by creating the cross point for the most frequent wave periods.

"*It should be considered as an advantage that practically all the volume, of e.g a heaving − float system could be used to displace fluid and thus to generate outgoing waves. Several proposed wave − energy converters have, however, relatively large proportions of "dead" volume not participating in such wave generation*". (Falnes)

If a power take off machinery only applies a simple breaking force to the motion, the response one would get in terms of power is represented by the lowest line (passive loading), which is often used as a reference case. Most of the PTO's installed in modern WECs apply a solution that behaves similar to this curve. However, if one would be able to control the motion optimally, one would achieve

the black line (reactive control). To achieve this the machinery has to apply forces to the buoy, which make the system move differently in relation to the incoming waves than it would naturally. In order to apply these forces one has to predict the incoming wave before it hits the buoy. Some kind of prediction tool is therefore needed with this kind of phase control. This kind of control, however, faces more challenges than solutions. Jørgen Hals Todalshaug has nonetheless, developed a solution which introduces negative stiffness terms and negative mass terms in your control actuation of the machinery. The machinery adds some forces that behave like a negative spring and like a negative mass, the inventor called it therefore the WaveSpring.

3.5 Power-Take-Off

The wave conditions do not only set the size of the WEC, it also determines the characteristics of the PTO (Elforsk, 2011). Most WECs are designed to have a relative motion between two or more bodies induced by the interaction with the waves. The relative motion or the wave-induced mechanical power is what drives the power process (Muliawan, 2014). This is usually referred to as the Power-Take-Off (PTO), and eventually the generator. As discussed earlier, the wave energy flux is dependent on the wave height and the wave period. Machines working in ocean swells need PTOs that are able to manage the large, but slow, forces associated with such waves (note: hydraulic systems have these qualities)(Elforsk, 2011). In smaller wind driven waves a directly driven system, like for example a linear generator, is to be preferred since it responds to velocity changes more rapidly. In order to maximise economic returns, all wave energy converters try to absorb as much of the incoming wave energy as they can to convert the energy to electrical power. The amount of absorbed energy is regulated by the control system.

3.6 ”It’s All about the Phase”

Figure 3.6 shows firstly how the energy in the seas is distributed (orange curve). As can be seen waves have typically a period of 5 to 20 seconds. In addition the heave response for different marine structures is seen. Typical marine structures

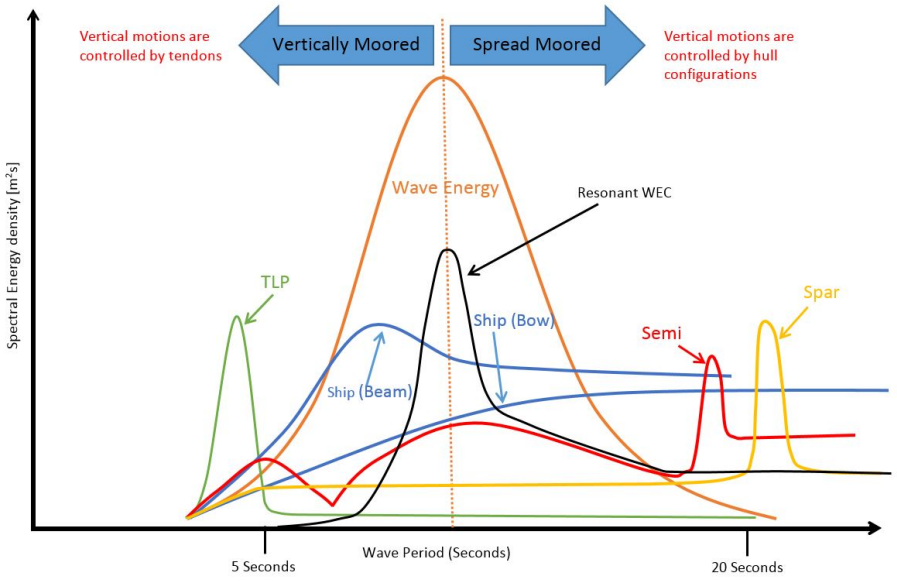

FIGURE 3.6: Energy distribution of the seas and response of different marine structures

are designed to not absorb any of the wave energy and for this reason they have there resonance period outside of the energy spectrum. A structure with resonance at a period of for example 10 seconds would not survive and probably collapse within the first storm. They are therefore designed to be in resonance outside of the sea spectrum. Some at larger resonant periods and some at lower periods, like the tension leg platform (TLP). A wave energy converter is, however, only efficient if it is inside of the energy spectrum. It needs to have good response, wherever wave energy is available. A resonant WEC in heave would typically have a response curve like shown in Figure 3.6 (black curve). Resonance is when the system is in its best condition to absorb energy, yet it is not really the resonance that is important for a WEC. It is more the phase that is relevant. If one would be able to improve the phase response of the WEC one would get a system with a large bend width as shown in Figure 3.7.

The WEC would then be able to respond to both the resonance period of the device and to all the neighbouring periods of the incoming waves (blue curve). Phase control is therefore one of the main challenges when designing a WEC.

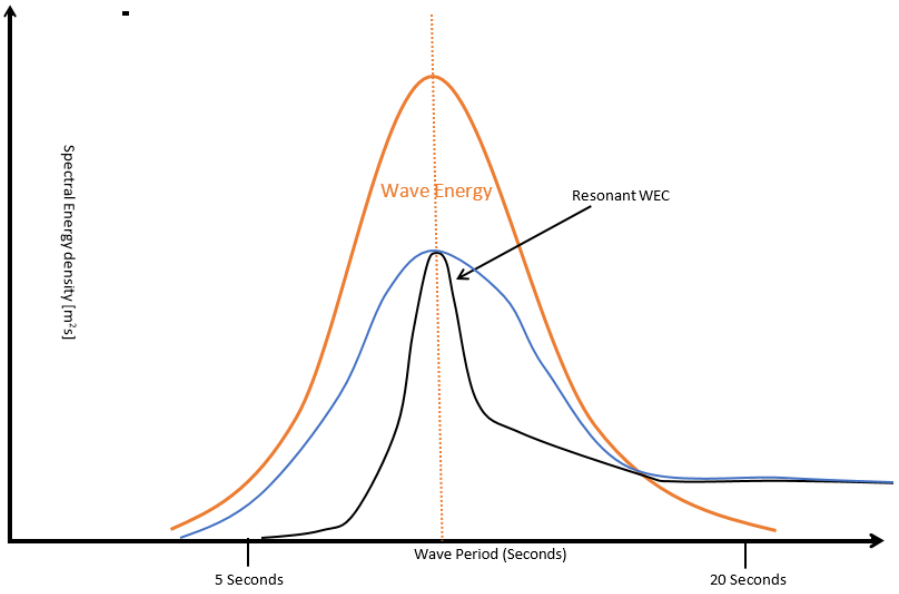

FIGURE 3.7: Energy distribution of the seas and response phase controlled WEC

3.6.1 Control systems of WECs

The control in wave energy devices can be been categorized into three types;

- Geometry control
- PTO control
- Power regulation

When designing a wave power device it is important to consider which control type is the most suitable. Geometric control changes the shape and therefore the added mass-damping. It is also possible to change the mass by the use of flume tanks, to control the centre of gravity and the buoyancy in order to transform the response characteristics of the device.

PTO control of the device is carried out to maximise the absorption force compared to the incident wave force (Cruz, 2008). Many WECs are using a PTO with a single damping coefficient or in other words real control. This form of control is the easiest as it only involves a force that is proportional to a damping coefficient times a velocity (Elforsk, 2011). A more developed type of control system is that of reactive control. Here two or more coefficients are used in the PTO, generally spring-damping coefficients. Using this type of control it is possible to get both the absorption force and wave excitation force in phase. In theory, this is very

easy to implement but in order to execute it in a physical WEC, it requires more complex and expensive components and a power take off that can both produce and consume power (Muliawan, 2014).

3.6.1.1 Latching

One type of PTO control is that of latching. Here the WEC is held (latched) in position at both the trough and peak of a wave and released at a time in order to achieve maximum power absorption like the wave power buoy of Falnes (Falnes and Budal, 1978). In Figure 3.8 the curves indicate incident wave elevation and vertical displacement of a heaving body as function of time (Falnes, 2002). Curve

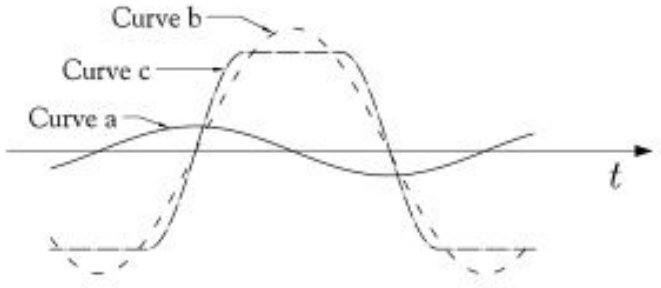

FIGURE 3.8: Latching, resonance and phase control (Falnes, 2002)

a shows the elevation caused by the incident wave. Curve *b* shows the vertical displacement of a heaving body with a mass so large that its natural period is equal to the wave period (resonance). Curve *c* shows the vertical displacement of a body with smaller mass and therefore a shorter natural period. We obtain phase control by keeping the body in a fixed vertical position during a certain interval. To summarize, latching control aims to control the phase that the device oscillates with, whilst in reactive control both the phase and the amplitude of the oscillations are controlled. The difference between latching and reactive control is that the device itself has to arrive at the holding position in latching control. In reactive control the PTO is allowed to function as a motor and drive the device to the optimal holding position.

Power regulation control refers to the quality and quantity of the delivered electricity. This form of control can include power smoothing via energy storage, control of the voltage and frequency.

3.6.2 WaveSpring

There is, however, a new and promising technology developed by Jørgen Hals Todalshaug, which one could classify as a PTO control system. The following is based on a conversation with (Todalshaug, 2015). In Figure 3.9 a buoy in equilibrium, downwards and upwards heave motion was sketched in 2D to give an idea of how the WaveSpring technology is working. It can be seen that two pneumatic cylinders are mounted to the buoy on the one end and to the center road which is connected to the sea bottom. The CorPower buoy is equipped with three of these pneumatic cylinders with an angle of 120 degrees in between them. The cylinder chambers are filld with high pressurised air. In equilibrium position

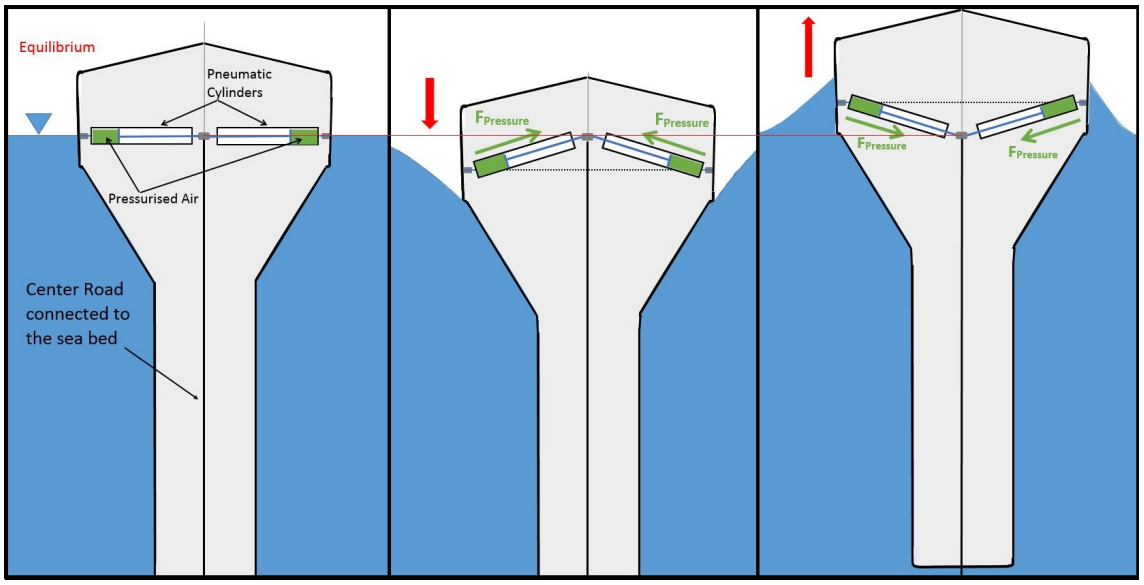

FIGURE 3.9: WaveSpring phase control

the air will give a force outwards in both directions, respectively. In order to effect the buoy the system has to be set in motion. For the vertical motion of the buoy it will not give any force to the buoy, but ones the buoy starts moving for example in heave a vertical component will be acting on the buoy. The buoy will feel an upwards force pushing it even further than it would naturally as can be seen from Figure 3.10. As it moves even more the force will increase. As can be seen the force is a function of the angle and increases therefore with increasing angle. The same happens when the buoy is moving downwards but in opposite direction. Since a negative spring would do exactly the same, the inventor named his invention WaveSpring. The WaveSpring widens with this additional force to the WEC the response bandwidth of the point absorber. There are, however,

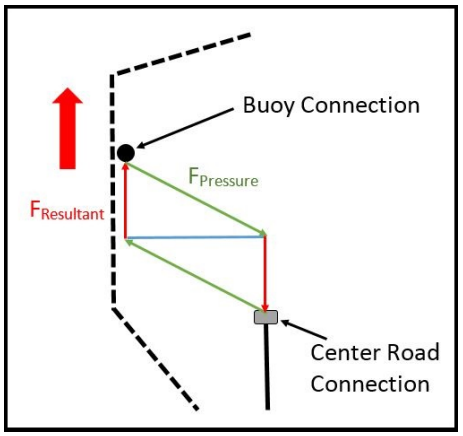

FIGURE 3.10: Effect of WaveSpring

some more major benefits with this technology. Real time wave information or prediction algorithms are not needed anymore, since the WaveSpring answers to any kind of incoming wave. In addition the buoy is moving continuously then for example with reactive control like latching. The result is a smoother power curve. Since the device is spared from abrupt energy transmissions due to the unnecessary latching of the system, fatigue and wear challenges of the PTO are reduced significantly. This reduces the cost of the PTO and improves reliability and component lifespan. Since no real-time information on the incident waves is required for making the buoy resonant, the number of sensors and active control loops can be reduced as well, making the system less complex (CorPower).

3.7 Wave Power Technologies

Many different options have been presented to convert wave energy in the last decades. The amplitude of the waves and their phase direction are irregular and highly weather dependent. Such variations have to be compensated by the power supply system. Wave power plants are exposed to extreme weather conditions, which can cause damages. Furthermore corrosion resistant materials have to be used which makes their production even more expensive (Graw, 1995). Another challenge is to pair the energy generated from wave motions with a frequency of less than one Hertz to electrical generators with a few hundred Hertz (Elforsk, 2011). This and more challenges make it difficult to harvest energy from the oceans. However, many inventors and engineers have tried to come up with a feasible technology. In the following the operation details of different concepts are

explained further and some of the advantages and disadvantages are presented.

3.7.1 Classification Of Devices

The waves of the oceans represent an enormous energy potential. Yet the utilization of wave power is limited. Offshore wave power devices can roughly be divided into three different categories:

- A Point Absorber (axisymmetric and small in relation to wave length)
- A Terminator (large horizontally and the main axis is perpendicular to propagation direction of the waves)
- A Attenuator (also large horizontally, but the main axis is in line with the propagation direction of the waves)

A schematic showing the incoming wave and the scale and orientation of a Terminator, Attenuator and Point Absorber is shown in the figure below.

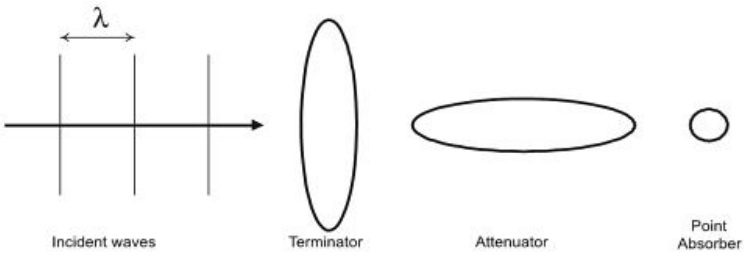

FIGURE 3.11: Schematic of Terminator, Attenuator and Point absorber (Cruz, 2008)

However, the classification system above is not sufficient if all device categories are to be encompassed, since the above is only targeted at floating devices. Thus, although the usual method of classification is primarily based upon the mode of operation, it is more informative to add more detailed qualifiers to describe the device (Cruz, 2008). All the concepts presented below should have the possibility to be combined with wind power (apart from the Pelamis), without discussing the economical feasibility.

3.7.1.1 Point Absorber

This device is a buoy floating on the water surface that is referenced to a fixed system. The devices are usually axisymmetric about a vertical axis. Compared to the incoming wavelength they are smaller then the Terminator or the Attenuator. The concept of such a device is very appealing from a modelling point of view because the scattered wave field can be neglected and forces to the body are only to the incident waves (Cruz, 2008). Point absorbers are capable of absorbing the energy from a wavefront multiple times the key horizontal dimension of the absorber and so possess a large potential capture width.
The point absorber extracts power from the waves due to the heave displacement caused by the incoming wave and due to the relative heave motion between the buoy and a the mooring system. The PTO system used is often hydraulic due to high forces and slow motion, but there are some concepts using linear generators as well. The WEC concept Typ E of Johannes Falnes and Kjell Budal from 1974 and the quite new concept called Wavebob (2010) are classic examples of a point absorber.

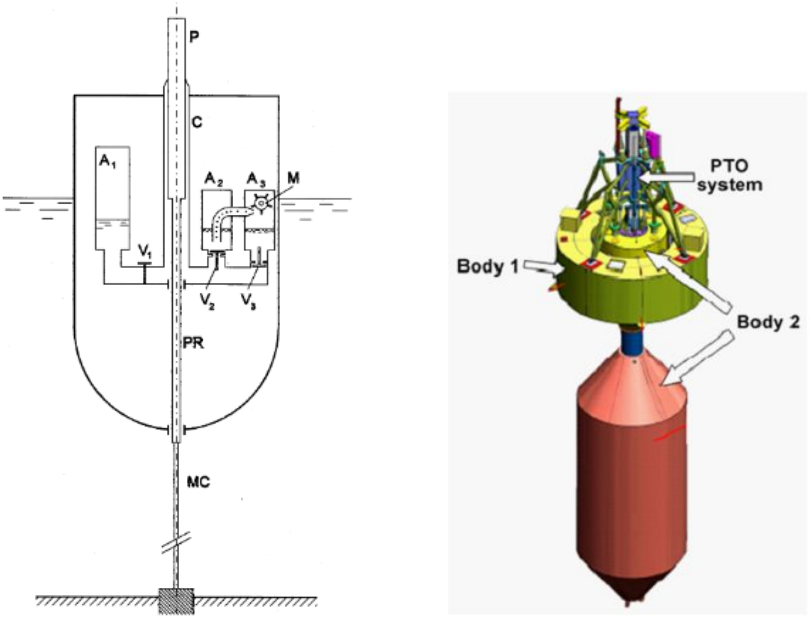

FIGURE 3.12: Concepts of Typ E (Falnes and Budal, 1978) and Wavebob (Wavebob, 2008)

Point absorbers can be designed to operate at near and offshore sites and at most sea states. When choosing a small diameter and light weight the point absorber allows a high absorption for small and high waves (short T_e and high

H_s) and is ideal for North Sea climates. As waves become longer (T_e increases) absorption starts to drop rapidly for systems without active control absorption. Active control can be used to tune a small buoy into higher absorption even for longer waves ($T_e > 12s$). How much more absorption is unknown at this stage, but it is estimated that for a system without active control the absorption is usually 10-30%. Heavy (100s of tonnes) and big (10-25m) point absorbers like the Wavebob are designed to harvest energy from longer waves ($T_e < 7s$). The diameter of a point absorber should be less than 1/6 of the wavelength, otherwise it will notably start counteracting itself. Active control has however shown absorption of 40%-50% for specific wave sites (Elforsk, 2011).

3.7.1.2 Overtopping Devices

Over topping devices can be referred to as terminators. Overtopping devices, reflector arms or slopped surfaces to drive the waves to a reservoir of stored seawater. The difference in water head is then used to derive low head turbines (wavedragon). A good example for this kind of device is the joined EU research project called the Wave Dragon, which is shown in the figure below. A big advantage for this kind of

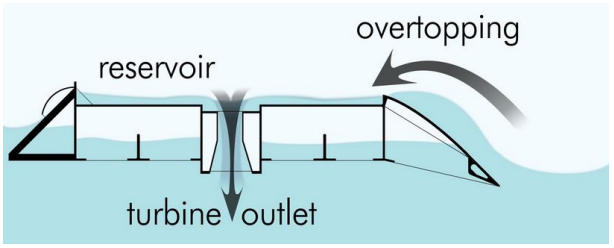

FIGURE 3.13: Illustration of the Wave Dragon (wavedragon)

device is that the turbine technology is well understood and used in hydropower. Overtopping devices are often large and heavy installations and can be installed on the shore line as well as offshore. To increase the range of sea states the reservoir is typically built up in several vertical heights to extract more energy from higher waves. In order to adjust for different wave heights the wave dragon uses mass to stay in place while changing height through an air cushion(wavedragon). The PTO is, as mentioned before,a low turbine (Kaplan type) coupled to a generator. The turbine efficiency can go up to 90% and the generator efficiency is 85-98% according to the Wave Dragon website(wavedragon). Overall wave to wire efficiency has been reported to be 18-20%.

3.7.2 Oscillating Water Column (OWC)

The Oscillating water columns can also be referred to as terminators. They are partially submerged structures that encloses a column of air above a column of water as shown in the figure below. The water level inside the chamber rises and

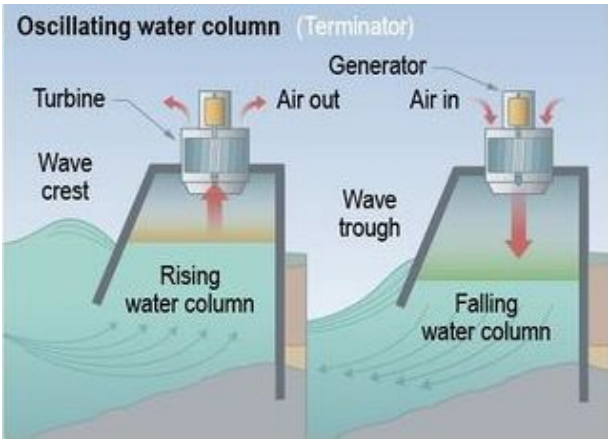

FIGURE 3.14: Illustration of an OWC (OpenEi)

falls due to wave action, alternately pressurising and rarefying the air within the chamber. Pressurized air escapes from the chamber through a turbine-generator unit producing electrical power. On the other hand, when the water level falls, the air is sucked back into the chamber through the turbine-generator assembly to continue power production. The turbine generator most commonly used is the Wells turbine (OpenEi). OWCs are suitable for shoreline installations, where mooring is not an issue and maintenance is more cheaper compared to offshore installations. Offshore OWCs are usually catenary moored devices (Elforsk, 2011). To combine an OWC with a wind power device seems convenient. Ideas of integrating an OWC into an offshore wind turbine foundation are yet to be put to practice. The PTO system used for OWCs usually suffer from high noise levels and have a quite narrow bandwidth. Depending on working conditions the efficiencies for the turbine are in the range of 40-70%. The generator efficiency is usually somewhere between 85-95% (Elforsk, 2011). Active control of the PTO is difficult to implement to these kind of devices, nonethless possible.

3.7.2.1 Attenuator

Attenuators are aligned with the incident wave direction with their beam much smaller than their length (Cruz, 2008). Attenuators are floating devices. The

energy is extracted as waves pass along the length of the device. The most known example for an attenuator is the Pelamis from Scotland. Devices like the Pelamis

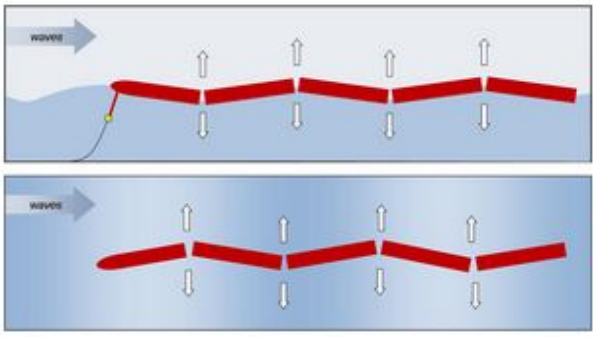

FIGURE 3.15: Illustration of the Pelamis (Falcao, 2009)

are floating semi-submerged on the surface of the water and are always facing the direction of the incoming waves. This is usually achieved by a mooring system attached to the front of the device. As waves pass down the length of the device and the sections bend in the water, the movement is converted into electricity via hydraulic PTOs housed inside each joint of the device tubes. The power is transmitted to shore using standard subsea cables and equipment (Falcao, 2009). The length of an attenuator segment should be smaller than 1/4 of the incoming wavelength otherwise the segment will start counteracting itself notably (Falnes, 2005). An attenuator can therefore only be designed to suit specific wave climates. The Pelamis for example, is most suited to relatively long waves $T_e > 7s$.
The hydraulic PTO systems drive an electric generator. The PTO can be equipped with active control to increase the energy absorption. This active control can double or triple the absorption from 20% without control to 40-80% with active control according to the Pelamis website (Falcao, 2009).

Chapter 4

Combined Wind and Wave Power

In the previous chapters, wind turbines and wave energy converters were explained separately. In this chapter different already existing technologies, which combine wave and wind power are briefly presented to give an overview of the state of art. Their profitability is uncharted to this point, as the combination of wave- and wind power is still in a trial phase and is still being researched.

4.1 Why Combining Wind and Wave Power?

The idea of combining wind and wave energy devices to use the synergy effects and reduce cost of electrical energy from offshore units while increasing the quality of the delivered power to the grid seems tempting. In the last decades more and more offshore wind farms have been installed in the ocean. Hence, the possibility of integrating other marine renewables, such as wave energy converters or ocean current turbines has increased. The combination introduces several advantages, such as better utilization of the ocean space and decreasing the associated costs. Installation (substructures) and maintenance costs, as well as sharing infrastructures between the devices are some of the key advantages (Karimirad, 2014). Adding a wave energy device to a floating support structure of a wind turbine is without a doubt increasing the stability. The motion of the structure will be damped by extracting the energy of the incident wave. This will increase the produced wind power while making simultaneous use of the wave power. It is questionably, however, whether this attempt is economically feasible. The floating wind energy industry is compared to the wave energy industry more mature, but none of them

are yet fully developed. The combination of these two underdeveloped technologies seems therefore far-fetched. Many engineers believe, however, that a hybrid system could be the key to success, since a combination could improve the survivability and stability in harsh environmental conditions. In the following some of these hybrid devices are presented.

4.2 The Floating Power Plant Poseidon

In 2008 FPP launched a 37 meter test- and demonstration plant at an open sea test site in the southern part of Denmark. Poseidon is an example of hybrid platforms combing wave energy and wind power in one unit to use the synergy and increase the power production as mentioned above. The floater absorbs the inherent energy from the waves, and by use of a double function piston pump it transforms the energy from the wave into water pressure that is then sent through a turbine, thus generating electricity. The wave absorption from the floater reduces the height

FIGURE 4.1: Floating Power Plant Poseidon (FPP)

of the waves and creating calm waters behind the front of the plant making the platform easy to access for maintenance purpose. The wind turbines are standard

offshore wind turbines. The mooring system ensures that the waves always meet the front of the plant (Wanan Sheng, 2012).

4.3 W2Power

The W2Power is a concept combining standard wind turbines and wave pumps in semi-sub platforms.

FIGURE 4.2: W2Power (W2Power)

Arrays of wave pumps are installed along the 90 meters at each of the platform sides. According to the W2Power website the pumps will deliver an additional 3[MW], thus bringing the total installed capacity of [9MW]. The platform itself is a triangular, standard semi-submersible. The mooring system is supposed to ensure that the wind turbines will be operating under optimal wind direction conditions. The wave pumps can be lifted when the wave height gets to high and will therefore withstand storm waves.

4.4 Wave Treader

The Wave Treader is attached to the transition piece of an offshore wind turbine. It is designed to provide easy access to the turbine and in addition to power smoothing in the offshore farm (Treader).

FIGURE 4.3: Wave Treader (Treader)

The attached floaters are 50 meters long and have 20 meter beams. If one of the floaters fails the other can still be used. The device has a fore arm, aft arm and sponson, which together function through a submerged structure at the foundation of the offshore wind turbine. The energy is converted by hydraulic pumps between the arms and the submerged structure. It is projected to have 500-700$[kW]$ of peak rating. As waves pass, the floating bodies are lifted up and fall down, which pressurises the hydraulic fluid. The hydraulic motor turns a generator to produce electricity.

4.5 NEMOS

The NEMOS-system consists of an elongated floating body which is connected to the seabed by three ropes as can be seen in Figure 4.4. Excited by the movement of the waves, it transmits mechanical energy to a generator positioned at a monopile where it is protected from the sea water. Due to innovative trajectories and control algorithms, up to 80% of the incoming wave energy can be used to drive electric generators. Conventional systems with vertical movement only achieve efficiencies up to 50%. With a change in the wave direction the orientation of the body and it's trajectory can be adapted by a patented system. For protection from extreme wave loads in heavy storms, the system can be lowered to calmer water.

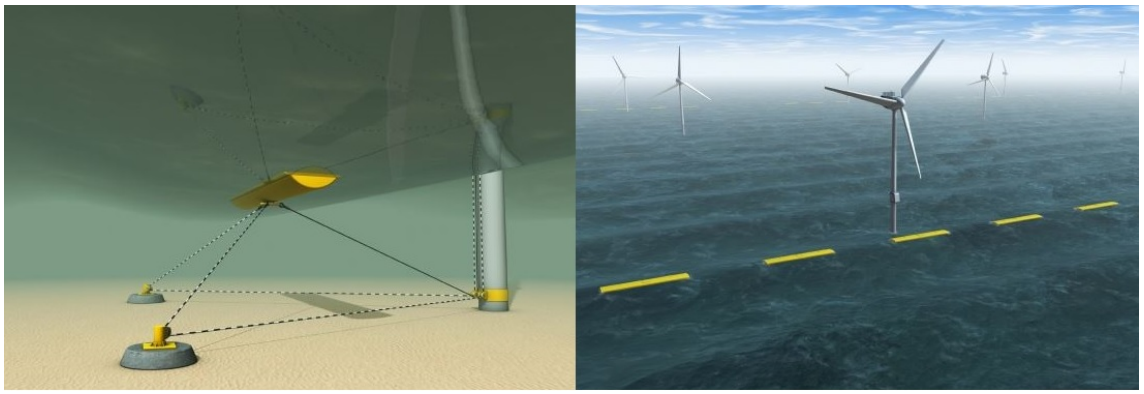

FIGURE 4.4: NEMOS (NEMOS, 2013)

Chapter 5

Design Proposal of a Combined Wind and Wave Power Device

In the following a proposal for combining wind and wave power with an underwater-electrical energy storage tank as a possible offshore energy harvesting system is presented. The elaborated system relates to a pump storage power plant for temporary reversible storage of potential energy developed by (Schramm, 2013).

5.1 The Concept

Combined wind and wave power is a demanding challenge for several reasons. Wave energy converters need motion, while offshore wind energy is most efficient at little motion. Common wind power parks are therefore installed at sites with little waves. The work of Torgeir Moan and Made Jaya Muliawan (Muliawan, 2014) has shown that by mounting a torus shaped WEC device directly to a floating wind turbine it can result in a positive synergy effect. This is due to the WEC damping the motion of the wind turbine (as mentioned in Chapter 4), which results in a smoother power curve of the latter. In other words, the WEC is acting as a protector against incoming waves. The additional effect the wind turbine achieved was, however, not more than approximately a 100 $[kW]$ according to (Muliawan, 2014). The economic feasibility of such a combination is therefore questionable.
In Chapter 4 some of many different attempts for combining wind and wave power were presented. None of them have shown promising results yet. The reason for this might be that the proposed solutions are not technically developed enough.

The authors opinion is, however, simply that wind energy is extremely difficult to harvest at sites with high wave energy occurrence.

The proposed solution in this thesis is therefore not combing the two power sources directly, but rather through a common energy storage tank. Sea water is flowing into one or several underwater tanks. The kinetic energy of the flowing water is harvested by a Kaplan water turbine similar to the power generation procedure in common hydroelectric power plants. The idea is to use wind driven electric centrifugal pumps and wave driven piston pumps to empty the tanks of the inflowing sea water. This allows a continuous flow of water into the tanks. A sketch of the concept is shown in Figure 5.1, developed in the CAD software Rhinoceros version 5. The sketch is not taking into account dimensions or technical details, but is supposed to give a basic understanding of the authors idea.

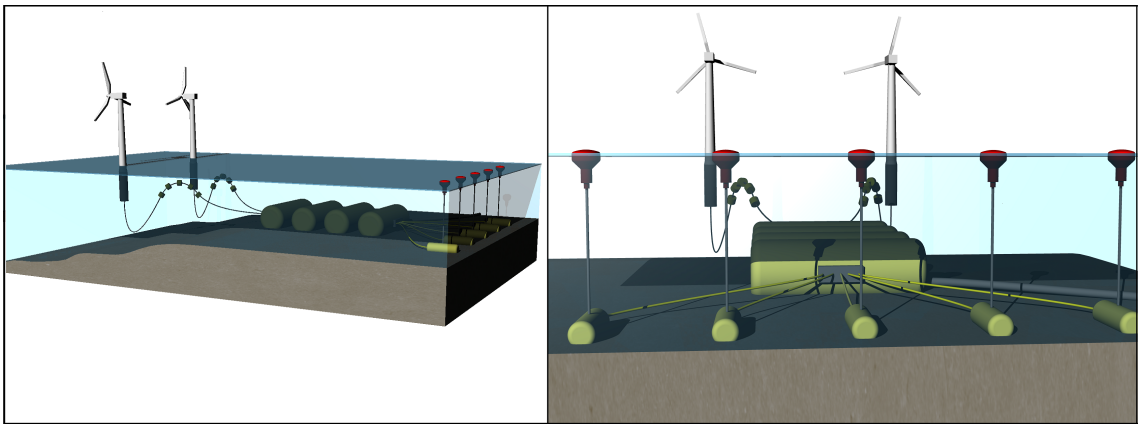

FIGURE 5.1: Sketch of the developed concept

From Figure 5.1, one can see that the author has chosen to use several WECs. As discussed in Section 3.4, wave power is only profitable when mass-produced. The amount of WECs was, however, not set when elaborating the concept. A typical approach is to install 3 WECs per wave length which is typical for the investigated offshore site (Todalshaug, 2015). It was also decided to have a local "small" tank under each WEC. This will make it easier to spread the buoys, instead of pumping the fluid directly out of the main tanks. The wind turbines need to have a certain distance from each other, depending on the rotor size. This is due to the wake behind a wind turbine. A typical approach is to install the wind turbine with 200 meters in between. The picture illustrates floating wind turbines. This is, however, not a requirement. The wind turbines could be fixed to the sea floor as well.

According to the author of this thesis, there are several potential benefits with such a system:

- The HAWT can be installed at deep offshore sites, while the WEC can be installed near shore (However, the power cable connecting the HAWT to the centrifugal pump is expensive. The distance between HAWT and pump should therefore be kept as short as possible)
- The installation of expensive batteries is not needed since the tanks store the energy from both wind and waves.
- Only one power cable connecting the energy storage tank and the power supply system onshore. This should cut down the total power cable length.
- The tanks can be pumped empty at night time, when the power demand is lowest in order to store potential energy for times with higher power demands.
- Generating power through the Kaplan turbine and pumping sea water can be done simultaneously.
- Several tanks can be installed with power producing turbines in between, to harvest as much kinetic energy as possible.
- Reducing the hours of zero produced electricity, which is one of the major concerns with renewable sources. In addition a smoother power output can be expected.

In the following a more detailed explanation of the system and the different components will be given.

5.2 Choice of Offshore Site

Before deciding what kind of wind turbine and wave energy converter should be considered, an appropriate offshore site has to be chosen. One necessary step when evaluating different geographic ocean sites would be to analyse wind and wave resources, as well as finding pumping heights and overall power requirements.

5.2.1 Evaluation of the Wind and Wave Resource

The power in the wind varies with the cube of the wind speed. Thus, if the wind speed doubles, the available power increases by a factor of eight. Wind speed increases with elevation above ground, usually by 15-20 percent with every doubling of height. A rule of thumb recommends that the average wind speed at the height of the wind rotor should be at least $2.5m/s$ (Manwell, 1988). In this thesis the wind and wave data was obtained from (Li, 2015). The paper (Li, 2015) examines joint distributions of environmental conditions at five European offshore sites for the design of combined wind and wave energy devices. The five sites investigated are circled out in Figure 5.2. The results for all sites can be found in

FIGURE 5.2: Location of potential European offshore sites

Appendix B.4. To estimate the power output of the proposed system, site 15 was chosen. This is because of a relatively high average wind power density. As can be seen from the results the average wind power density at 80m above sea level was 871.03 $[W/m^2]$ and the average wave power density 14.29 $[kW/m]$. The wave power density is not particularly high compared to the others, but site 15 has a water depth of only 29 meters, which should be suitable for our water pumping WEC. In Figure 5.3 a joint distribution of the significant wave height H_s and the wind speed U_w for the chosen offshore site is shown. Figure 5.3 was established

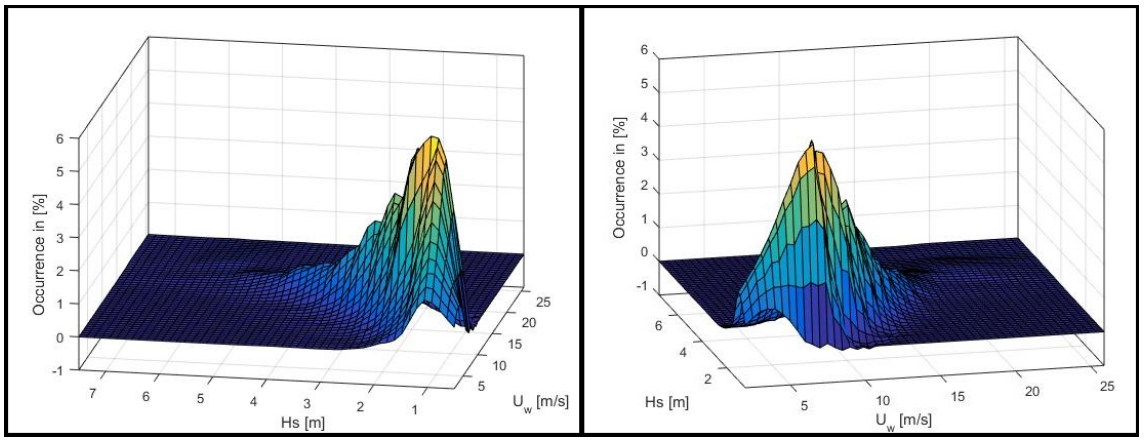

FIGURE 5.3: Joint distribution of wind speed U_w and significant wave height H_s from 10 years hindcast data

in MATLAB and is based on hindcast data over a period of 10 years. The joint distribution which Figure 5.3 is based on can be found in Appendix B.2. Hindcasts are historical weather data that provide valuable information for the analysis of marine environments at specific sites (Solutions, 2015). The whole wave scatter diagram for the site can be found in the Appendix B.3. The wind speed U_w was measured at a height of 10 meters above sea surface. From the figure it can be seen that a wind speed of 10 [m/s] is occurring the most. By using Eq.(2.5) the maximum wind speed at the offshore was calculated to be 27.2 m/s at 80 meters above sea surface, which is approximately the height of an offshore wind turbine nacelle. (Bachynski, 2015) proposed an operational wind speed of 10 m/s, for a wind turbine placed in the North Sea. This values is significant when designing a wind turbine.

5.2.2 Pumping Height and Total Power Requirement

The total elevation, or head, that the pump must work against is always greater than the static depth where the water is pumped from. The power required to pump water is proportional to its mass per unit volume, or density, the acceleration of gravity, the total pumping head, and the volume flow rate of water. This can be expressed as a formula:

$$Power = Density \cdot Gravity \cdot Head \cdot Flowrate \tag{5.1}$$

If we for example assume a water density of 1025 kg/m^3, a tank 29 meters above the sea surface and a pumped volume of $50m^3$ a day it would require:

$$Power = 1025kg/s^3 \cdot 9.81m/s^2 \cdot 29m \cdot 0.000579m^3/s \approx 168.83\ Watts \quad (5.2)$$

The actual power required ...would be higher, caused by losses due to pump inefficiency and the pressure difference between the tank and where the water exits the pump. Eq.(5.2) will, however, be used in this thesis to determine the maximum pumped volume for both the wind driven centrifugal pump and the wave driven piston pump.

5.3 Choice of the Wind Turbine

Wind energy has historically been used for many different purposes like grinding grain, sawing wood and pumping water (Manwell, 2009). Applications for wind water pumping dates back to 13^{th} century Europe. Earlier wind pumps were purely mechanical devices. There are, however, fundamental limits to the efficiency of mechanical wind pumps. Due to the mechanical pumping system the windmill must be located directly over the source from which it is drawing water (Argaw, 2003). Mechanical wind technology devices are often designed with as many as twenty blades. This high rotor solidity provides high torque at low wind speeds, but limits their productivity as wind speed increases (Ackermann, 2000). In addition high inefficiencies of the mechanical pumping process have to be expected, even with modern design improvements. Modern mechanical wind pumps are still limited to an overall conversion efficiency of 7-27% (Argaw, 2003). Nowadays there are other possible arrangements as well, which include electric water pumps and conventional water pumps in a hybrid power system (Manwell, 2009). Electric wind pump systems can be designed with lower solidity rotors than traditional wind pumps. This makes them more suitable in regards to offshore wind power devices - especially if the HAWT is floating. With lower solidity rotors the nacelle is lighter, capable to generate higher tip speed ratios and able to produce more power (Ackermann, 2000). Further, they have fewer moving parts, reducing the need for maintenance. Since electricity can be transmitted over long distances, the device can be placed far away from the site of water pumping as well. In Figure 5.4 two onshore wind water pumps are shown, the mechanical system to the left

and the electrical system to the right. Applications for offshore wind pumps have not been developed to this date.

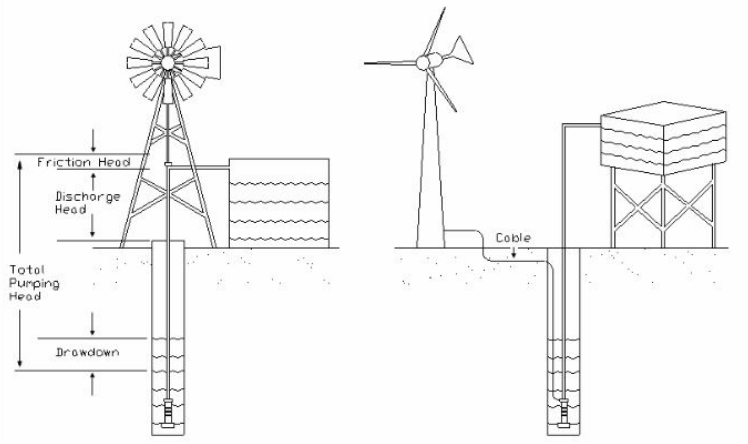

FIGURE 5.4: Mechanical and Electrical Wind Pump (Ziter, 2009)

Since the mechanical wind pump system seams less suitable for offshore sites, an electrical system driven by the wind should be the best choice for this concept proposal. Key components of an offshore electrical wind pumping system include the tower, the floater, the mooring, the turbine rotor, an electrical generator, a motor and pump as well as electrical wiring. Generally a three blade design is selected, with composite airfoil blades for optimal performance and durability (Ziter, 2009). The wind turbine chosen for this concept is a NREL 5MW wind turbine. The reason for this choice is mainly because of available data from the software SIMA, which is needed for the later analyses. Other wind turbine types should, however, be considered, since the choice of a floating wind turbine is highly dependent on the wind and wave distribution of the offshore site. Due to the high workload of this thesis it was, however, decided to stick to the NREL 5MW wind turbine.

5.3.1 Generator

A synchronous generator is ideal for wind pumping applications, as this type of generator is capable of outputting AC current at variable frequency, which is directly proportional to the rotor speed of the turbine(Ackermann, 2000). As the turbine rotor accelerates, the rotational speed of the generator increases, providing a corresponding increase in output frequency and more power is therefore delivered to the pump (Muljadi, 2000). Variable speed systems are ideal as they require no

gearbox and can operate at high rotor speeds with less structural loading on the turbine. They are considered more reliable and less costly to maintain, which is important in offshore applications where maintenance can be difficult (Ackermann, 2000).

5.3.2 Motor

To power the electric pump, an induction motor which is capable of operating according to the frequency provided by the generator is needed. The torque supplied by the motor is a function of its RPM for a given operating frequency. This means that the generator output changes with the ratio of torque to speed based on the new operating frequency. This makes it possible that the motor always can respond to changing wind speeds to produce a desirable output torque (Muljadi, 2000).

5.3.3 Pump

An appropriate pump must be selected to match the output conditions of the motor. There are many pumps that are designed with built in multi-stage motors. These can operate over a range of input conditions from the motor. A possible solution could be the KDT Series Multistage Split Casing centrifugal pump by (Shandong). This pump has a capacity of 6000 m^3/h and can be placed underwater. The type and size should, however, be investigated more in detail. A large pump will pump more water at high wind speeds, however, it will pump less or even nothing at low wind speeds. A detailed investigation of the pump will, however, not be performed in this thesis.

5.4 Choice of the WEC

5.4.1 Historical Investigation of Wave Driven Piston Pumps

The paper (Nielsen, 1986) investigated the possibility of pumping water due to the motion of a floating buoy connected to a piston pump. The danish wave power explorer had the idea to create artificial waterfalls through pipelines by utilizing

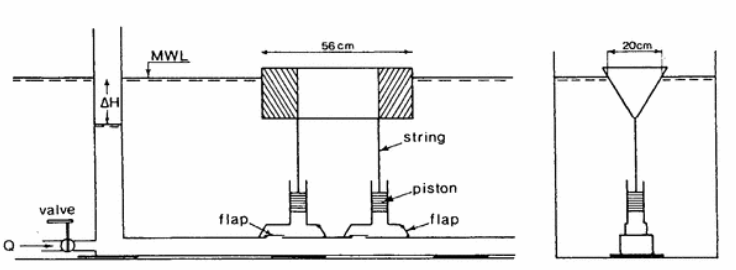

FIGURE 5.5: Experimental set up

the depth of the ocean. The kinetic energy of the flow was then supposed to be extracted by a turbine. When the water reached a tank at the ocean floor, wave driven piston pumps pushed the water up again. In Figure 5.5 the experimental set up of the proposed system is shown. Other attempts of pumping water and utilizing the kinetic energy in a water flow are not known to the author. Earlier work on wave energy converters have been performed more in relation to directly generating energy.

5.4.2 Design Criterias for the WEC

WECs are usually designed to perform at certain frequency ranges. These frequency ranges are often quite narrow because they are designed for specific sea states at specific ocean locations. The most occurring significant wave height of the chosen offshore site was found to be approximately 2[m]. A small WEC should therefore be suitable for the chosen offshore site. However, a wave energy converter will still be able to produce energy in other sea state conditions; although not as much in waves of other frequencies then it is designed for. The full frequency range that the converter can produce in is called the bandwidth of the machine (Falnes, 2005). Wave energy converters are in other words designed to operate in certain wave climates or sea-states, and most of the device developers today have machines designed for Atlantic conditions where the wave energy potential is the greatest (Graw, 1995). There are some developers however, that aim to provide wave energy converters designed for low to moderate energy seas, what is incidentally recommended by (Falnes, 2005).

5.4.2.1 List of Fundamental Requirements for a WEC

Over the years many lessons have been learned about the conversion of wave energy. Many different devices have been tested in small scale and some even reached full scale trials in the ocean. Many of the test results are often kept confidentially. However, many articles and reports have been published. In the following a list of the most important requirements for a wave energy converter is presented. The list is based on literature research and several educational conversations with well known profiles at NTNU, like Professor Torgeir Moan, Professor Johannes Falnes, Jørgen Hals Todalshaug, Professor O.M. Faltinsen and my supervisors Professor Dag Myrhaug and Bernt Leira.

- The most fundamental task of a WEC is to generate a wave that interferes destructively with the incident wave (Muliawan, 2014, Falnes, 2005, Hals, 2010, Cruz, 2008). In principle wave energy absorbers have to be good generators (Hals, 2010). This means that the radiation resistance is the key factor for the income side of wave energy conversion. It influences the amount of power that can be absorbed and consequently the earnings.

- A WEC should rather consist of many small units than a few large ones. The WEC will most of the time operate in sea states with low or moderate wave heights. A to big and heavy WEC will not be able to harvest energy from this sea states because of to little convertible movement. It will lie motionless on the ocean surface. (Falnes and Budal, 1978) introduced a rule of thumb in the late 70's. The WEC should not have a bigger volume than 300 m^3 and should not be designed for a power output of more the 300 kW.

- The WEC has to resist extreme loads as well as repetitive influences due to storm waves. A device that can lower itself over or under the ocean surface during a storm is probably the best survival measure. For convenient point absorbers it is obvious that lowering the WEC is the best choice. However, the land based Wavestar, e.g., lifts the floating devices up during storm (Wavestar).

- The point above brings us to the next preferable requirement. Controlling mass, stiffness or/and volume of the WEC. Some WECs that are designed for several sea states can control their shape by changing their mass, which is called tuning. WECs designed for large ocean swells will experience large

forces and low velocities compared to moderate wind driven sea states (Hals, 2010). WECs within these conditions require larger masses and more inertia to produce power instead of just following the waves. In moderate sea states it is instead, preferable to have smaller and lighter device that can exploit the velocity of the motion (Hals, 2010).

- To predict the incoming waves some other device like a heave based, acoustic surface tracking or pressure based measurement device can be considered implementing. This will make the tuning more efficient (Hals, 2010).
- Since power is a product of force and velocity it is important, that a WEC is designed to endure a combination of relatively large forces and large motions, so as to minimise forces and motions (Hals, 2010).
- All wet surfaces should be smooth, to avoid viscous losses through vortex shedding (Falnes, 2002).
- Station-keeping moorings should not reduce the power capture (Muliawan, 2014).
- Phase control should also play a major role when deciding the WEC type.

5.4.2.2 The Chosen Wave Energy Converter

One WEC that shows promising experimental results is the already mentioned CorPower buoy. The small size should be suitable for the aforementioned offshore site. The company strictly followed the proposed design criteria elaborated by Johannes Falnes, Kjell Budal and other wave energy experts. In addition the CorPower WEC includes modern technology like the WaveSpring. In Figure 5.6 the chosen CorPower WEC is shown.

FIGURE 5.6: CorPower buoy and PTO (CorPower)

The CorPower buoy is, however, not designed to mechanically drive a piston pump. This has to be accounted for when modeling the wave pump system. The CorPower technology should be suitable to electrically drive a centrifugal pump. This will not be examined in this theses, but one should look further into this before implementing a potential experimental test of the system.

5.4.2.3 Piston Pump

From Figure 5.1 it can be seen that each WEC is connected to an additional smaller tank further away from the main tanks. These smaller tanks are connected to the main tanks by pipelines. The water is directly pumped out of these tanks by the wave driven piston pump, see Figure 5.7 The piston pumps have two valves to

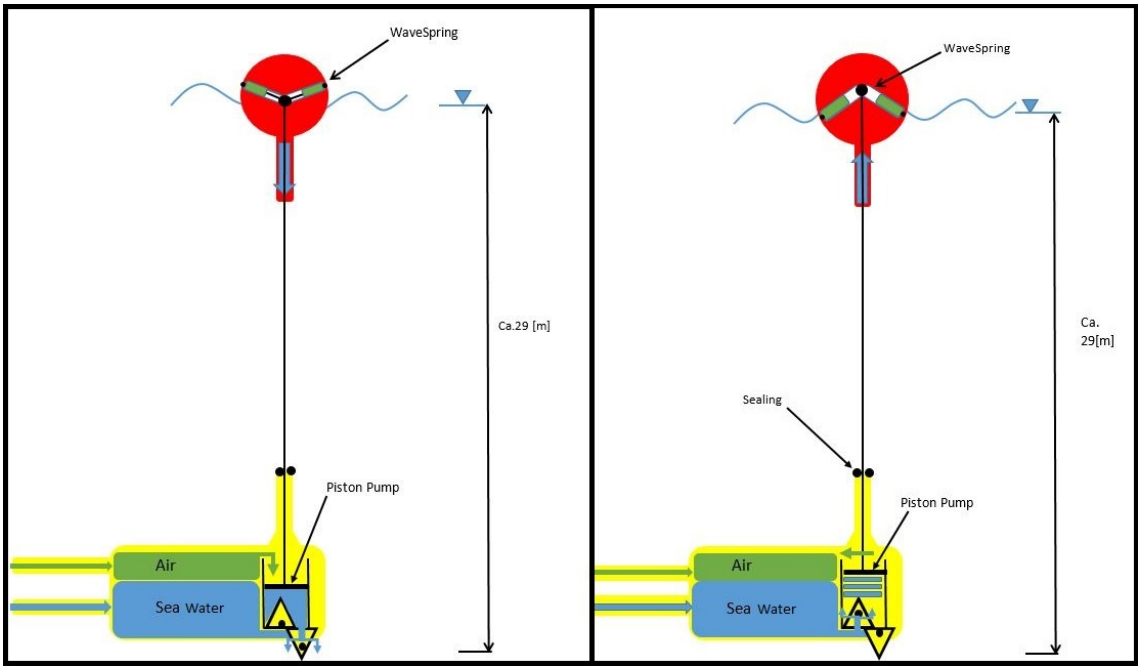

FIGURE 5.7: Sketch of the wave driven piston pump

insure unidirectional flow. In the upward stroke the piston has to pull against the pressure in the tank. On the downward stroke, when the valve toward the turbine side is closed, the wave driven pump has to press the water through the outlet valve. The design of valves are essential to ensure a good performance, as return losses should be minimized.

5.4.3 The Storage Tank

The idea of using a storage tank at the bottom of the sea was adapted from (Schramm, 2013). In Figure 5.8 the proposal is illustrated in basic.

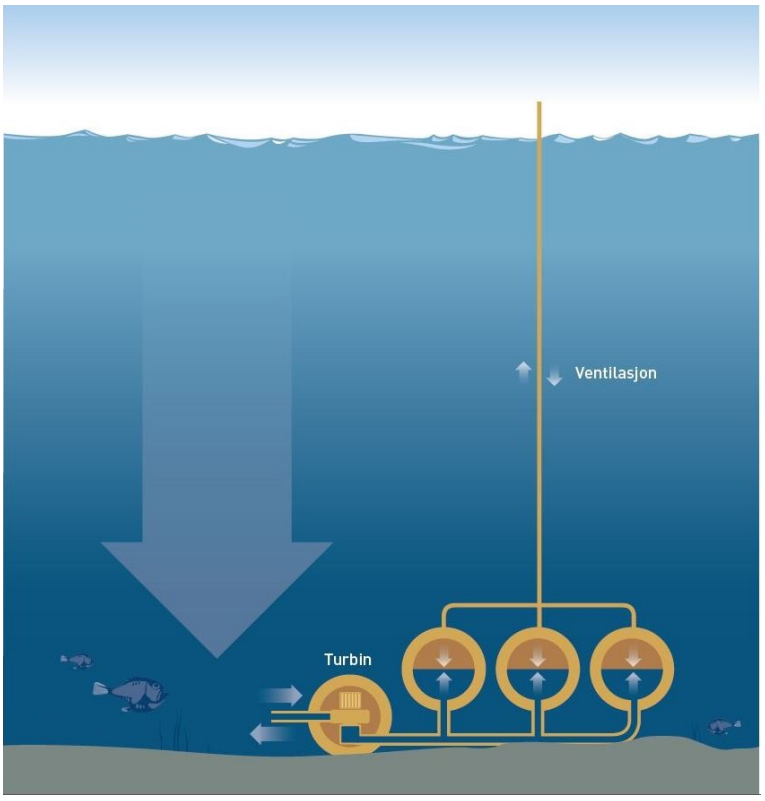

FIGURE 5.8: Storage power plant on the seabed (Benjaminsen, 2013)

In an interview with Gemini.no Schramm explained his idea as following: "*Imagine opening a hatch in a submarine under water. The water will flow into the submarine with enormous force. It is precisely this energy potential we want to utilize. Many people have launched the idea of storing energy by exploiting the pressure at the seabed, but we are the first in the world to apply a specific patent – pending technology to make this possible.*"(Benjaminsen, 2013)

To exploit the pressure on the seabed in practice, the power is captured in a turbine as in normal hydroelectric dams storing energy by keeping water at a high potential. To pump the water out of the tanks the turbines are running in reverse functioning then as a pump. In this thesis the water will, however, be pumped out through additional piston pumps driven by the waves and wind driven centrifugal pumps. The storage power tanks designed by Schramm are supposed to be placed at a water depth of 400-800 meters. This is, however, to deep for a mechanical

wave driven piston pump. The water depth of the chosen site is 29 meters. This will drastically reduce the pressure difference, and therefore the kinematic energy of the water flowing into the tank. The reduced pressure the pumps have to overcome should, however, compensate for some of the lost power. When choosing deeper waters it would probably be more rational to use wave driven electric centrifugal pumps to pump out the water. In Figure 5.9 a summary of the proposed concept is schematically shown.

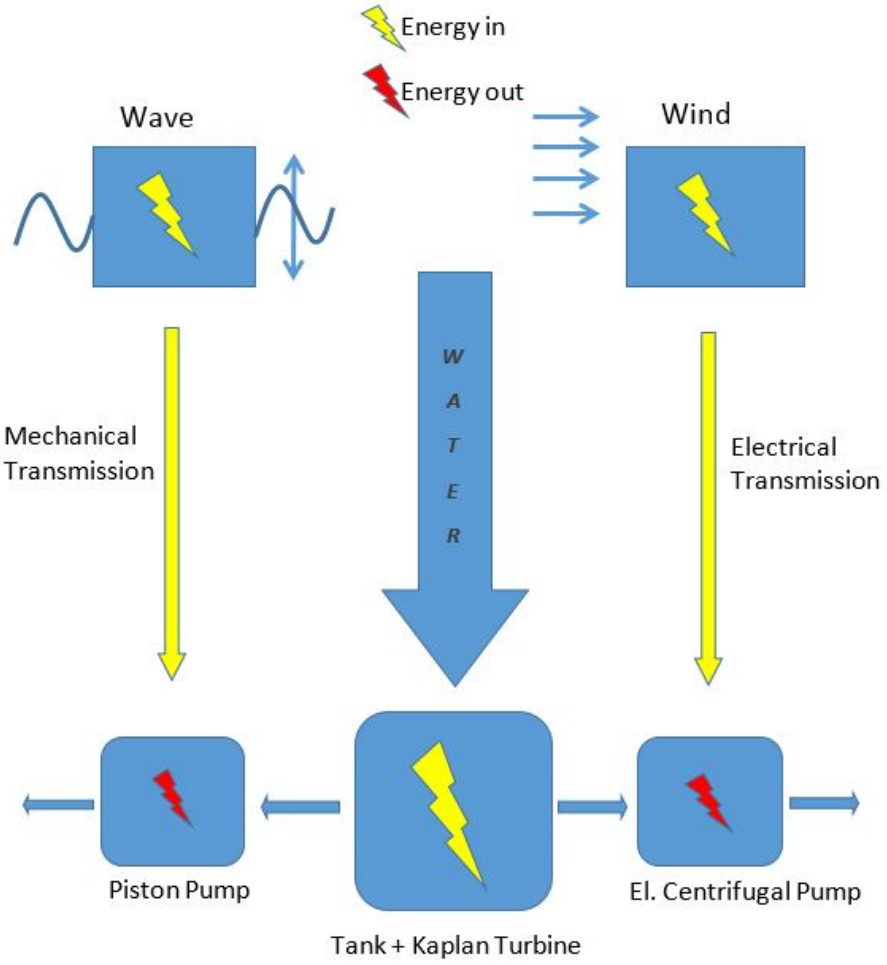

FIGURE 5.9: Schematic concept description

Chapter 6

Wind Power Model

The purpose of this chapter is to predict the power output for a three-bladed wind turbine which is connected to a centrifugal pump. To calculate the power output of a wind turbine, optimal geometric properties of a blade were established in MATLAB by using the Blade Element Moment (BEM) method. Additionally the software ASHES was used to check the blade in a more realistic setting.

6.1 Simplifications and Predefined Parameters

Due to the complexity and time limitations of this thesis, simplifications had to be made. The BEM method used to calculate the power output in this thesis is a simplified approach. It will never give the exact blade performance, and it will not reach the same level of accuracy as is possible with using for example Computational Fluid Dynamics (CFD). The advantage, however, is that the BEM method is considerably faster and typically takes only a few seconds to calculate the performance of the blade. The BEM theory assumes for instance steady state wind speed, which means that the wind profile is uniform and that abrupt changes in wind speed are not taken into account. In addition, it was assumed that there is no flow between the blade elements and that the blades are stiff (not effected by the forces acting on it).

6.1.1 Choice of Blade

The NREL 5MW wind turbine from the software SIMA was used as a reference (MARINTEK, 2014a). The reference wind turbine has a radius of 63m, where the NACA0064 airfoil profile was used for the last 20,5m of the blade. The last 20,5 meters are the main contributors to the performance of the blade, since the thrust distribution increases with increasing radius. This will be discussed in Chapter 7 in detail. For simplification it was therefore decided that the entire blade is composed of a NACA0064 airfoil (Figure 6.1) for which the lift and drag coefficients were known from the software SIMA at $Re = 10^7$.

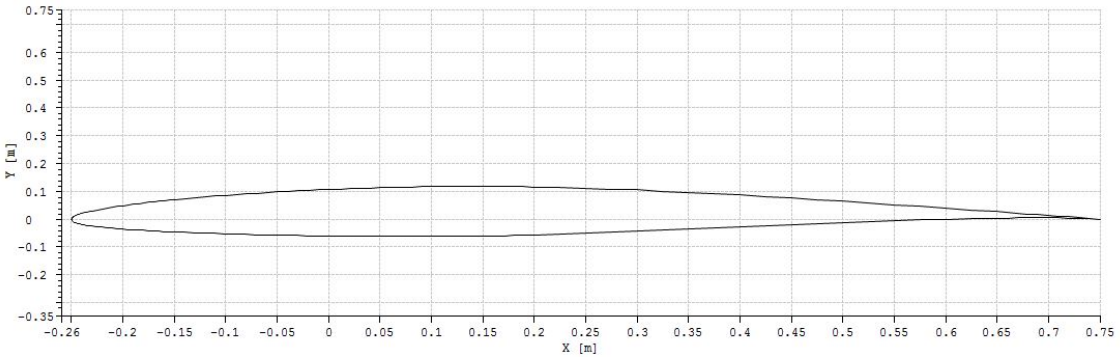

FIGURE 6.1: Geometry of the NACA0064 airfoil (SIMA, 2015)

In reality a wind turbine blade is composed of many different airfoil profiles and is experiencing highly varying Reynolds numbers. The NACA0064 airfoil is typically used for the last 20% of a wind turbine blade. In Figure 6.2 it is illustrated that the Reynolds number increases with increasing turbine diameter. The chosen Reynolds number of $Re = 10^7$ is most likely too high, but should give a reasonable estimation of the lift and drag coefficients (Bachynski, 2015).

Due to the optimization of each blade element by using the BEM theory it is, however, justifiable to just use one airfoil profile for a first power output prediction. The operational wind speed for the chosen offshore site was set to 10 m/s (Section 5.2.1) and the blade is therefore optimized for this wind speed.

6.1.2 Choice of the Tip Speed Ratio

The optimal tip speed ratio (TSR) of the rotor is partly chosen from Figure 6.3. In this figure the power coefficient C_p as a function of the TSR for different wind

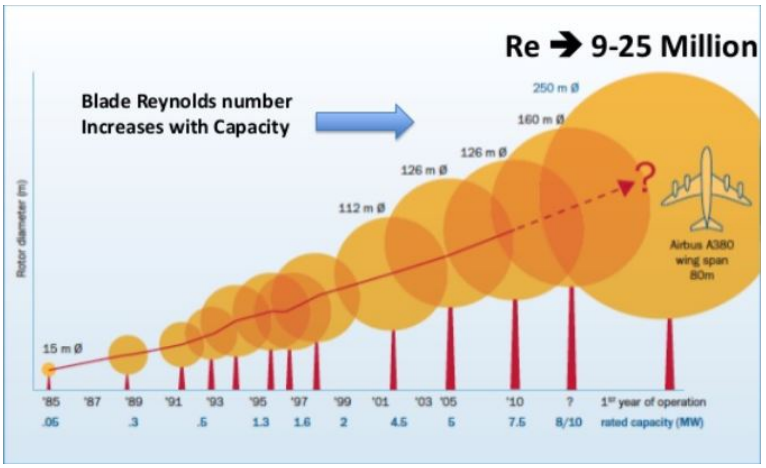

FIGURE 6.2: Increasing Reynolds number (Doolan, 2013)

machine designs is shown.

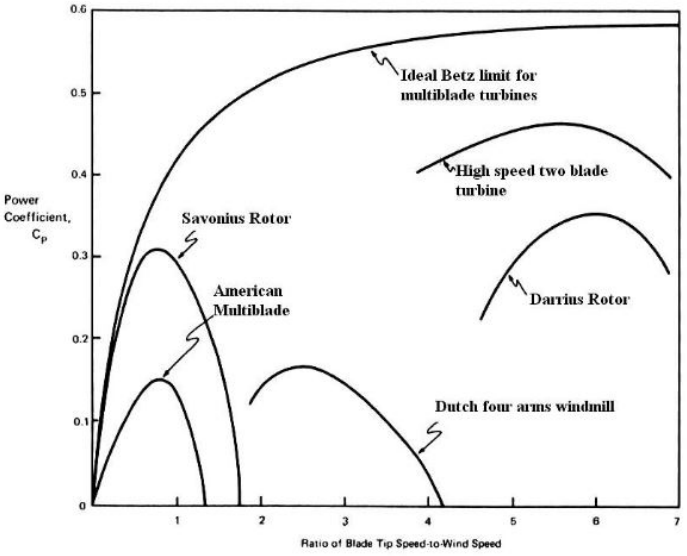

FIGURE 6.3: Power vs TPR (Schubel and Crossly, 2012)

It can be seen that the maximum efficiencies of the multibladed turbines, the Darrieus concept and the Savonius reach levels above 30 percent but below the Betz limit of 59%. The American multibladed design and the historical Dutch four bladed designs peak at 15 percent. These are not suited for electrical generation but are ideal for onshore mechanical water pumping (Schubel and Crossly, 2012). For a multibladed wind turbine it can be seen that a TSR of over 5 is optimal. The TSR is defined as the relationship between rotor blade velocity and relative

wind velocity.

$$TSR = \frac{\Omega R}{V_{wind}} \tag{6.1}$$

where Ω is the rotational speed of the rotor, R the radius of the blade and V_{wind} the wind velocity.
Wind turbines must be designed to operate at their optimal wind tip speed ratio in order to extract as much power as possible from the wind stream (Schubel and Crossly, 2012).

The TSR is the primary design parameter around which all other optimum rotor dimensions are calculated (Boyle, 2004). If the TSR is increased above or below the design TSR it will affect the turbine performance. The relative velocity vector will move the blade elements angle of attack towards a condition of lower lift to drag ratio and possibly toward a situation with stall.
The efficiency of a turbine can be increased with higher Eventough higher tip speeds increase the efficiency of a turbine, effects of torque, mechanical stress, aerodynamics and generated noise are primarily considered when selecting an appropriate TSR (Ragheb, 2014). Table 6.4 gives an overview of how decreasing or increasing the TSR effects the blade.

Tip Speed Ratio	*Low*	*High*
Value	Tip speeds of one to two are considered low	Tip Speeds higher than 10 are considered high
Utilisation	traditional wind mills and water pumps	Mainly single or two bladed prototypes
Torque	Increases	Decreases
Efficiency	Decreases significantly below five due to rotational wake created by high torque [4]	Insignificant increases after eight
Centrifugal Stress	Decreases	Increases as a square of rotational velocity [4]
Aerodynamic Stress	Decreases	Increases proportionally with rotational velocity [4]
Area of Solidity	Increases, multiple 20+ blades required	Decreases significantly
Blade Profile	Large	Significantly Narrow
Aerodynamics	Simple	Critical
Noise	Increases to the 6th power approximately [4]	

FIGURE 6.4: TSR desgin considerations
(Schubel and Crossly, 2012)

An increase of the TSR demands a reduction in chord widths, which leads to narrow blade profiles. This leads to reduced material usage and lower production costs (Schubel and Crossly, 2012). Although an increase in aerodynamic and centrifugal forces is associated with higher TSRs. The increased forces signify that difficulties exist with maintaining structural integrity and preventing blade failure

(Quaschning, 2013). As the tip speed increases the aerodynamics of the blade design become increasingly critical. A blade which is designed for high relative wind speeds develops minimal torque at lower speeds. This results in a higher cut in speed (Duquette, 2001) and in difficulties when self-starting. A noise increase is also associated with increasing tip speeds as noise increases approximately proportionately to the sixth power (Gasch, 2002, Oerlemans, 2006). Modern HAWT generally utilise a tip speed ratio of six to nine for three bladed rotors (Hau, 2006). This setting turned out to produce efficient conversion of the winds kinetic energy into electrical power (Hau, 2006, Burton, 2011). Due to Figure 6.3 and the argumentation above it was decided to optimize the blade at a TSR of 8.

6.1.3 Summary of Predefined Parameters

- Reference wind turbine = $NREL\ 5MW$
- Turbine diameter = $126[m]$
- Airfoil profile = NACA0064
- Average wind speed $V_{average} = 12[m/s]$
- Temperature $T_{average} = 10[C^{\circ}]$
- Density of air $\rho_{air} = 1.204[kg/m^3]$
- Tip speed ratio $TSR = 8$
- Kinematic viscosity $\upsilon = 1.48 \cdot 10^{-5}[m^2/s]$
- Reynolds number $Re = 10^7$

6.2 Maximum Wind Turbine Power Output

The wind turbine extracts the energy from the wind by transforming it into mechanical energy in the device. If all of the kinetic energy in the wind was captured by the wind turbine, the wind velocity behind the rotor would be zero . This is physically impossible, which is why a wind turbine can never achieve 100% efficiency. If knew the magnitude of how much the wind behind the wind turbine is slowed down, we would be able to find out how much kinetic energy in the wind is absorbed by the wind turbine. By considering three different sectors of the airflow, we can find out how much the wind velocity is slowed down by introducing the axial induction factor. In Section 6.2.1 the momentum theory is used to derive the so called Betz Limit.

6.2.1 Betz Limit

The maximum power output from a wind turbine is capped by the Betz limit (Quaschning, 2013). The law is derived from the principles of conservation of mass and momentum of the air stream flowing through an idealized "actuator disk", which extracts energy from the wind stream. According to this law, no turbine can capture more than 59,2% of the kinetic energy in wind. Modern wind turbines achieve their peak at 75% to 80% of the Betz limit.

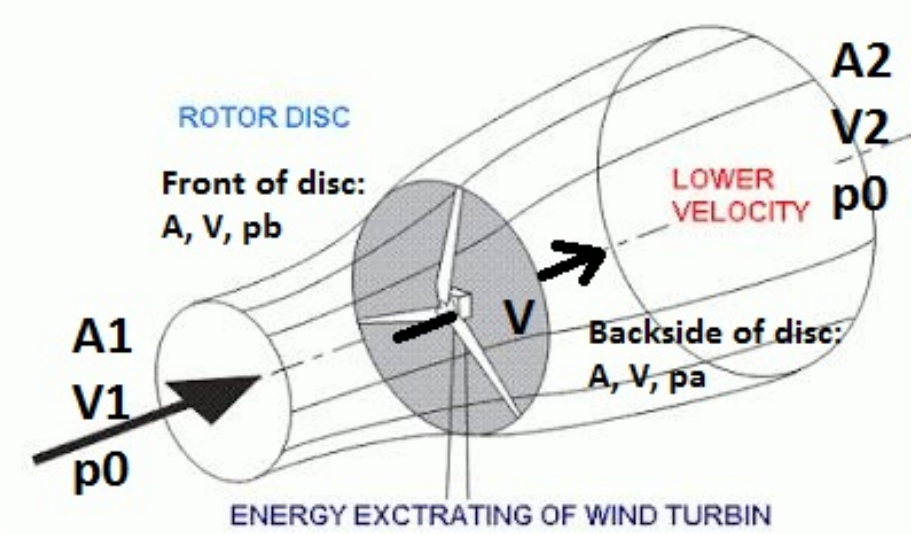

FIGURE 6.5: Schematic of fluid flow through a disk-shaped actuator (Quaschning, 2013)

As mentioned the Betz theorem is derived from the principles of conservation of

mass and momentum of air flowing through a tube as can be seen in Figure 6.5. Since incompressible flow is assumed we get

$$V_1 A_1 = V_2 A_2 = V A \tag{6.2}$$

where V_1 is the velocity when entering the tube (the free stream velocity), V the velocity through the disc and V_2 the velocity leaving the tube. Since the areas A_1, A and A_2 change, the velocities have to change due to the assumption of incompressible flow. After Newton's second. law we can balance the forces as

$$ImpulseForce - PressureForce = ImpulseForce \tag{6.3}$$

$$\rho V_1 A_1 V_1 - (p_b - p_a)A = \rho V_2 A_2 V_2 \tag{6.4}$$

which leads to the energy flux over the wind turbine:

$$P_{Windturbine} = (\rho \frac{V_1^2}{2} V_1 A_1 + p_0 V_1 A_1) - (\rho \frac{V_2^2}{2} V_2 A_2 + p_0 V_2 A_2) \tag{6.5}$$

By expressing $V_2 = aV_1$ where a is an axial induction factor representing the change of velocity from V_1 to V_2 it can be shown that the power efficiency, C_p becomes:

$$C_p = \frac{1}{2}(1 + a - a^2 - a^3) \tag{6.6}$$

Hence, we get the maximum efficiency at

$$\frac{\delta C_p}{\delta a} = 0 = \frac{(-3a^2 - 2a + 1)}{2} \rightarrow a = -1 \;\; a = \frac{1}{3} \tag{6.7}$$

which gives us the Betz limit of

$$C_p = \frac{1}{2}(1 + \frac{1}{3} - (\frac{1}{3})^2 - (\frac{1}{3})^3) = 0.5926 \rightarrow 59.26\% \tag{6.8}$$

The maximum power can then be calculated through the formula

$$P = \frac{1}{2}\rho U^3 \pi R^2 C_p, \tag{6.9}$$

where ρ $[kg/m^3]$ is the air density, U $[m/s]$ the wind velocity, $R[m]$ the turbine radius. For a wind turbine with a swept area of $1m^2$, Eq.(6.9) (with C_p=0.59) is plotted exemplary in Figure 6.6 over a range of wind speeds.

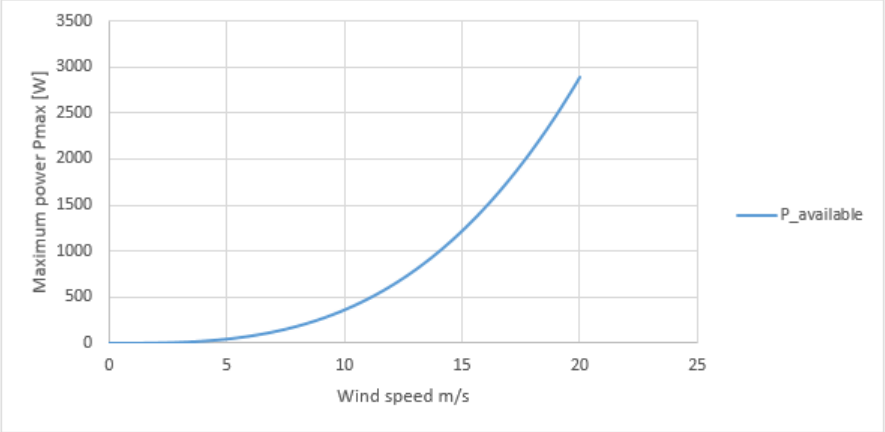

FIGURE 6.6: Maximum power output for wind turbine with swept area A_{swept}=1m^2

6.2.2 Thrust Force and Thrust Coefficient

By using Bernoulli combined with continuity the thrust force can be derived. The thrust force F_T is the force in the axial direction that is acting on the wind turbine (Frøyd, 2010). This force is expressed as:

$$F_T = \frac{1}{2}\rho U^2 \pi R^2 C_T, \tag{6.10}$$

where C_T is the thrust coefficient. To find C_T an empirical relation has to be used to find out how the thrust force develops with respect to the axial induction factor. The ideal expression for the thrust force can be found by a similar deduction as done with the power coefficient C_P in Section 6.2.1. C_T can then be expressed as:

$$C_T = \frac{\Delta p \cdot A}{\frac{1}{2} \cdot \rho \cdot V^2 \cdot A} = 4 \cdot a \cdot (1 - a) \tag{6.11}$$

This expression is only valid for very small values of the axial induction factor a. For most applications a correction based on an empirical relation is needed. This is discussed more in detail in Appendix A.2.3.2. The thrust force is mainly used to calculate the structural parameters, such as strength and material, for the wind turbine blade (Bachynski, 2015). It will also affect the overturning moment which affects the tower- and support structure. This will, however, not be investigated in this thesis.

6.3 Aerodynamics of a Blade

To understand how the HAWT produces power it is necessary to briefly take a look at the blade aerodynamics of wind turbine blades. The HAWT produces power by manipulating the wind the same way boats and airplanes do. A wing is shaped in such a way that free stream airflow hitting the trailing edge is separated into two different streams. One is going over and the other is going under the wing. The distance the upper stream is traveling is longer than the distance around the lower side. For the airflow to meet up at the trailing edge at the same time, the air at the upper surface must travel faster, which leads to a pressure difference, as illustrated in Figure 6.7.

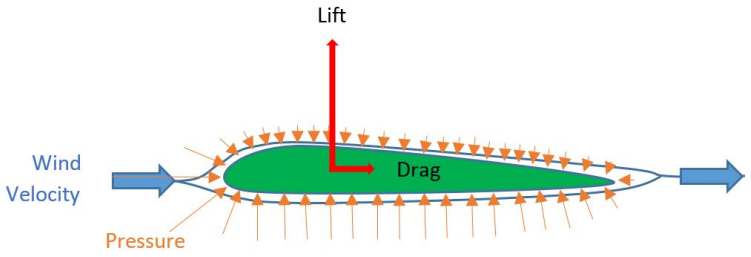

FIGURE 6.7: Pressure and velocity field around an airfoil

In order to extract energy, the blades must receive a force from the airflow around them. Newton's third law states that a body affecting another body with a force will experience an equal and opposite directed force. Newton's second law states that an uncontained body that experiences a force will accelerate. In this case the airflow around the blade is inducing lift and drag forces on the blade, while the drag force is mainly due to the skin friction on the surface of the airfoil.

6.3.1 Forces on the Blade

The magnitude of the lift and drag force depends on the angle of attack. The angle of attack is defined as the angle between the chord line and the relative air velocity U_{rel} as can be seen from Figure 6.9. The lift force is defined as:

$$F_L = \frac{1}{2} \cdot \rho_{air} \cdot U_{rel}^2 \cdot C_L \cdot L_C \cdot dr \tag{6.12}$$

where C_L is the lift coefficient, L_C is the chord length and dr is the depth of the airfoil or the span of the wing. The drag force is defined as:

$$F_D = \frac{1}{2} \cdot \rho_{air} \cdot U_{rel}^2 \cdot C_D \cdot L_C \cdot dr \tag{6.13}$$

where C_D is the drag coefficient. The lift and drag coefficients are found by wind tunnel experiments or CFD, since they are dependent on the Reynolds number Re. C_L and C_D are mainly given with respect to a certain Re. The Re for a wing is defined as:

$$Re = \frac{L_C \cdot U_{rel}}{\upsilon} \tag{6.14}$$

where υ is the kinematic viscosity $[kgm^2]$, which changes with temperature and pressure. Re is highly dependent on the angle of attack, but for a first attempt on analysing a wind turbine blade, one can disregard Reynolds number effects without much error. The Reynolds number is therefore chosen to be constant over the hole airfoil and blade.
The lift and drag coefficients are as mentioned taken from SIMA at $Re = 10^7$. Because of the airfoil being sensitive to variations in Re, it is appropriate to use the constant Re at approximately 80% of the blade radius. One would expect the most influence of the blade performance here. As we will see later this fits approximately for the chosen Re.

6.3.2 Rotational Induction Factor

Since the turbine is rotating, we have to consider the rotational speed of the airflow behind the rotor. This is done by introducing the rotational induction factor a'. The rotational induction factor is defined in much the same way as the axial induction factor a, but here we have to add the induced velocity as we have acceleration, not declaration of the air in the tangential direction. The difference is in this case that the turbine is not extracting the wind for energy but transferring energy to the airflow through the rotational induction. The rotational induction describes therefore a source of energy loss (Frøyd, 2010). The tangential velocity U of a blade at radius r is defined as:

$$U = \omega \cdot r \tag{6.15}$$

The rotational velocity U which the blades experience at a given radius can then be derived as:

$$U + a' \cdot (\omega \cdot r) = U_2 = (1 + a') \cdot \omega \cdot r) \tag{6.16}$$

where a'[-] is the rotational induction factor, ω $[m/s]$ and r $[m]$ the radius. In Figure 6.8 it is shown how the combination of wind speed and the rotational speed results in the relative velocity U_{rel}.

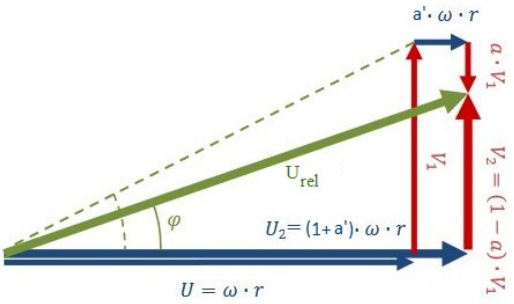

FIGURE 6.8: Velocity diagram with the induced velocities

6.3.3 Blade Element Theory

The lift and drag both push the turbine backwards and forces the blade to rotate. From Figure 6.9 it can be seen that the lift force is normal on the relative velocity, which is the sum of potential wind velocity U and peripheral velocity Ωr. The velocity triangle contains also the angle of attack, α, the twist angle, θ and the flow angle φ.
An important characteristic for HAWT blades is seen through Figure 6.9. As the radii r increases and U remains constant the magnitude of the peripheral vector increases. This causes the flow angle to reduce. To maintain an angle of attack of high lift and low drag with increasing radii the blade has to decrease the twist in the peripheral direction.

6.3.4 Design of the Blade

The blade is fully defined when a set of chord lengths, twist angles, airfoil geometries and airfoil alignments are found. For this purpose, the Blade Element Momentum (BEM) theory is used, which is explained more in detail in Appendix

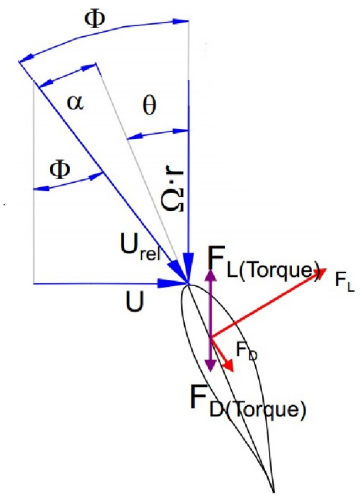

FIGURE 6.9: Airfoil
(Quaschning, 2013)

A.

To predict the power output of a wind turbine, it was decided to design a optimal blade with BEM theory. The details of this theory are, however, not discussed in this Chapter due to its complexity. The theory used in this thesis is described in detail in Appendix A. This method combines momentum theory and blade-element theory to analyze how a wind turbine operates. By expressing velocities with respect to the axial and rotational induction factors, a and a', as in Figure 6.10, BEM develops expressions for the forces on each blade element and the rate of change of momentum.

The BEM method is most commonly used for analysis of wind turbine blades (Manwell, 2009). One of the many different computer tools that do blade analysis using BEM theory is *ASHES*, which has been used in this thesis. BEM method can also be used to design an idealized turbine. The method used in the following is based on (Gasch, 2002) and is developed in MATLAB. The method has been developed based on creating an initial design disregarding drag, which was suggested by Glauert (for more details see Appendix A).

6.3.5 Universal parameter table

By using ideal BEM theory with a given TSR it is possible to create an ideal parameter table consisting of local speed ratios, δ_r, induction factors a and a', flow

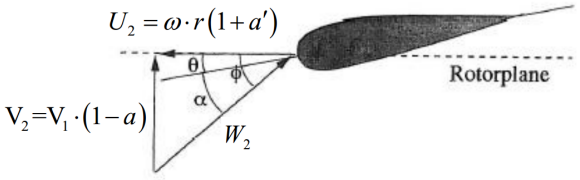

FIGURE 6.10: Velocity Triangle (Frøyd, 2010)

angles ϕ and blade element parameters B_{EP}, which will be used in the algorithm creating an initial blade design (Gasch, 2002). The parameters are found by the following equations.

$$\lambda_r = (4a-1)\sqrt{\frac{(1-a)}{(1-3a)}}, \tag{6.17}$$

$$a' = \frac{(1-3a)}{(4a-1)}, \tag{6.18}$$

$$\phi = \arctan\frac{(1-a)V_1}{(1+a')\omega r}, \tag{6.19}$$

$$B_{EP} = \frac{a}{(1+a')} 4\sin\phi, \tag{6.20}$$

The origin and derivation of these parameters is discussed in Appendix A.2.5. The universal parameter Table A.1 is shown in Appendix A.

6.3.6 Determining the twist angle, θ

The twist angle was optimized for each blade element by the following equation.

$$\theta = \phi - \alpha_{opt}, \tag{6.21}$$

where α_{opt} is the optimal angle of attack for the given airfoil. By choosing the same airfoil for each blade element, the optimal angle of attack will be theoretically constant for the whole blade. The optimal angle of attack is where the ratio C_L/C_D is highest (Gasch, 2002). This is found by identifying which angle of attack that corresponds to the maximum C_L/C_D ratio, given by the airfoil information from SIMA.

6.3.7 Determining the Chord Length, L_C

The chord length was optimized for each blade element by the following equation.

$$L_C = B_{EP}\frac{2\pi V_1}{ZC_L\omega}, \tag{6.22}$$

Eq.(A.54) is also found by an approach using BEM explained in Apendix A. It is desirable having the forces acting in the torque direction to be approximately constant. The velocity U in rotational velocity, and consequently also the relative velocity W, is increasing with the radius, yielding in a decreasing chord length to keep the force distribution constant. The chord length will in an idealized design decrease from root to tip in a non-linear manner.

6.4 Power Output of the Wind Turbine

The torque distribution is given by

$$dM = C_r\frac{1}{2}\rho W^2 L_C dr z \tag{6.23}$$

It is desirable having the forces acting in the torque direction to be approximately constant. The velocity U in rotational velocity, and consequently also the relative velocity W, is increasing with the radius, yielding in a decreasing chord length to keep the force distribution constant. The chord length will in an idealized design decrease from root to tip in a non-linear manner. When the iterative calculations of the element-wise forces and the induction factors are done for each blade element, the power output and power coefficient over the entire blade can be calculated as

$$M = \int_r \mathrm{dM}\, r\, \mathrm{d}r \tag{6.24}$$

$$P_{rotor} = M\omega \tag{6.25}$$

$$C_p = \frac{P_{rotor}}{\frac{1}{2}\rho V^3 A} \tag{6.26}$$

6.5 Electric Wind Pumping

With the wind turbine performance obtained, it can be analyzed how much water may be pumped out of a tank for a range of average wind speeds. For a wind resource with probability distribution $p(v)$, the average power available in the wind for the investigated wind turbine can be calculated as

$$\bar{P}_{wind} = \int_0^\infty P(v)p(v)dv \tag{6.27}$$

where $P(v)$ is the calculated power output of the wind turbine (Ziter, 2009). If the chosen offshore site is assumed to closely follow a Rayleigh probability distribution $p(v)$ is defined by Eq. (2.4). If we now assume that all of the power in the wind is used to pump water, the theoretical maximum pumping rate over a given averaging period can be calculated as

$$\dot{V}_{avg} = \frac{\bar{P}_{wt}\eta_p}{\rho g H} \tag{6.28}$$

where $\dot{V}_{avg}$ $[m^3/s]$ is the theoretical maximum volume flow rate of water over the averaging period, η_p $[-]$ the pump efficiency, ρ $[kg/m^3]$ the water density, g $[m/s^2]$ the acceleration due to gravity and H $[m]$ the head where the fluid exits the pump (Milnes, 2010). In Eq. (6.28) it should be noted that the power is divided by hydrostatic pressure $p_{sta} = \rho g H$ to obtain the volume flow rate.

Using Eq.2.4 with $\bar{v}$ ranging from 3 m/s to 12 m/s, $\dot{V}_{avg}$ can be calculated numerically (Here Simpson's rule was used to integrate Eq. (6.27)) for a range of heads. In Figure 6.11, the theoretical maximum volume flow rate $\dot{V}_{max}$ is shown exemplary over a period of one day for a wind turbine with a swept area A_{swept}=$1m^2$ as in Figure 6.6.

The power output $P(v)$ of the wind turbine in Figure 6.11 is calculated by Eq. (6.9), also in agreement with the maximum power output used in Figure 6.6. The black straight line is marking the water depth of the chosen offshore site in the North Sea and the red curve the mean wind speed of the site.

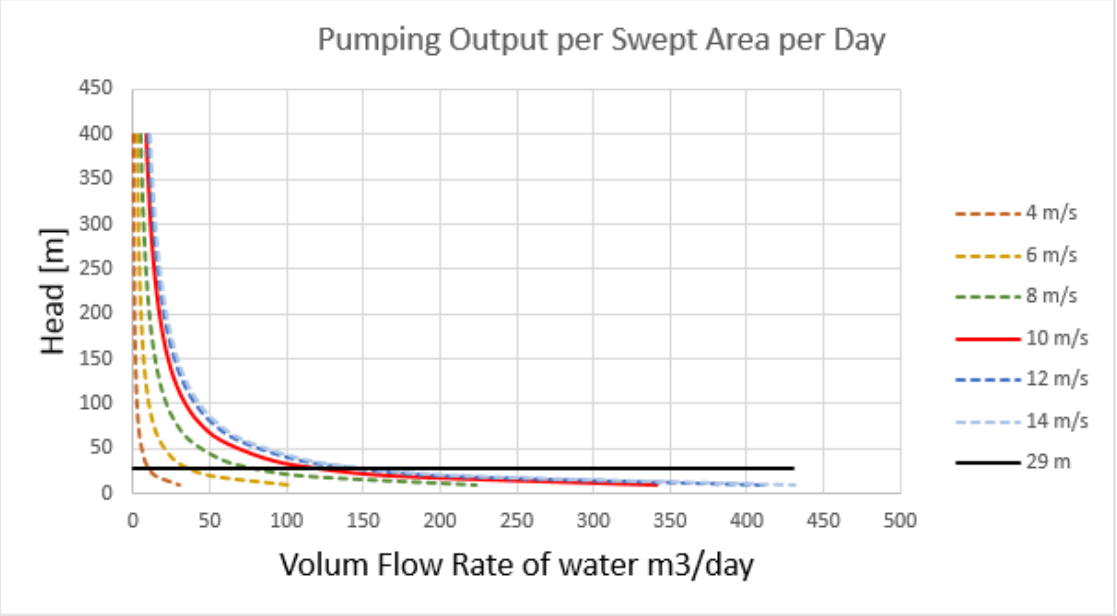

FIGURE 6.11: Volume flow rate $\dot{V}$ m^3/day per swept area

Chapter 7

Results and Discussion of the Wind Power Analysis

In this chapter the results from the MATLAB script are presented. In addition ASHES was used to find the power coefficient for different wind speeds and TSRs.

7.1 MATLAB Script

The script for analyzing the power output of the wind turbine was developed by using MATLAB version R2015a and is based on the BEM method, explained in Chapter A. In Figure 7.1 the procedure of the wind power analysis conducted in this thesis is shown. In addition, Figure 7.2 shows the sequence of the BEM theory calculations made in MATLAB.

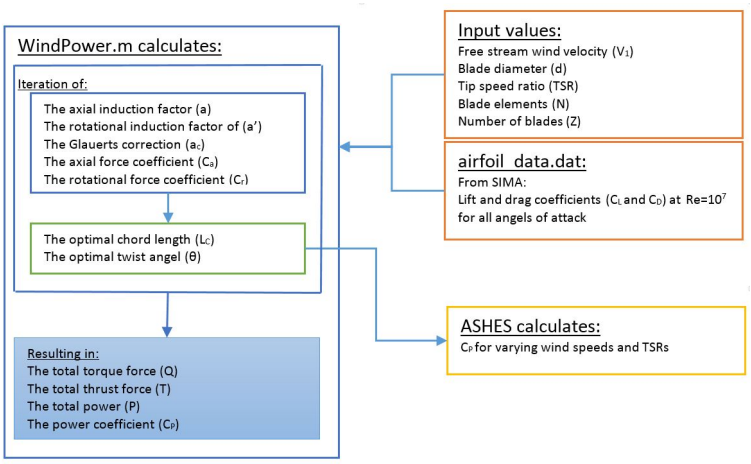

FIGURE 7.1: Workflow

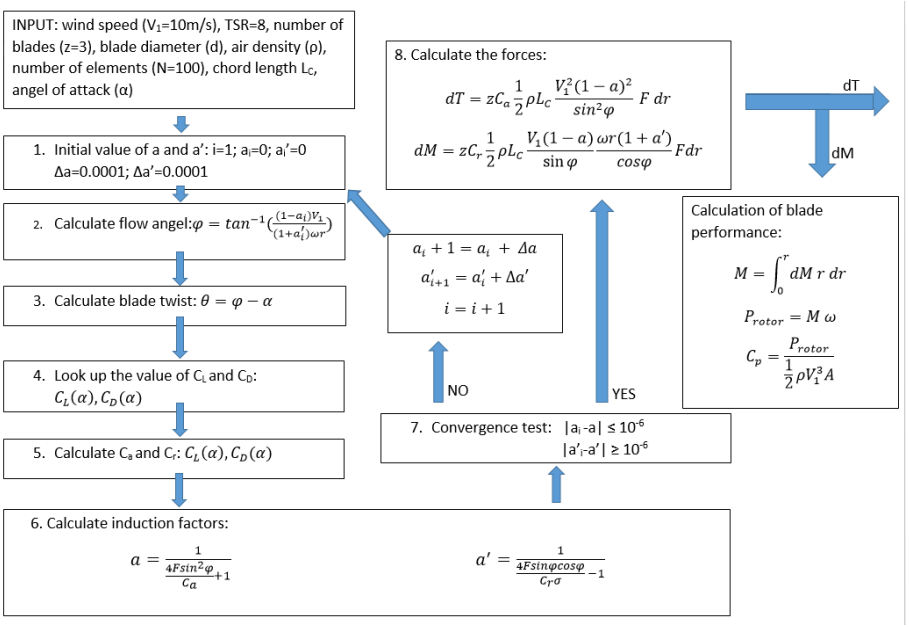

FIGURE 7.2: MATLAB script sequence

7.1.1 MATLAB Results

Figure 7.3 and Figure 7.4 show the results from the initial and final design after optimizing the blade with the BEM method for a operational wind speed of 10 m/s and a TSR of 8.

In Figure 7.3 it can be seen that the chord length is decreasing for increasing blade radii as expected. This is also the case for the twist angle (θ) shown in Figure 7.4. The chord length of the blade decreases from 6.8 meters at the hub, to 1.2 meters at the tip. The twist angle decreases from 25 to -8 degrees at the tip of the blade.

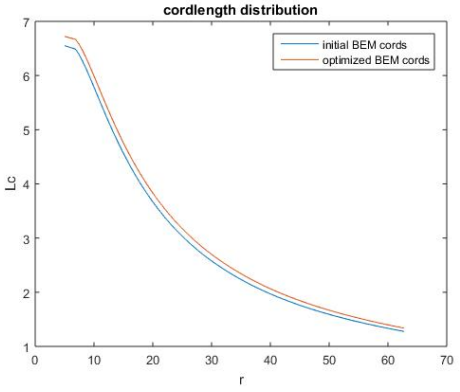

FIGURE 7.3: Chord Distribution

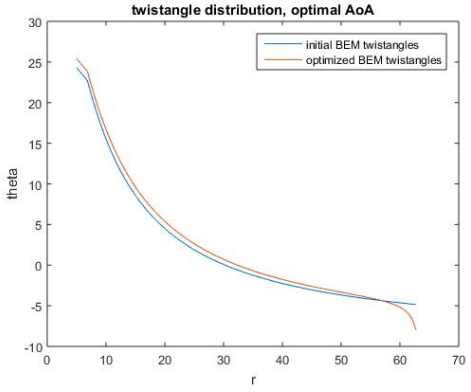

FIGURE 7.4: Twist Distribution

It can also be seen that the optimal chord length and twist angle are slightly larger than for the initial blade. This resulted in a total thrust increase from $T_{blade,initial}$ =620.28kN to $T_{blade,optimal}$= 629.85kN. The total produced power is increased from $P_{blade,initial}$ = 3.77MW to $P_{blade,optimal}$= 3.92MW. The power coefficient calculated by Eq.(6.26) for the initial design increased from 0.513 to 0.528. The torque,dM, and thrust,dT, distribution for one of the three "optimal" blades is shown in Figure 7.5. It can be seen that the torque and thrust are influenced by the tip loss,

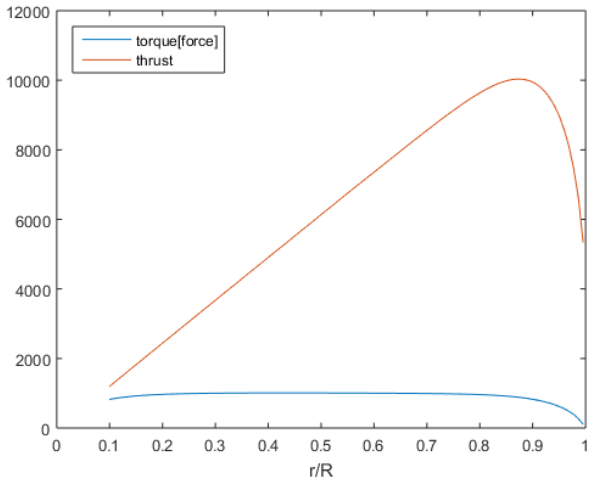

FIGURE 7.5: Torque and thrust distribution over the blade

since both reduce towards zero at the tip. It can also be seen that the thrust reaches a maximum at approximately 80% of the total blade radius as expected. The thrust will not The torque is approximately constant over the whole blade length but dropping at the tip, as expected.

The chord length and twist angle distribution was then imported to ASHES to investigate how the wind turbine is operating at different wind speeds.

7.2 Testing in ASHES

ASHES is a software that performs integrated analysis of wind turbines. The input data is the structural design specifications of the blade for each blade element including airfoil type, chord length, twist angle and distance from airfoil centre to the pitch axis. The input specifications are derived from the BEM analysis done in MATLAB. ASHES utilizes BEM analysis to determine aerodynamic loads (ASHES, 2014), but the method used in ASHES is not identical to the method used to determine the design in this thesis. It is a more comprehensive method resulting in a more correct analysis than what was done in MATLAB. In Figure 7.6 the blades generated by the MATLAB script WindPower.m are shown after importing them to ASHES.

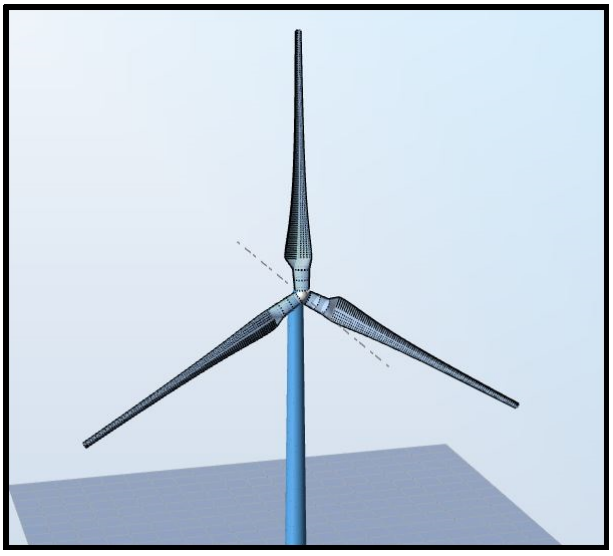

FIGURE 7.6: ASHES 2.0 simulation

7.2.1 Power Output

In Figure 7.7 the aerodynamic power of one blade is shown. It can be seen that the aerodynamic power is stabilizing at ≈4.35[MW]. The power output of the optimal blade calculated in MATLAB was $P_{blade,optimal}$ ≈3.92MW, which means that the results obtained from ASHES are approximately 10% higher. The blade

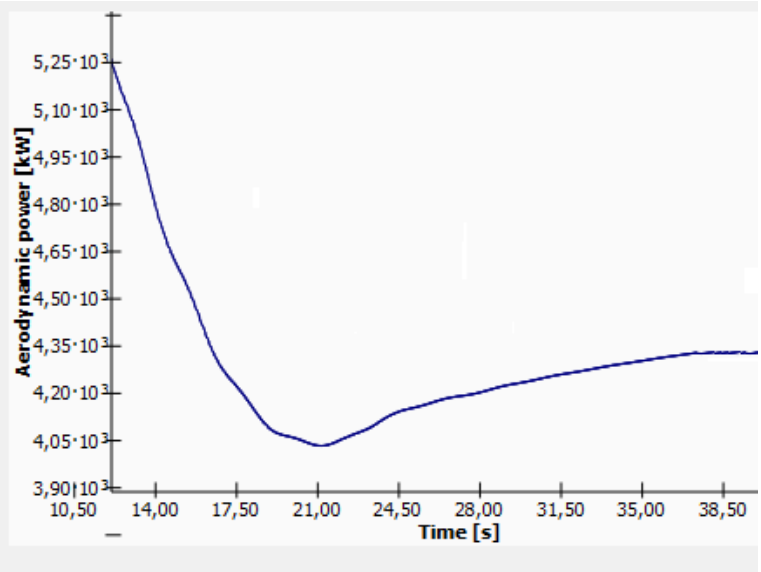

FIGURE 7.7: Caption

design is chosen with the aim of obtaining a fixed and optimal AoA along the blade in MATLAB. In ASHES the angle of attack is varying as seen in Figure 7.10. The wind velocity V_1 and the twist angle θ is set, so a varying AoA must be due to a different simulated ratio of V_2/U_2 in MATLAB and ASHES (see Figure A.4) resulting in a different angle of the relative velocity W. The lift and drag coefficients in MATLAB are calculated from the tabulated values at $Re = 10^7$. ASHES calculates more precisely over a wider range of Re, ranging from $2.4{\cdot}10^6$ to $8.8{\cdot}10^6$ with increasing radii. This is clearly seen in the C_L figure, where the maximum C_L is about 2.7, while the largest C_L for the tabulated value is 1.452 (see Appendix A.2). This is believed to be the main reason for the much higher power output of the blade in ASHES compared to MATLAB. If airfoil data for a wider range had been chosen, a much more realistic MATLAB prediction could have been made. The ASHES simulation is done with a stiff blade approximation. The power output variation due to flexible blades were a few watts and therefore ignored in the ASHES analysis.

Figure 7.9 was also exported from ASHES. It is seen that a TSR between 9 and 11 would result in a higher power output. This is rather unexpected as the design optimization was made for a top performance at TSR=8. It can also be seen that the top area is rather flat, meaning that the airfoils will perform well at a range of angle of attacks. It was, however, decided to keep TSR=8 even though the power output would increase. Due to time constrains it was decided to stick with this

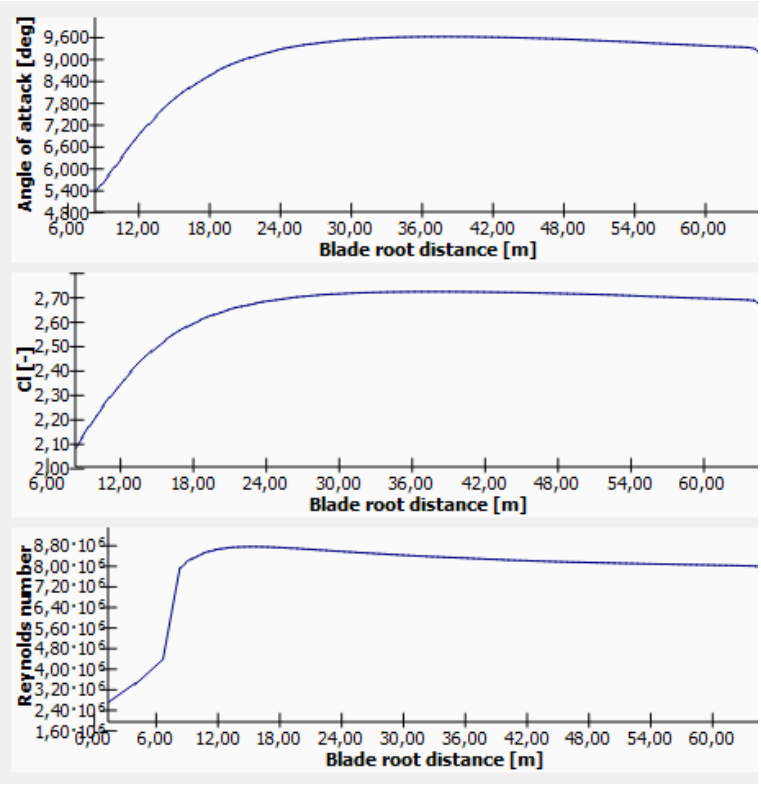

FIGURE 7.8: Wing element performance (ASHES)

result instead of modifying the MATLAB code to get the TSR value on the top of the slope.

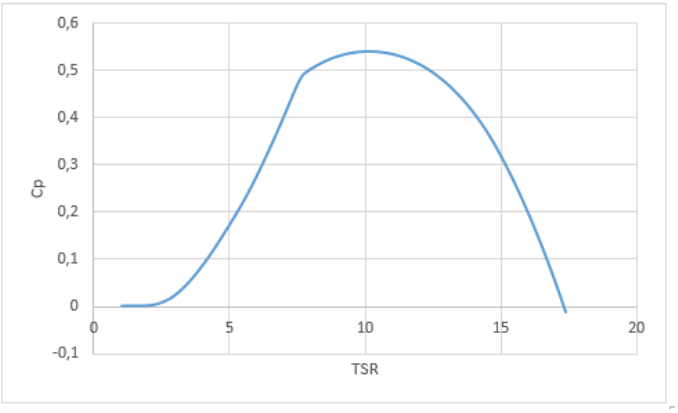

FIGURE 7.9: C_p vs TSR

7.2.2 Strength analysis

If the decision of blade design and material choice is insufficiently, the risk of blade deflection will be significant. A blade deflection will lower the total area swapped

by the blades and alternate the angle of attack. This will lower the power output (Ziter, 2009). In the worst case the blade will hit the tower as it rotates.

In version 2.0 of ASHES, a flexible blade analysis was used to check deflection. This simulation utilizes the finite element method together with a co-rotational beam element formulation to determine the structures' dynamic response (ASHES, 2014). The test results showed an acceptable level of deflection and insignificant levels of power reduction, and is therefore ignored in the analysis.

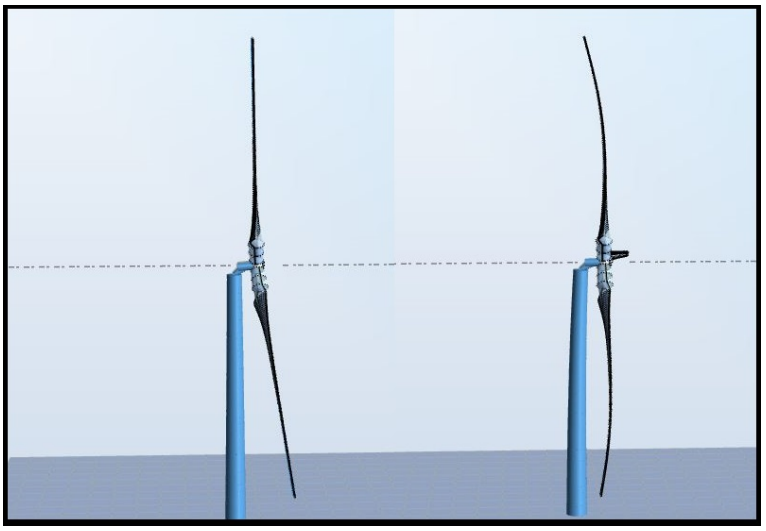

FIGURE 7.10: Flexible and stiff blade

7.3 Electric Wind Pumping

Since the turbine output is now obtained, we can calculate the maximum volume flow rate that can be pumped out of a underwater storage tank. As in Section 6.5 the Rayleigh probability distribution was used to determine the average power of the wind turbine over one day (see Eq.(6.27)). This calculation was done in EXCEL and gave an average power at a mean wind speed of 10 m/s of 3,22MW. The maximum average pumping rate can then be determined by Eq.(6.28), where it was assumed that the centrifugal pump has an efficiency η_p of 0,8. This gave a maximum pumping rate of 8,82 m^3/s or 762.491,62m^3/day. In Figure 6.11 the maximum flow rate for different mean wind speeds is shown with respect to the water depth. The red line represents the volume flow rate at a wind speed of 10 m/s, which is the operational wind speed of the investigated wind turbine. The

chosen offshore site has a water depth of 29 meters, which is indicated by the straight black line in the figure.

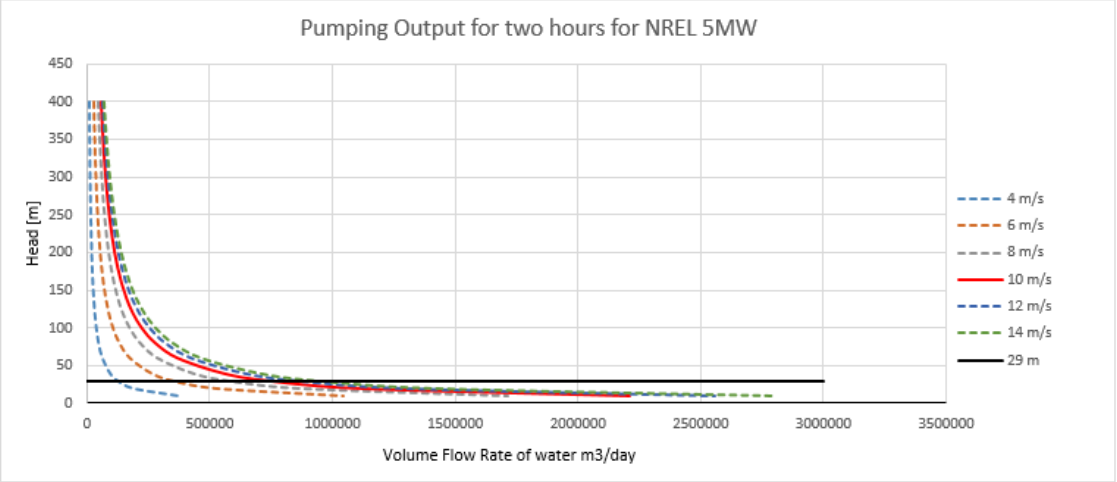

FIGURE 7.11: Pumping output of NREL 5MW

The maximum pumping output of the wind turbine can also be determined from this graph. For a mean wind speed of 10 m/s and a water depth of 29 meters the turbine can approximately pump 750.000 m^3/day which agrees with the already stated.

Chapter 8

Wave Power Model

In this chapter a numerical analysis of the point absorber by CorPower in frequency domain was performed to find the piston pump performance, driven by the WEC. The study of the hydrodynamics of a floating WEC is largely similar to dynamics of ships in wavy seas. The presence of a power take off mechanism (PTO), which in this case is the piston pump, and the requirement of maximizing the extracted energy introduces additional issues (Wanan Sheng, 2012). To maximize the motion of the WEC the WaveSpring technology introduced in Chapter 3.6.2 was included in the calculations. The numerical validation, which was performed in MATLAB, rests on (Wanan Sheng, 2012), (Falnes, 2002) and (Myrhaug, 2007).

8.1 WAMIT

To calculate and analyse the interaction between waves and the surface of floating and submerged offshore structures the program WAMIT can be used. WAMIT is a hydrodynamic 3D panel code, based on the potential theory. The program computes the frequency dependent added mass, damping coefficients and excitation force from the geometric description of the buoys. The PTO machinery was not taken into account in WAMIT. A MATLAB model was therefore developed to calculate the power output of the device. The MATLAB model is based on the theory presented in this chapter.

8.2 Simplifications and Predefined Parameters

The investigated dynamic system is assumed to be fully linear and moving only in heave direction, thus its motion responses and power capture responses will be linear with regard to wave heights (Faltinsen, 1999). In case of a nonlinear system, the motion responses and the hydrodynamic coefficients may be nonlinear. In this regard non linear viscous damping was also neglected to simplify the calculations. It is, however, as long as the power capture response is not strongly nonlinear, possible to provide a reliable assessment of a the power capture capacity of a device (Wanan Sheng, 2012). The frequency domain analysis was assumed to be valid for irregular waves, which is not correct. A time domain analysis would give more reliable results, but the frequency domain has shown to give reasonable results not only for regular waves if small wave amplitudes and motions are assumed (Falcao, 2010). Since no reference values for the PTO damping of the CorPower WEC were given, the damping was set to maximum for all sea state conditions.

8.2.1 Geometry of the CorPower Point Absorber

The geometry and size of the wet surface of the CorPower point absorber is shown in Figure 8.1.

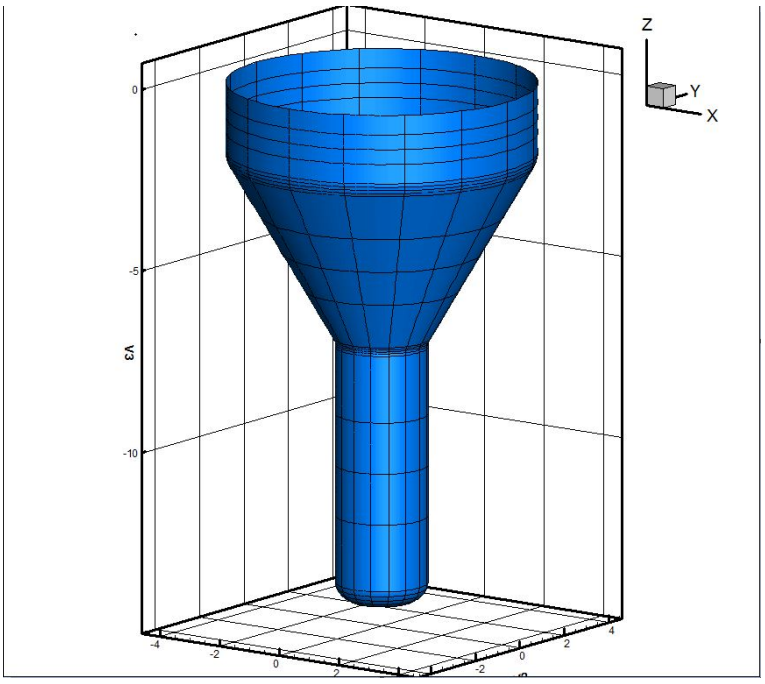

FIGURE 8.1: Geometry of CorPower wave energy converter

The buoy has a diameter of 8 $[m]$ in the waterline, which was set to 0 $[m]$, hence the draft of the device is 15 $[m]$. The buoy has a total weight of approximately 80 tons.

8.2.2 Summary of Simplifications and Predefined Parameters

- Analysis in frequency domain
- Assuming deep sea $H > (\lambda/2)$
- Dynamic system is fully linear
- Only the heave motion is investigated
- Wave spectrum = JONSWAP
- Reference WEC = CorPower 300$[kW]$
- WEC diameter = 8$[m]$
- WEC weight 80.000$[kg]$
- Density of water $\rho_{water} = 1025[kg/m^3]$

8.3 Hydrodynamic Coefficients

The results of the WAMIT analysis were plotted in MATLAB. Figure 8.2 shows the added mass and damping coefficient.

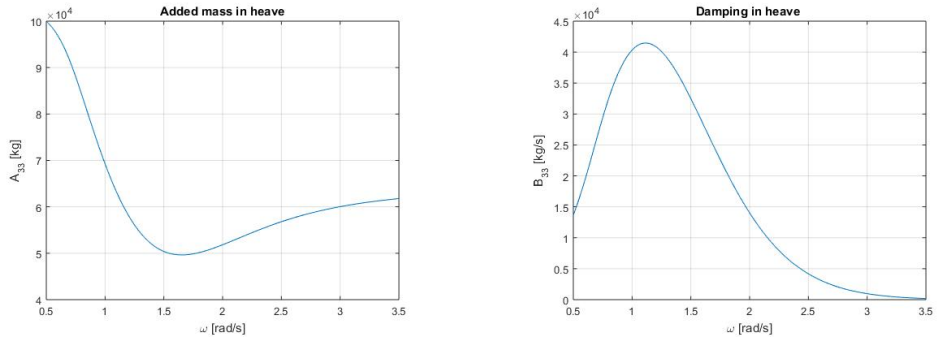

FIGURE 8.2: Added mass and damping coefficient

In Figure 8.3 the excitation force and the motion response (RAO) in heave are shown, which were also assessed from WAMIT. From the heave RAO, it can be

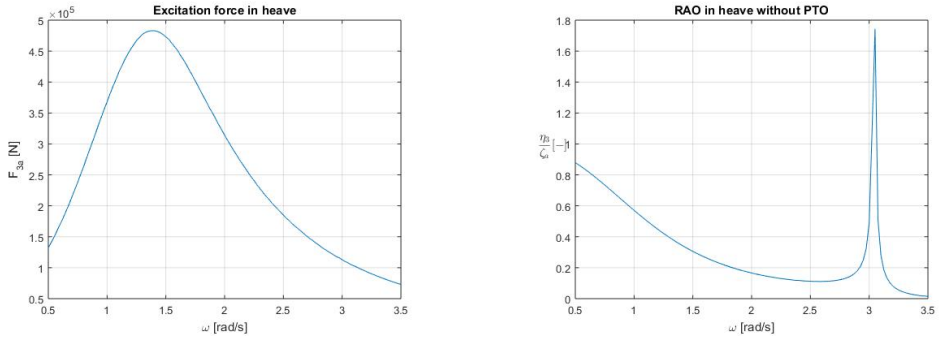

FIGURE 8.3: Excitation force and RAO for heave motion

seen that WAMIT has given a reasonable prediction for the heave motion of the floating buoy.

The stiffness coefficient was set to be constant in WAMIT and is defined as

$$S = C_{33} = \rho g A_w \tag{8.1}$$

where A_w is the waterplane area. However, when including the already mentioned WaveSpring technology the stiffness coefficient has to be modified. This will be discussed further in Section 8.6.

8.4 Mechanical Oscillator

In Figure 8.4 a mass M is immersed in water and suspended through a spring $S = C_{33}$ and the mechanical resistances R_f, $R_u = R_{PTO}$ and R_r, which are friction losses, convertible useful damping and radiated damping.

We now apply an external force

$$F_e(t) = \Re\{\hat{F}_e e^{i\omega t}\} \tag{8.2}$$

to the body, resulting in a forced oscillatory motion with velocity

$$u(t) = \Re\{\hat{u} e^{i\omega t}\} \tag{8.3}$$

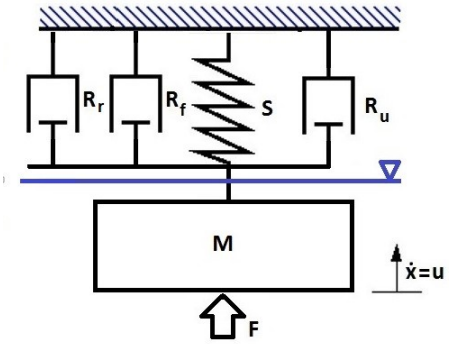

FIGURE 8.4: Mechanical Oscillator

where $\hat{F}_e$ and $\hat{u}$ are the complex amplitudes of the excitation force and the vertical velocity of the moving body, respectively. F_e is the wave excitation force, the wave force the body would experiences if it would be kept in position, hence when u=0. The excitation force is the sum of Froude-Krylov and the diffraction force (Faltinsen, 1999)

$$\hat{F}_e = F_{Froude-Krylov} + F_{Diffraction} \tag{8.4}$$

The complex amplitude $\hat{F}_e$ is defined as

$$|\hat{F}_e| = |f_e||\zeta_a| \tag{8.5}$$

where f_e is the excitation force coefficient obtained from WAMIT and ζ_a the wave amplitude, which is defined as $H/2$ in regular waves and as Eq.3.4 for irregular waves. The equation of motion can then be defined as

$$M\ddot{x} = \hat{F}_e - R_r\dot{x} - Sx + F_{PTO} \tag{8.6}$$

Where the PTO force is assumed to consist of a linear damper and a linear spring:

$$F_{PTO} = -R_u\dot{x} - Kx \tag{8.7}$$

In this analysis the PTO is, however, assumed to only contribute to damping. Hence, the force applied by the PTO can be expressed as

$$F_{PTO} = -R_u\dot{x} \tag{8.8}$$

The useful converted power, which can be extracted from a linear PTO is calculated as:

$$\bar{P}_u = \frac{1}{2} R_u \hat{u}^2. \tag{8.9}$$

The wave generated power away from the oscillating body can be determined by

$$\bar{P}_r = \frac{1}{2} R_r \hat{u}^2 \tag{8.10}$$

where over bar denotes the average value over time. The power lost by friction is calculated as

$$\bar{P}_f = \frac{1}{2} R_f \hat{u}^2 \tag{8.11}$$

the friction loss was, however, neglected in the following. Since the body is surrounded by water the added hydrodynamic mass, $M_r = A_{33}$ must be included in the dynamic system. In frequency-domain, the dynamic equation for the floating body has a form as (Falnes, 2002)

$$[i\omega(M + M_r) + R_u + R_r + \frac{S}{i\omega}]\hat{u} = \hat{F}_e \tag{8.12}$$

From the dynamic equation, an expression for the complex velocity amplitude can now be obtained:

$$\hat{u} = \frac{\hat{F}_e}{[-\omega^2(M + M_r) + i\omega(R_u + R_r) + S]} \tag{8.13}$$

8.5 Useful Converted Power

With the equation of motion in place, we can now calculate the useful converted power P_u. For simplification we neglect that M_r and R_r depend on frequency. Thus, if M_r and R_r are constants the convolution multiplication is just ordinary multiplication.

From Eq.(8.9) we can now determine the average captured power given in frequency-domain as

$$\bar{P_u} = \frac{1}{2}\Re(R_u\hat{u}^2) = \frac{1}{2}\frac{R_u|\hat{F_e}|^2}{(R_r + R_u)^2 + (\omega M + \omega M_r - \frac{S}{\omega})^2} \tag{8.14}$$

note that $\bar{P}_u \to 0$ when $\omega \to 0$ and when $\omega \to \infty$. Thus there is a maximum of absorbed power when $\frac{\delta P_u}{\delta R_u} = 0$ (Falnes, 2002), which occurs if

$$R_u = \{R_r^2 + (\omega M + \omega M_r - \frac{S}{\omega})^2\}^{\frac{1}{2}} = R_{u(opt)} \tag{8.15}$$

The maximum energy absorption P_{max} for different incident wave frequencies can be reached when the oscillating body is at resonance (Falnes, 2002). The body is at resonance when

$$\omega M + \omega M_r - \frac{S}{\omega} = 0 \tag{8.16}$$

which means that the maximum absorbed power can be expressed as

$$P_{max} = \frac{R_u|\hat{F_e}|^2}{2(R_u + R_r)^2} \tag{8.17}$$

Combining Eq.(8.16) and Eq.(8.15) the optimum choice of the PTO damping becomes

$$(R_u)_{opt} = R_r \tag{8.18}$$

Since we neglected the losses due to friction (including viscous losses in the water), including friction the optimum choice would be

$$(R_u)_{opt} = R_r + R_f \tag{8.19}$$

8.6 Including the WaveSpring

To include the WaveSpring technology the stiffness coefficient S has to be modified. As mentioned in Section 3.6.2 the WaveSpring forces the WEC to be in resonance triggered by the pneumatic cylinders by reducing the stiffness coefficient S. To include the WaveSpring in the calculations, we have to introduce the

natural angular frequency, which can be derived from Eq. (8.16) as

$$\omega_0 = \sqrt{S/(M + Mr)} \tag{8.20}$$

In Figure 8.5 an example of a JONSWAP wave spectrum for a significant wave height of H_s=4 and a wave period T_p=6 is shown. It can be seen that the spectrum

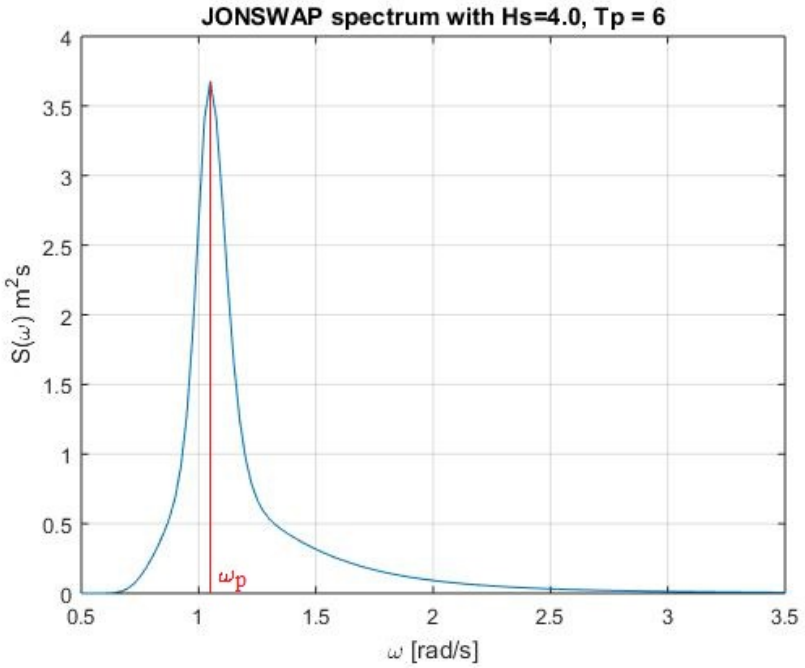

FIGURE 8.5: JONSWAP wave spectrum

has its peak at $\omega_p \approx$1.1 [rad/s]. If we set $\omega_0 = \omega_p$ the wave energy converter will be in resonance when the wave spectrum has its peak. This can be achieved by choosing the stiffness coefficient S as

$$\omega_0 = \omega_p = \sqrt{S/(M + M_r)} \Rightarrow S = \omega_p^2 \cdot (M + M_r) \tag{8.21}$$

There is, however, an additional benefit provoked by the new WaveSpring technology. By also introducing the damping coefficient of the oscillator δ (Falnes, 2002),

$$\delta = \frac{1}{2} \frac{(R_u + R_r)}{(M + M_r)} \tag{8.22}$$

we can rewrite Eq.(8.14) as

$$\bar{P}_u(\omega) = \frac{1}{2}\frac{R_u|\hat{F}_e(\omega)|^2}{(R_r+R_u)^2}\frac{1}{1+(\omega_0/2\delta)^2(\omega/\omega_0-\omega_0/\omega)^2} \tag{8.23}$$

If we now rearrange Eq.(8.23) we get

$$\frac{(R_r+R_u)^2}{R_u|\hat{F}_e(\omega)|^2}\bar{P}_u(\omega) = \frac{1}{1+(\omega_0/2\delta)^2(\omega/\omega_0-\omega_0/\omega)^2} \tag{8.24}$$

,which is called the frequency response of the absorbed power (Falnes, 2002). By replacing ω with ω_0 we see that Eq.(8.24) has its maximum value 1 at resonance:

$$\frac{(R_r+R_u)^2}{R_u|\hat{F}_e(\omega_0)|^2}\bar{P}_u(\omega_0) = \frac{1}{1+(\omega_0/2\delta)^2(\omega_0/\omega_0-\omega_0/\omega_0)^2} = 1 \tag{8.25}$$

In Figure 8.6, Eq.(8.24) was plotted against ω/ω_0 for two different values of the dimensionless damping factor δ/ω_0. One with δ/ω_0=0.05 and one with δ/ω_0=1. The damping factor of the device is defined as

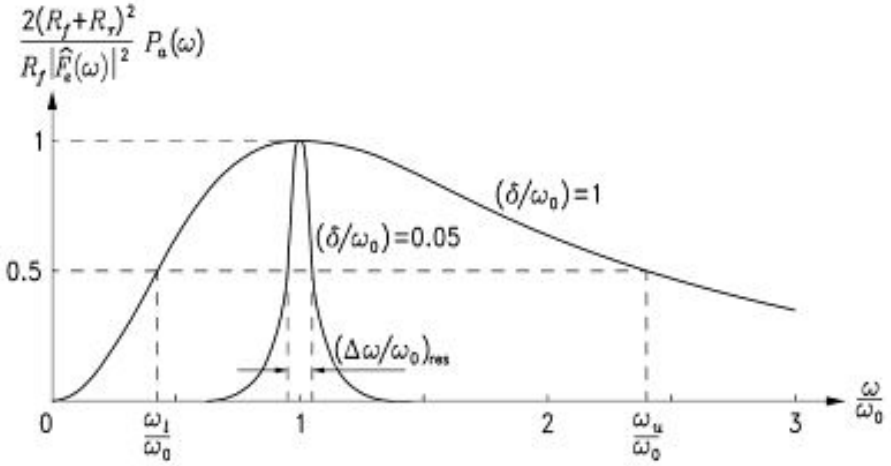

FIGURE 8.6: Frequency response of absorbed power for two different values of a damping factor δ/ω_0 (Falnes, 2002)

$$\frac{\delta}{\omega_0} = \frac{R_u+R_r}{2\omega_0(M+M_r)} = \frac{R_u+R_r}{2\sqrt{S(M+M_r)}} \tag{8.26}$$

We now introduce the resonance bandwidth, which is the frequency interval $(\Delta\omega)_{res}$, where the kinetic energy exceeds half of the maximum (Falnes, 2002). The resonance bandwidth is expressed as

$$\Delta\omega = \omega_u - \omega_l = \frac{R_m + R_r}{M_m + M_r} = 2\delta \tag{8.27}$$

where ω_u and ω_l are the upper edges of the interval. From Figure 8.6 one can observe, that the curve for δ/ω_0=1 has a much bigger resonance bandwidth $(\Delta\omega)_{res}$ then the curve for δ/ω_0=0.05. If we now replace δ with Eq.(8.26) we get

$$\Delta\omega = \frac{R_u + R_r}{\sqrt{S(M + M_r)}} \tag{8.28}$$

From this the second benefit of the WaveSpring becomes clear. Since the WaveSpring is reducing the stiffness S, $(\Delta\omega)_{res}$ is getting bigger. This means that the WEC is able to be at resonance at a larger frequency bandwidth. Hence, the WEC is capturing power over a larger range of frequencies.

8.6.1 Wave Power Captured in Regular Waves

If we define the complex excitation force amplitude $\hat{F}_e$ in Eq.(8.14) as per unit wave amplitude, then $\bar{P}_u$ becomes the power capture response H_p (Wanan Sheng, 2012).

$$\frac{|\hat{F}_e(\omega)|}{|\zeta_a\omega|} = |f_e(\omega)| \tag{8.29}$$

where $\zeta_a = A = H/2$ is the wave amplitude in regular waves. We then get for the power capture response

$$H_p = \frac{1}{2}\frac{R_u|f_e|^2}{(R_r + R_u)^2 + (\omega M + \omega M_r - \frac{S}{\omega})^2} \tag{8.30}$$

The captured power in regular waves over a period of time can then be defined as

$$P_{re}(w,t) = A|H_p(\omega)|cos(\omega t) \tag{8.31}$$

for the oscillating device. The problem is divided into time steps, and each frequency component of the irregular sea is treated individually to calculate the captured power response. The response of each frequency component is summed

up to a total power response. Thus, we can find the quasi-steady power, before moving on to the next time step. The thrust is finally averaged over the time series to find the mean power captured by the WEC. A time series of two hours with 0.5 second time steps was used in the MATLAB script. The wave energy capture width W_{re} for the device in regular waves can then be defined as

$$W_{re} = \frac{\bar{P}_{re}}{\frac{\rho g^2}{32\pi} H^2 T} \tag{8.32}$$

where P_{re} is the average power absorbed in regular waves. The capture width, or absorption length, is the width perpendicular to the wave direction, in which the WEC takes up power from the waves. The maximum capture width for a heaving body, with no constraints on the amplitude was first derived by Budal and Falnes, Evans and Newman (Falnes, 2002). A point absorber is of very small extension compared to the wavelength. The maximum energy, which may be absorbed by a heaving axi-symmetric body equals the wave energy transported by the incident wave front of width equal to the wavelength divided by 2π (Falnes, 2002). This can be expressed as

$$W_{max} = \frac{\lambda}{2\pi} \tag{8.33}$$

where the wave length λ is defined as

$$\lambda = \frac{T^2 g}{2\pi} \tag{8.34}$$

for deep waters. This maximum capture width is, however, assuming that the WEC is moving in all 6 degrees of freedom. In our case we assume that the WEC is only moving in heave. Which means that all of the wave energy only contributes to heave motion of the buoy Falnes (2002). The maximum capture width can then be expressed as

$$W_{max} = (3/2\pi)\lambda \tag{8.35}$$

Early experimenters, not being aware of this relationship, were surprised by measuring absorption widths larger than the physical width of a tested point-absorber model(Falnes, 2002). The WEC can capture more power because on average the radiation to the far field is reduced by destructive interference. The radiation damping of the WEC will be correspondingly reduced (Falnes, 2002). In other

words, to capture more power the device must move more than the incident wave. The efficiency of the device capturing wave energy can be expressed by

$$\eta_{re} = \frac{W_{re}}{B} \tag{8.36}$$

where B is simply the width of the device. Because of the wave energy capture width being able to reach values larger than the width of the device, the efficiency can be over a 100%. The expression efficiency could therefore be misleading, if the physical background is not understood.

8.6.2 Wave Power Captured in Irregular Waves

In agreement with Section 8.6.1, the captured power of the WEC in irregular waves over a period of time is obtained by

$$P_{irr}(w,t) = \sum \zeta_a |H_p(\omega)| cos(\omega t + \epsilon) \tag{8.37}$$

where ζ_a is defined by Eq.(3.4), the power capture response H_p is equal to Eq.(8.30) and ϵ is a random phase angle uniformly distributed between 0 and 2π. A reasonable approximation for a sea state to last is 2 hours, which was used to find the mean captured power of the WEC. To find the total energy [kWh/year] the WEC is producing over a period of one year, the captured power P_{irr} for every sea state was multiplied by the respective occurrence of the sea state (in %). This will give an approximate overview of how much produced energy one can expect from one WEC, if it is operated the whole year. One should, however, not expect the WEC to produce useful energy more than 1/3 of the year (Falnes, 2015). The wave energy width, W, for the device can be defined by dividing Eq.(8.37) by Eq.(3.22), such that

$$W_{irr} = \frac{\bar{P}_{irr}}{\frac{\rho g^2}{64\pi} H_s^2 T_e} \tag{8.38}$$

where $\bar{P}_{irr}$ is the average captured power over a period of time for one specific sea state condition. Knowing the capture width, the efficiency of the device capturing the wave energy is given by

$$\eta_{irr} = \frac{W_{irr}}{B} \tag{8.39}$$

Chapter 9

Results of the Wave Power Model

This chapter presents the results obtained from calculations made in MATLAB. The hydrodynamic coefficients for the WEC were, as mentioned, obtained by an analysis in WAMIT.

9.1 Sea State Analysis

To calculate the power output of the WEC both regular and irregular waves were investigated. The scatter diagram for the chosen North Sea offshore site can be found in Appendix B.3. The calculated tables were simplified, in the manner of merging several peak periods and significant wave heights by assigning them to just one number of occurrence. In this regard, only the upper bound values of T_p and H_s have been utilized. The wave probability distribution for the offshore site is shown in Table 9.1 with T_p from 1s to 9s and H_s from 0m to 3.5m. In addition, the probability distribution is graphically shown in Figure 9.1.The color bar on the right hand of the table shows the percentage. The darker the color in the table, the more common is the sea state.

From Table 9.1 and Figure 9.1 it can be seen that waves with a period of T_p between 4-8s and a wave height H_s between 1-3m have been occurring the most over the 10 years of measuring.

TABLE 9.1: Wave probability distribution in [%] measured over 10 years

Hs[m] \ Tp[s]	1.0-2.0	2.0-3.0	3.0-4.0	4.0-5.0	5.0-6.0	6.0-7.0	7.0-8.0	8.0-9.0	>6%
0.0-0.5	0.00342	0.10953	1.13636	1.53112	0.37080	0.17913	0.24302	0.28865	5-6%
0.5-1.0	0.00000	0.13463	1.98521	8.74521	6.66073	3.11587	0.94012	0.93100	4-5%
1.0-1.5	0.00000	0.00000	0.08671	3.91452	7.85414	5.29961	2.90708	1.29723	3-4%
1.5-2.0	0.00000	0.00000	0.00000	0.32174	4.68008	5.29961	2.35145	1.41931	2-3%
2.0-2.5	0.00000	0.00000	0.00000	0.00342	0.95153	5.00525	2.15407	0.99147	1-2%
2.5-3.0	0.00000	0.00000	0.00000	0.00000	0.04564	2.41534	2.27615	0.90247	0.5-1%
3.0-3.5	0.00000	0.00000	0.00000	0.00000	0.00228	0.45865	2.38340	0.63550	<0.5%

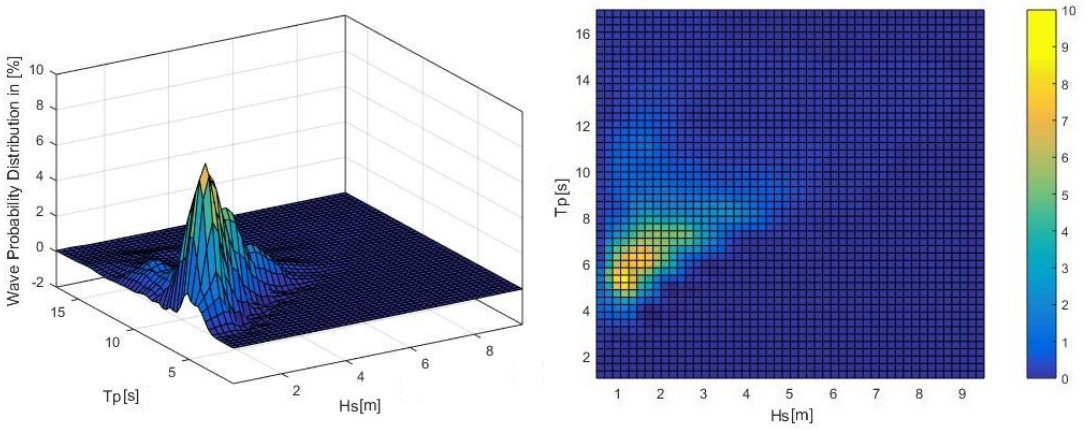

FIGURE 9.1: Wave probability distribution in [%] measured over 10 years

9.1.1 MATLAB Results for Regular Waves

The results in this section were obtained by running the MATLAB scribed RegularWaves.m. The calculations are based on the theory discussed in Chapter 8. The WaveSpring was, however, not included in the calculations made in RegularWaves.m. The damping coefficient of the power takeoff system was set to R_{opt}

In table 9.2 the wave power in unidirectional regular waves is shown for the most common wave periods and wave heights of the offshore site. Since the wave power calculated by Eq. (3.21) is per meter wavefront [kW/m], the values in Table 9.2 were multiplied by the width of the CorPower buoy,B_{WEC}, to obtain the power of the incident wave hitting the WEC. The average power captured by the device in regular waves is presented in Table 9.3. It can be seen that the wave power is increasing with increasing H_s and T_p.

In Figure 9.2 the power captured of the device is shown over a period of 30 seconds. The wave height was exemplary set to H=2m and the wave period was set to T=6s. From this figure it can be seen that the power curve has a period of 6 seconds,

TABLE 9.2: Wave power in regular waves [kW/B_{WEC}] per WEC width (B_{WEC}=8m)

T/H	1	1.5	2	2.5	3	3.5
5	39.248	88.309	156.99	245.30	353.24	480.79
6	47.098	105.97	188.39	294.36	423.88	576.95
7	54.948	123.63	219.79	343.42	494.53	673.11
8	62.797	141.29	251.19	392.48	565.18	769.27
9	70.647	158.96	282.59	441.54	635.82	865.43

TABLE 9.3: Average captured power from the WEC [kW]

T/H	1	1.5	2	2.5	3	3.5
5	206.04	695.39	1648.3	3219.4	5563.1	8834.0
6	97.737	329.86	781.89	1527.1	2638.9	4190.5
7	58.276	196.68	466.21	910.56	1573.5	2498.6
8	39.736	134.11	317.89	392.48	1072.9	1703.7
9	28.625	96.609	229.00	447.26	772.8	1227.3

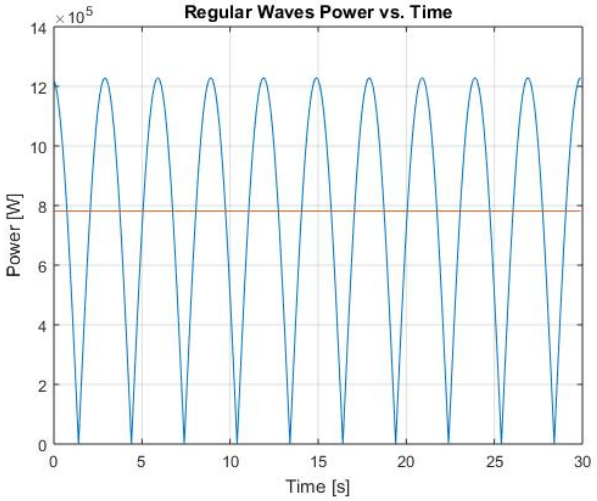

FIGURE 9.2: Power over a period of 80s in regular waves for H=2m and T=6s

which agrees with the wave period of the regular wave. The mean captured power for this specific sea state condition was marked with a red line.

In Table 9.4 the capture width for the device is shown. The capture width is

TABLE 9.4: Wave capture width [m]

T/H	1	1.5	2	2.5	3	3.5
5	5.2496	7.8745	10.4993	13.1241	15.7489	18.3738
6	2.0752	3.1128	4.1504	5.1879	6.2255	7.2631
7	1.0606	1.5909	2.1211	2.6514	3.1817	3.7120
8	0.6328	0.9491	1.2655	1.5819	1.8983	2.2147
9	0.4052	0.6078	0.8104	1.0130	1.2155	1.4181

decreasing for increasing T and H. At T=5 and H=3.5 the capture width is more than twice the width of the WEC. As mentioned in Section 8.6.1 the maximum capture width is expressed by Eq. (8.33). For T=5s the wavelength becomes $\lambda \approx$40m, which means that the maximal capture width is achieved by using Eq.8.35 W_{max}=19m. The high capture width values at T=5 are therefore justifiable. This results also in the efficiency reaching values over 100% for high wave heights at T=5, as can be seen in Table 9.5.

TABLE 9.5: Wave power capture efficiency %

T/H	1	1.5	2	2.5	3	3.5
5	65.62	98.43	131.24	164.05	196.86	229.67
6	25.94	38.91	51.88	64.85	77.82	90.79
7	13.26	19.89	26.51	33.14	39.77	46.40
8	7.91	11.86	15.82	19.77	23.73	27.68
9	5.06	7.60	10.13	12.66	15.19	17.73

From Table 9.5 it is clear that the capacity of the device capturing power decreases with increasing wave period. This is simply because of the WEC moving slower compared to shorter wave periods. This can be easily seen from the general equation for kinetic energy

$$E_k = \frac{1}{2}mv^2 \tag{9.1}$$

where v is the velocity of a mass m. The kinetic energy E_k decreases with the quadratic velocity v^2. Hence, the captured power must decrease.

9.1.2 Wave Power in Irregular Waves

The irregular sea states were assumed to be reproduced by a JONSWAP spectrum as discussed in Section 3.2.1. The MatLab script JONSWAP.m calculates the JONSWAP spectrum for each H_s and T_p, from which the wave energy period T_e for each sea state was obtained. The results are given in Table 9.6.

From Table 9.6 it should be noted that the energy period T_e calculated by Eq. (3.16) is higher then the wave period T_p. In Figure 9.3 the JONSWAP spectrum generated by JONSWAP.m for $H_s = 3$ and $T_p = 8$ is exemplary shown.

The next step was to calculate the potential wave power in the irregular waves by equation 3.22, which was also done in the MATLAB script JONSWAP.m.

TABLE 9.6: Energy period T_e [s] values calculated by JONSWAP spectrum

T_P/H_s	1	1.5	2	2.5	3	3.5
5	5.1330	5.3554	5.4155	5.4155	5.4155	5.4155
6	6.1586	6.1941	6.3913	6.4746	6.4984	6.4984
7	7.1848	7.1848	7.2055	7.4013	7.5064	7.5620
8	8.2111	8.2111	8.2211	8.2111	8.3831	8.5110
9	9.2375	9.2375	9.2375	9.2375	9.2375	9.3365

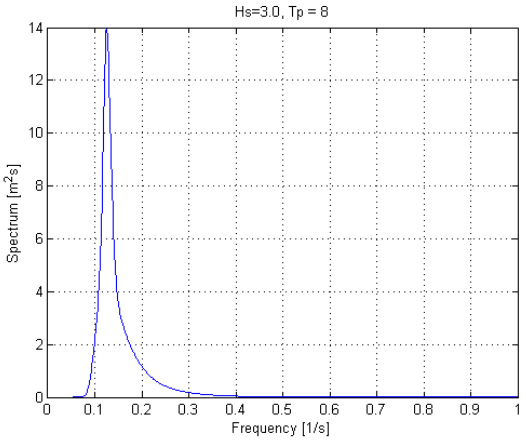

FIGURE 9.3: JONSWAP spectrum for $H_S = 3$ and $T_p = 8$

The results are shown in Table 9.7. Equivalent to Table 9.2 the wave power was multiplied with the width, B_{WEC}, of the buoy. In addition, the Table 9.7 shows the percentage of time every sea state is likely to occur.

TABLE 9.7: Wave power in irregular waves [kW/B_{WEC}] per WEC width B_{WEC}=8m)

Hs[m] \ Tp[s]	1.0-2.0	2.0-3.0	3.0-4.0	4.0-5.0	5.0-6.0	6.0-7.0	7.0-8.0	8.0-9.0	>6%
0.0-0.5	1.96	2.86	3.66	4.57	5.49	6.40	7.32	8.23	5-6%
0.5-1.0	0.00	11.61	15.32	18.31	21.97	25.63	29.29	32.960.00	4-5%
1.0-1.5	0.00	0.00	34.78	42.99	49.72	57.680	65.92	74.15	3-4%
1.5-2.0	0.00	0.00	0.00	77.29	91.21	102.84	117.19	131.84	2-3%
2.0-2.5	0.00	0.00	0.00	120.77	144.39	165.05	183.11	206.00	1-2%
2.5-3.0	0.00	0.00	0.00	0.00	208.68	241.05	269.20	296.64	0.5-1%
3.0-3.5	0.00	0.00	0.00	0.00	284.04	330.52	372.00	408.08	<0.5%
3.5-4.0	0.00	0.00	0.00	0.00	0.00	432.81	490.34	541.47	
4.0-4.5	0.00	0.00	0.00	0.00	0.00	547.78	624.06	692.67	

It can be seen that the wave power is increasing with increasing wave height H_s and increasing wave period T_p in accordance to Table 9.2. It can also be seen that the wave power from regular waves is much higher than from irregular waves - approximately halve the size. It is, however, understandable since for a same wave height, the wave energy in regular waves is double the wave energy in irregular

waves (compare Eq.(3.21) and Eq.(3.22)). In addition, the wave energy period T_e used to calculate the wave power is higher than the wave period T used in regular sea states.In Figure 9.4 the wave power was plotted for H_s=0.5-4.5m and T_p=1-12s.

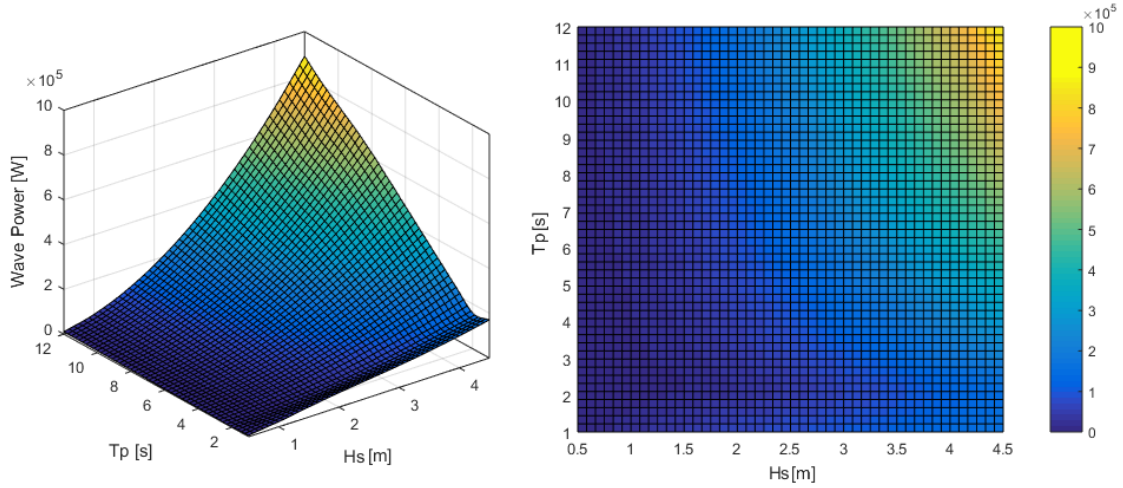

FIGURE 9.4: Wave power distribution in irregular waves

From Figure 9.4 it becomes even clearer for increasing wave height H_s and wave period T_p.

9.1.3 Power Captured by the WEC in Irregular Waves

The MatLab script WavePower.m reads in the hydrodynamic coefficients obtained from WAMIT and uses the wave spectra calculated in JONSWAP.m to find the mean power output for each sea state over a period of 2 hours. Unlike the calculations made for regular waves the WaveSpring technology was included as discussed in Section 8.6. The damping coefficient was than defined as in Eq.(8.15). The mean power captured in irregular waves P_{irr} for the different wave heights H_s and wave periods T_p is shown in Table 9.8 and Figure 9.5.

CorPower promises an average power output of 200-300kW, which is in accordance to the calculated values in Table 9.8. It can be seen that the WEC captures most of the power at H_s=3.5[m] and T_p=6[s] and very little at wave heights of 0.5m. It can also be seen that the captured wave power limit of 300kW, as defined in Section 3.4, is not exceeded. In Figure 9.6 the power captured by the WEC over a time period of two minutes and two hours is shown for a sea state condition with

TABLE 9.8: Power captured of the WEC in irregular waves [W]

Hs[m] \ Tp[s]	0.0-1.0	1.0-2.0	2.0-3.0	3.0-4.0	4.0-5.0	5.0-6.0	6.0-7.0	7.0-8.0	8.0-9.0	>6%
0.0-0.5	0	40100	38709	49914	50290	42727	36848	29985	24574	5-6%
0.5-1.0	0	0	91887	117900	96882	83871	66020	58915	50038	4-5%
1.0-1.5	0	0	0	190250	170530	128040	110980	88083	75017	3-4%
1.5-2.0	0	0	0	0	238950	181920	139030	117430	100400	2-3%
2.0-2.5	0	0	0	0	269870	235530	180260	149550	122820	1-2%
2.5-3.0	0	0	0	0	0	273560	216090	172650	149000	0.5-1%
3.0-3.5	0	0	0	0	0	322800	259670	205950	178660	<0.5%
3.5-4.0	0	0	0	0	0	0	284730	235540	198010	

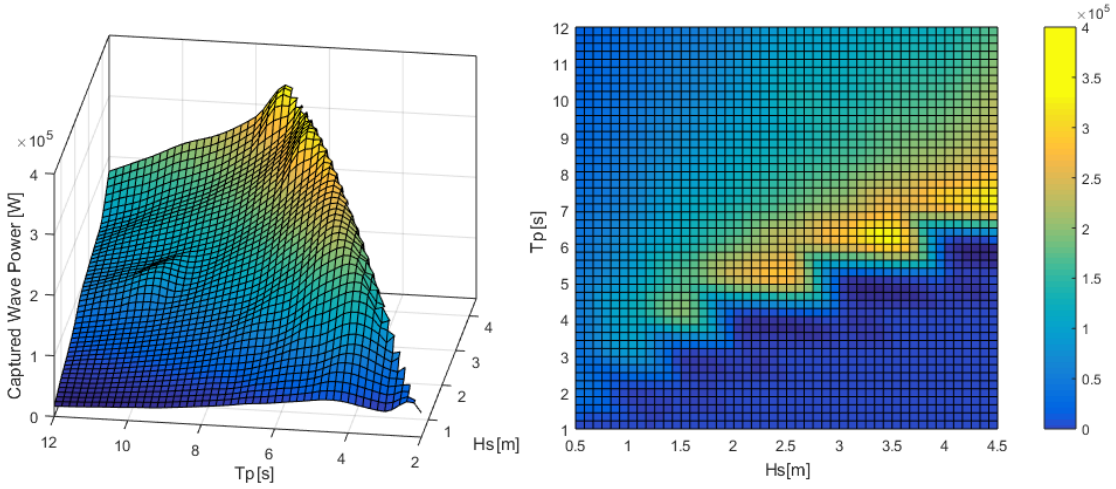

FIGURE 9.5: Power captured of the WEC in irregular waves [W]

H_s=2m and T_p=6s, respectively. The red line indicates the mean captured power of the device over the given time period.

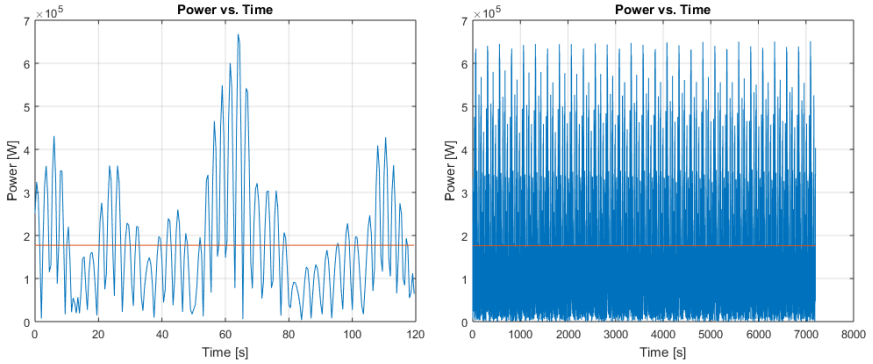

FIGURE 9.6: Captured wave power over 2min and 2hours

In Figure 9.7 the mean captured power of the WEC over a time period of one year for all sea state conditions is shown. It was here assumed that each sea state condition is stable over a time period of 2 hours. The table, which Figure 9.7

is based on, can be found in Appendix B.6. From Figure 9.7 and Table B.7 it

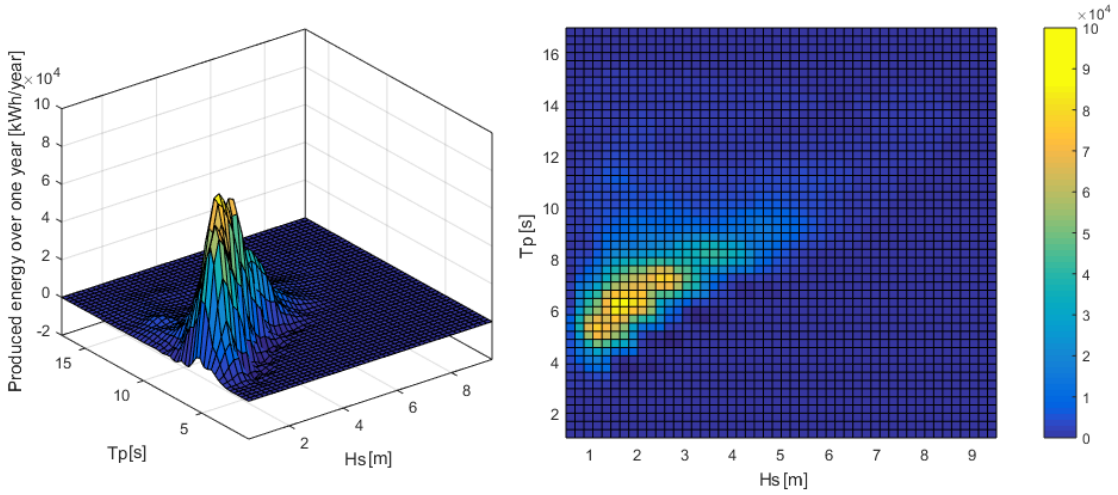

FIGURE 9.7

can be seen that the WEC is annually producing approximately 1120[MWh/year] if it would be in operation the whole time. As mentioned in Section 8.6.2, a reasonable operating time is one third of a year, which means that the WEC would approximately produce 375[MWh/year]. This rather low power output value could be explained by the low wave power density of the chosen offshore site.

9.1.4 Wave Capture Width and Efficiency

The wave capture width for H_s=0.5-4.5m and T_p2-9s is given in Table 9.9 and Figure 9.8.

TABLE 9.9: Wave capture width [m]

Hs[m] \ Tp[s]	1.0-2.0	2.0-3.0	3.0-4.0	4.0-5.0	5.0-6.0	6.0-7.0	7.0-8.0	8.0-9.0	>6%
0.0-0.5	7.4184	7.22928	6.80088	6.25128	5.8672	5.5616	3.9872	3.0336	5-6%
0.5-1.0	0	6.96	6.624	5.308	4.06	2.6288	2.04	1.5928	4-5%
1.0-1.5	0	0	5.2304	3.8008	2.58	1.8048	1.3008	1.0224	3-4%
1.5-2.0	0	0	0	3.108	2.0376	1.3376	1.0416	0.768	2-3%
2.0-2.5	0	0	0	2.4192	1.5856	1.1008	0.7864	0.6304	1-2%
2.5-3.0	0	0	0	0	1.3584	0.8096	0.6632	0.5232	0.5-1%
3.0-3.5	0	0	0	0	1.1056	0.7576	0.5512	0.4224	<0.5%
3.5-4.0	0	0	0	0	0	0.6496	0.4696	0.3728	
4.0-4.5	0	0	0	0	0	0	0.4112	0.3232	

It can be seen that the wave capture width is highest for waves with small heights and low periods, which is understandable since the WEC will absorb most of the

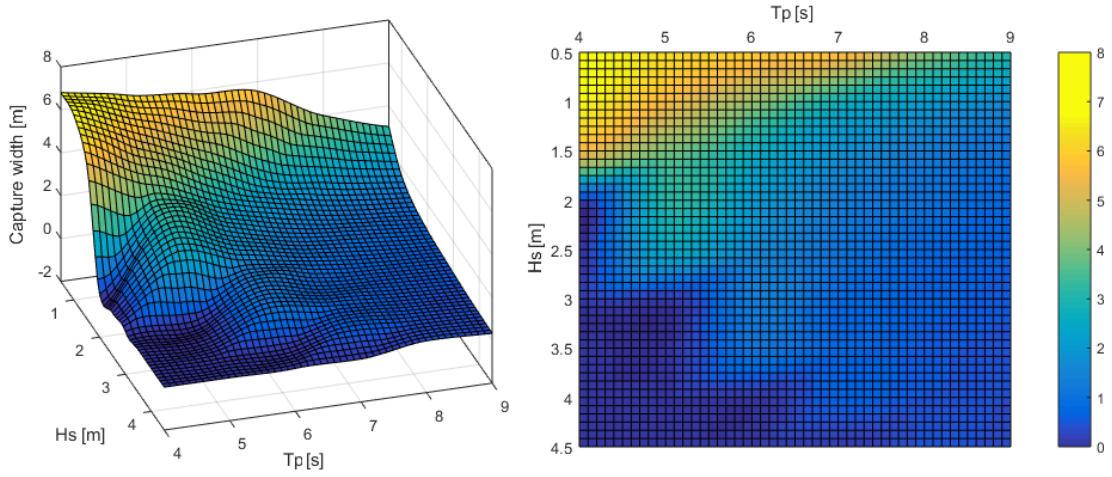

FIGURE 9.8: Wave capture width [m]

energy in the wave. The incident wave will have almost no energy after hitting the WEC, hence the wave will nearly vanish. The WEC is, however, not producing a noteworthy amount of power since the exploitable energy is low. For larger waves the preserved momentum increases and the WECs ability of capturing the wave energy decreases. The radiated wave from the WEC is not sufficient enough to cancel out the whole incident wave.

The efficiency of the WEC for the different H_s and T_p values is shown in Table 9.10 and Figure 9.9

TABLE 9.10: Efficiency η of the device capturing wave energy in %

Hs[m] \ Tp[s]	1.0-2.0	2.0-3.0	3.0-4.0	4.0-5.0	5.0-6.0	6.0-7.0	7.0-8.0	8.0-9.0
0.0-0.5	92.73	90.36	85.01	78.141	73.34	69.52	49.84	37.92
0.5-1.0	0	87	82.8	66.35	50.75	32.86	25.5	19.91
1.0-1.5	0	0	65.38	47.51	32.25	22.56	16.26	12.78
1.5-2.0	0	0	0	38.85	25.47	16.72	13.02	9.6
2.0-2.5	0	0	0	30.24	19.82	13.76	9.83	7.88
2.5-3.0	0	0	0	0	16.98	10.12	8.29	6.54
3.0-3.5	0	0	0	0	13.82	9.47	6.89	5.28
3.5-4.0	0	0	0	0	0	8.12	5.87	4.66
4.0-4.5	0	0	0	0	0	0	5.14	4.04

>6%
5-6%
4-5%
3-4%
2-3%
1-2%
0.5-1%
<0.5%

The efficiency follows the same distribution as the wave capture width, since they are related to each other by Eq.(8.39). For a sea state condition with a wave height of 0.5m and a period of 2 sconds the efficiency reaches 92.73%, but decreases rapidly with increasing wave height and period.

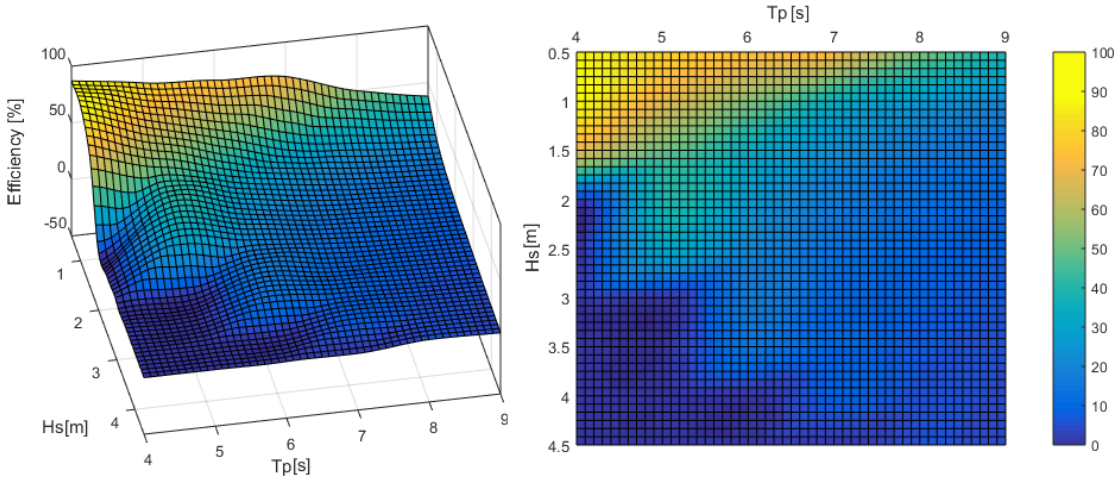

FIGURE 9.9: Efficiency η of the device capturing wave energy in %

9.1.5 Effect of the Wavespring

In Figure 9.10 the effect of the WEC capturing wave power for a sea state condition with H_s=2m and varying T_p is shown with and without the WaveSpring.

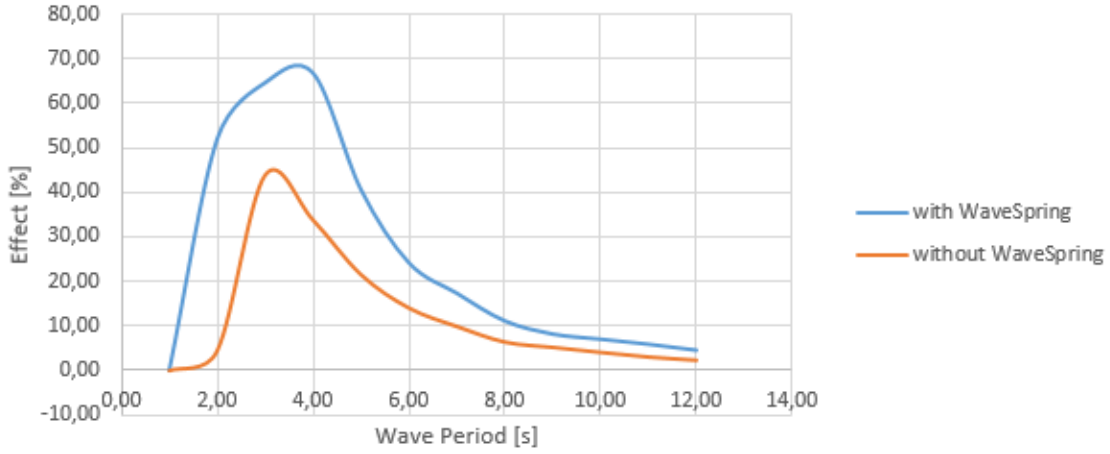

FIGURE 9.10: Effect of WaveSpring

It is apparent that the WaveSpring has a large effect on the efficiency of the device. The efficiency increased from 45% to almost 70%. It can also be seen that the efficiency without the WavesSpring is increasing slower. This might be due to the WaveSpring increasing the damping factor and therefore the resonance bandwidth of the device, as discussed in Section 8.6.

9.2 Wave Driven Pump

To calculate the average pumping rate of the wave driven piston pump, only the results from the analysis in irregular waves were used. If all of the power produced by the WEC is used to pump water the volume flow rate can ,according to Eq.(6.28), be expressed as

$$\dot{V}_{avg} = \frac{\bar{P}_{irr}\eta_p}{\rho g H} \tag{9.2}$$

where $\dot{V}$ is the volume flow rate,$\bar{P}_{irr}$ the mean power produced by the WEC for all sea state conditions in irregular waves, H the head where the fluid exits the pump, ρ the water density and η_p the pump efficiency of the piston pump. The mean power produced by the WEC can be calculated as

$$\bar{P}_{irr} = \sum P_{irr}(i) \cdot p(i) \tag{9.3}$$

where i denotes the the sea state condition for each H_s and T_p, $P(i)$ the produced power for each sea state condition and $p(i)$ the probability for each sea state to occur. The calculations done for $\bar{P}_{irr}$ were established in EXCEL and resulted in $\bar{P}_{irr}$=127617[W]. Inserted in Eq.(9.2) we obtain a mean volume flow rate $\dot{V}$ of 0,35$[m^3/s]$, where H was set to 29[m] and η_p to 0,8. Hence, the WEC is able to pump 30249,72 $[m^3/day]$ on average. In Figure 9.11 the volume flow rate is shown for varying water depth. It can be seen that the volume flow rate decreases rapidly due to the increasing static pressure when entering deeper offshore sites.

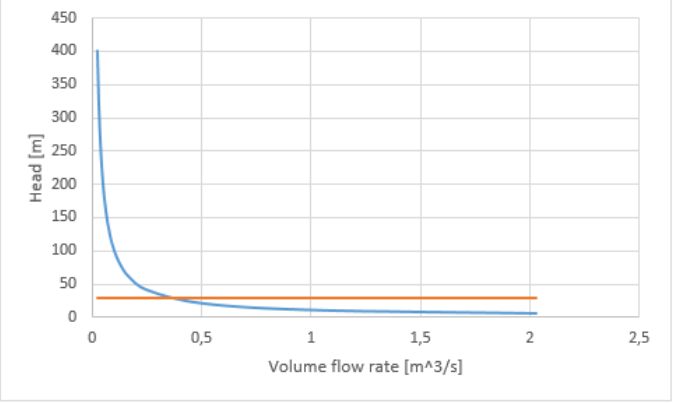

FIGURE 9.11: Volume flow rate $[m^3/s]$ vs. head [m]

Chapter 10

Modelling in SIMA

A model representation of the WEC was set up in SIMA, however, due to time constrains further analyses were not performed. The intention of the SIMA model was to describe the behavior of the WEC in a more realistic manner. This chapter gives a brief presentation of the software and the created model.

10.1 SIMA

SIMA is a simulation and analysis tool for marine operations and floating systems (MARINTEK, 2014a). The software is built on nonlinear time domain analysis which makes it able to deal with advanced structures and operations. SIMA is developed in co-operation between MARINTEK and Statoil. The motivation for creating this program was the need for a simulator to investigate marine operations. This could provide important information on quality assurance, feasibility evaluation, improve HSE performance, give familiarization to participants in the marine operation and what-if-analysis (Statoil, 2011). SIMA is the graphical interface for the two computer programs RIFLEX and SIMO. SIMO is used to analyze motions and station keeping of multibody systems. Riflex is a program for static and dynamic analysis of flexible risers and other slender structures (MARINTEK, 2014b).

10.2 Modelling in SIMA

The following three ways of modelling the WEC were considered, which were suggested by (Todalshaug, 2015).

- As a two-body system where one (the rack body) has the mass of the PTO and one has the mass of the buoy (buoy body). You would have to assume a somewhat lower centre of mass for the PTO part and a somewhat higher centre of mass for the buoy part. Such that the pretension force, the PTO force and the WaveSpring force to work between the two bodies. The rack body to be connected to the seabed or the floating platform through a taut mooring line.
- As a two-body system with the rack body having only a small mass and the buoy the rest of the mass.
- As a one-body system where the pretension force, the PTO force and the WaveSpring force to work between the body and the mooring point.

In both two-body alternatives, the rack body should be given without hydrodynamic properties, and constrained to move with the buoy in all modes except heave (or more precisely constrained to move along the buoy centre axis). It was, however, decided to go for the one-body system, since this one seemed to be the easiest to conduct.

10.2.1 The WEC Model

The hydrodynamic coefficients needed to model the WEC in SIMA were obtained from the WAMIT analysis mentioned in Section 8.1. This step was challenging and time consuming since SIMA is not directly compatible with WAMIT. The coefficients and geometry of the WEC were then imported to SIMA to create a SIMO body. In Figure 10.1 the model of the WEC is shown without having it connected to the sea floor. The information obtained from WAMIT are purely hydrodynamics. Mass coefficients therefore had to be applied to SIMA. The mass coefficients SIMA needs to run an analysis are the total mass of the WEC, the center of mass and the massmatrix. The precise mass properties of the CorPower prototype scale are not decided yet, but (Todalshaug, 2015) suggested the following values, which should give a representative behaviour of the WEC:

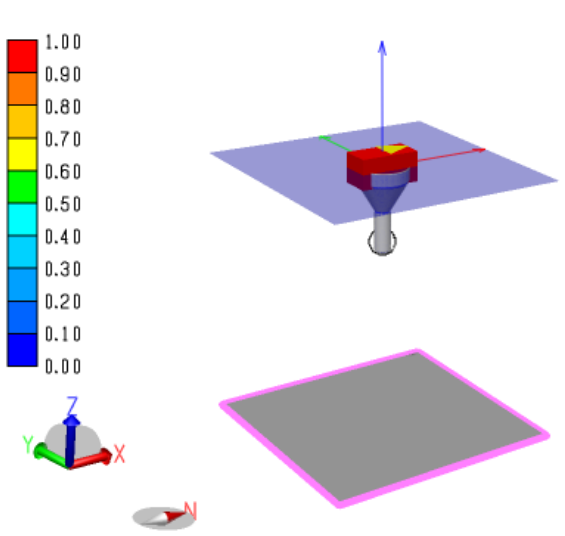

FIGURE 10.1: The model of the WEC in SIMA

- The total mass,m, of the buoy would be about 80 tonnes. About 25 tons are due to PTO components. The buoy hull and structure make up 55 tons.
- The centre of mass could be taken to lie about 2 m under the mean water line on the buoy
- The Mass matrix consists of the moments of inertia,I_{xx},I_{yz},I_{yy},I_{zx},I_{zy} and I_{zz}. Since the WEC is symmetric only I_{xx},I_{yy} and I_{zz} are of importance. These can be calculated by I_{axis}=mr_g^2, where r_g is the radius of gyration about a given axis. (Todalshaug, 2015) suggested the gyration radii to be chosen as: $r_{xx} = r_{yy} = 2.5m, r_{zz} = 1m$.

10.2.2 The Coupled WEC Model

To fix the WEC to the sea floor a mooring line has to be modelled. In addition a PTO (in this case a piston pump) and the WaveSpring have to be included to the model. The PTO will add an additional linear damping and the WaveSpring an additional hydrostatic stiffness parameter to the system. One way of including the PTO and WaveSpring is to calculate the effect of these to parameters for each sea state and then changing the damping and stiffness directly in SIMA, before running the analysis for the different sea state conditions. The additional linear damping from the PTO can be calculated by Eq.(8.15) and the stiffness coefficient by Eq.(8.21). This approach should of course only be considered if one assumes

linear motion of the WEC, since the calculations done in Chapter 8 are assuming linear theory to be valid.

To couple the WEC to a mooring line so called super nodes have to be defined. One at the under site of the WEC and one at the sea floor. The mooring line can then be defined in between those nodes. The parameters of the mooring line, such as thickness and material can also be defined in SIMA. In Figure 10.2 the finished coupled model is shown.

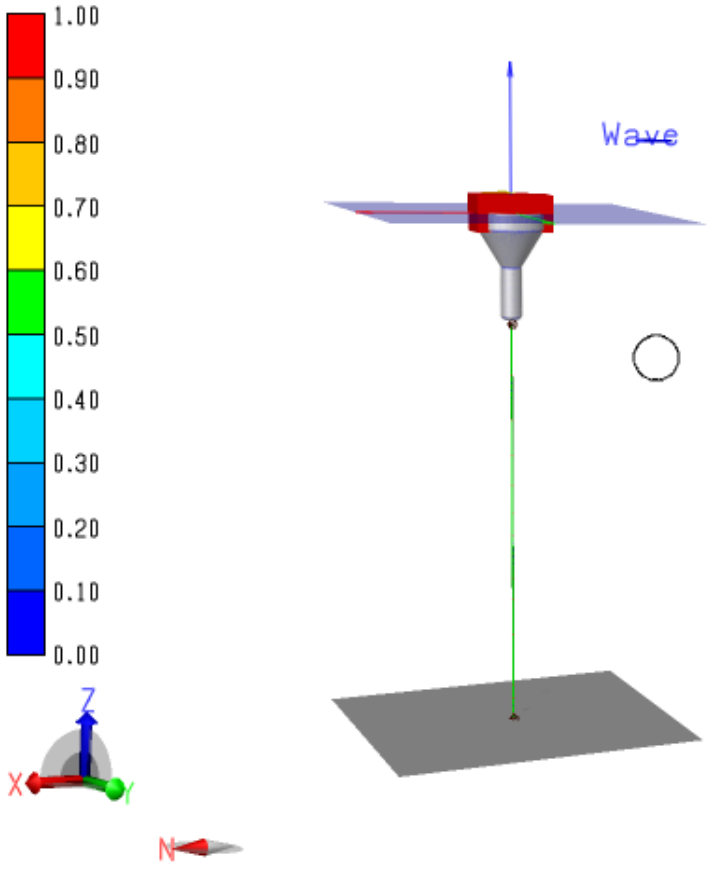

FIGURE 10.2: The coupled model

Due to time constrains and the high work load of this thesis, the author was not able to analyse the model in SIMA further. The SIMA file of the model is, however, ready to be used for a more realistic analysis of the WEC in the future.

Chapter 11

Combining Wind and Wave Power Proposal

The large hydrostatic head at the ocean floor provides a unique opportunity for storing energy as pumped hydro. As discussed in Chapter 5 pumped hydro stores potential energy by displacing water from the chamber of a subsea tank that rests on the ocean floor. In this Chapter the size of the chamber is estimated with respect to the calculated power production of the wind turbine and WEC.

11.1 Simplifications and Assumptions

The density of the water displaced from the chamber is assumed to be constant with ρ_{water}=1025kg/m^3. In Figure 11.1 the salinity content of the ocean on a per depth basis is shown. It can be seen that the density is not varying noteworthy, this assumption should therefore be justifiable. Another assumption is to that we will assume that the pumping devices are able to evacuate the chamber to a full vacuum. This assumption should be modified once the capabilities of the pumps have been investigated further, as was done in this thesis. In addition the ocean will be treated as a constant pressure head, which means that wave motions on the sea bed are not accounted for.

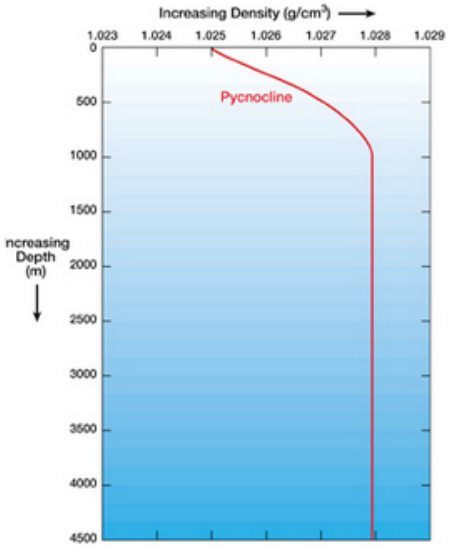

FIGURE 11.1: Salinity content of the ocean

11.2 Chamber Size Estimation

The energy stored by the chamber is equal to the chamber's volume and the hydrostatic pressure of its surrounding environment (Greenlee, 2009). This can be expressed as

$$E = V_{chamber}(\rho_{water} g H + 10^5) \tag{11.1}$$

where $V_{chamber}$ is the volume of the chamber, ρ_{water} the water density, g the gravitational constant and H the water depth. Since the chamber is being evacuated to vacuum, the atmospheric pressure p_{atm}=10^5 must be taken into account as the difference i pressure (Greenlee, 2009). The volume needed to store one kilowatt hour is therefore directly related to the depth of the chamber and can be expressed as

$$\frac{V_{chamber}}{kWh} = \frac{C}{(\rho_{water} g H + 10^5)} \tag{11.2}$$

where C is the conversion factor from Joules to kWh. In Figure 11.2 the amount of volume needed to store a constant amount of energy is shown. The figure was established in EXCEL and the table on which it is based can be found in Appendix C.1. It should be noted that the volume decreases non-linearly with increasing depth.

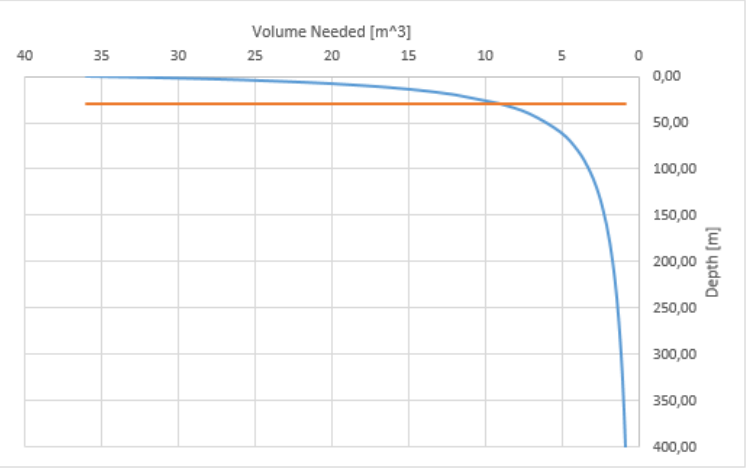

FIGURE 11.2: Volume required per unit of energy as a function of depth

11.3 Estimating the Volume of the Underwater Chamber

With Eq.11.2 in place we can now determine the required size of the chamber when combing wind and wave power. The mean power produced by the wind turbine at a operational wind speed of 10 m/s was determined in Section 7.3 as 3216,78[kW]. The mean power produced by the WEC was determined in Section 9.2 as 127,617[kW]. It can be seen that the difference in power output would be immense, if only consider one WEC. Installing only one WEC to pump water is therefore not reasonable. It was therefore decided to multiply the amount of WECs such that a series of WEC produce the same amount of energy as one wind turbine before calculating the size of the chamber. This results in 25 WECs per wind turbine, producing in total 3190,43[kW]. When combining the two power sources we get a total amount of energy E_{tot}=6407.21[kWh]. This results in a total required volume of 58901.58[m^3] at a water depth of 29[m], were Eq.(11.2) was used. In Table 11.1 the volume and amount, n, of tanks (cylinder shaped) needed to fulfill this requirement is shown for different diameters, D, with a length, L, of 150, 100 and 50 meters, respectively.

TABLE 11.1: Volume and number of underwater tanks

L/D,n	2	n	3	n	4	n	5	n
150	$1885m^3$	32	$4241m^3$	14	$7540m^3$	8	$11781m^3$	5
100	$1257m^3$	47	$2828m^3$	21	$5027m^3$	12	$7854m^3$	8
50	$628m^3$	94	$1414m^3$	42	$2513m^3$	23	$3926m^3$	15

11.4 Discussion

From Table 11.1 it becomes clear that one needs to install a large amount high volume underwater tanks to fulfill the requirement of 58901.58[m^3]. From Figure 11.2 it can be seen that the volume decreases rapidly when installing the underwater storage tanks at a greater water depth. The predetermined water depth of 29 meters at the chosen offshore site might therefore be reconsidered. By installing the tanks at a depth of e.g. 80[m] the tank volumes in Table 11.1 reduces to less than half. This will, however, complicate the approach of using a wave driven piston pump, due to higher mechanical losses. It seems more logical to discard the idea of combining the two power sources through a common storage tank, and look at the two sources separately. The power output for one WEC is comparatively small to the wind turbine. Hence, the volume pump rate is low, decreasing rapidly when entering deeper waters (see Figure 9.11). The depth of the chosen offshore site could therefore be suitable for locating a wave energy power park equipped with underwater energy storage tanks.

The intention of CorPower is to mass-produce their buoy and install many WECs at one wave power farm. If we would assume a wave power farm with e.g. 25 WECs, we would consequently reduce the calculated volume of 58901.58 [m^3] to approximately 30000 [m^3] (25 WECs per wind turbine). Aforementioned it was proposed that each WEC has its own local tank from which the water is pumped out. If we assume that each WEC has a local tank with volume 190[m^3](L=15m, D=4m), we would have approximately 25000[m^3] left to distribute between the main tanks. In Table 11.2 the volume and amount, n, of main tanks needed for this new proposal are given. Such a wave power farm would approximately pro-

Table 11.2: Volume and number of underwater tanks

L/D,n	2	n	3	n	4	n	5	n
150	$1885m^3$	13	$4241m^3$	6	$7540m^3$	3	$11781m^3$	2
100	$1257m^3$	19	$2828m^3$	9	$5027m^3$	5	$7854m^3$	3
50	$628m^3$	39	$1414m^3$	17	$2513m^3$	10	$3926m^3$	6

duce annually 0.03TWh. By using the current Norwegian price level this would correspond to 9 million NOK a year (norgesenergi).

Chapter 12

Conclusion

The question weather it is economically feasible to combine wind and wave power still remains. The intention of this thesis was to propose a design of a combined wind and wave power device. The analysis carried out in this thesis, showed that the combination through a common underwater energy storage tank is difficult to conduct. Wind turbines are able to pump large amounts of water and the under water storage tanks should therefore be installed at deep seas. This will reduce the required volume of the storage tanks significantly. The volume pump rate of a wave energy converter is comparatively low. Hence, when using wave power to pump water the underwater storage tanks should not be placed to deep under the sea surface. Due to the low power output of WECs, harvesting wave energy is only possible when the devices are mass produced. The author, is convinced that the proposed system is suitable for both wind and wave power farms. Especially for wave power farms an underwater storage tank seems well-fitting and could be the key to harvesting energy from waves in the future. Using wave driven piston pumps to pump water instead of implementing expensive and fragile gearboxes to the WEC should increase the power output and reduce maintenance cost.

The idea of developimg a realistic, yet feasible solution to reduce the infrastructure remains tempting. Since ocean waves are primarily generated by wind these two resources are correlated. Therefore it should be possible to exploit wave and wind power simultaneously. The connection to the grid is one of the most costly interventions, when harvesting energy offshore. To combine the two resources should therefore reduce the cost instead of operating the devices separately.

Chapter 13

Further Work

In the following suggestions for further work are mentioned.

One could investigate sites with higher wave energy density. This will increase the performance of the WEC. In addition deeper offshore sites could be analyzed. This will reduce the required volume of the underwater energy storage tank. In this regard, one has to investigate whether it is feasible to use a wave driven piston pump, or if a wave driven centrifugal pump is preferable. In addition, one could use a Weibull distribution to determine a more realistic average power output of the wind turbine.

One could look further into what kind of pumpscould be used for the proposed system. In this regard, more detailed calculations for the maximum pump rate could be performed. For this purpose a handwritten bond graph explaining the physical settings of the wave driven piston pump was developed, which can be found in Appendix B.9. Implementing the bond graph to the software 20-Sim one could calculate the pump rate more precisely, with regard to pressure differences and mechanical losses. In addition, one could perform a experimental test of the wave driven piston pump.

The wind turbine blade was composed of only one airfoil profile, the NACA0064. To obtain a better power output of the turbine different airfoil profiles should be used. Another important part of the wind turbine design is to balance the aerodynamic torque (T_b) and generator torque at the design RPM. If generator torque is too high, the system will stabilize at a lower speed while a too small resistance

will accelerate the turbine to a higher speed. The generator torque (T_{gen}) varies proportionally with RPM, while the blade torque (T_b) is non-linear. If the slope of T_{gen} is steeper than T_b, the blade will fail to start rotating.

ASHES has the ability to calculate this interaction through varying a parameter defining the slope of the T_{gen} vs RPM curve. With wind speed and TSR as inputs, this could be done to give a better power output for the wind turbine, since only the aerodynamic power was investigated, and not the delivered power by the generator.

In general, a more reliable analysis of a wave energy converter with less simplifications could be something to look into further. When investigating the WEC performance a time-domain simulation could be done, since this will increase the accuracy of the results. In addition, one should investigate the motion of the WEC in all 6 degrees of freedom. The software SIMA could be used for this purpose. As mentioned in Chapter 10 the CorPower buoy was already modeled in SIMA.

Building a WEC is generally very costly since it has to survive highly varying wave loads and still produce energy at as many different sea states as possible. Fatigue and high reparation costs have been a big issue in the wind power industry. Combining wave and wind power will cause even bigger costs. To make the wave power production economically feasible, several WEC's should be operated simultaneously due to the already discussed limit of 300$[kW]$. Since the WEC is "destroying" the incoming waves, it has to be investigated how far from each other and in what constellation the WEC's could operate without interfering with each other.

The final design of the proposed system must fulfill many functional requirements. First of all, the units have to maintain structural integrity for at least the lifespan of 20 years. The underwater storage tank must be able to sustain the high static and dynamic loads present at the ocean floor. Furthermore, the structures must resist the abrasion, fouling, and chemical attacks inherent to a marine environment. Maintenance is cost prohibitive, especially for the storage tank this will probably be difficult after its initial installation. Another potential problem is the mooring of the storage tank. The design must be able to accommodate the resulting cyclic loading when charging and discharging. These issues should therefore

be investigated further.

Bibliography

academia. Wind energy. 2015. URL https://www.academia.edu/5264334/06_Wind_Energy.

L. Ackermann, T.; Söder. Wind energy technology and current status: A review. 4, 2000.

R. E. A. Argaw, N.; Foster. Renewable energy for water pumping applications in rural villages. *Subcontractor Report No. 500-30361*, July 2003.

ASHES. What is ashes? 2014. URL http://www.ashes.no/what-is-ashes/.

E. Bachynski. Conversation about effect of reynolds number. April 2015.

C. Benjaminsen. Vannkraftverk p havbunnen. May 2013. URL http://gemini.no/2013/05/vannkraftverk-pa-havbunnen/.

G. Boyle. Renewable energy. Second Edition, 2004.

BP. Bp statistical review of world energy june 2014. *Technical report BP*, 63rd edition, 2014. URL http://www.bp.com/content/dam/bp/pdf/Energy-economics/statistical-review-2014/BP-statistical-review-of-world-energy-2014-full-report.pdf.

T. Burton. Wind energy handbook. Chichester, UK 2011.

CorPower. Wavespring technology. URL http://www.corpowerocean.com/corpower-technology/wave-spring-technology/.

J. Cruz. Ocean wave energy, current status and future perspectives. 2008.

C. Doolan. Developing a quieter wind turbine- understanding the effects of blade generated turbulence and noise. November 2013. URL http://www.slideshare.net/informaoz/dr-con-doolan-university-of-adelaide.

E. S. Duquette, M.A. Understanding flight. *New York*, USA 2001.

EIA. International energy outlook 2013. 2013. URL http://www.eia.gov/forecasts/ieo/pdf/0484%282013%29.pdf.

Elforsk. Wave power, surveillance study of the development. 2011.

EOM. Global scale circulation. 2013. URL http://www.earthonlinemedia.com/ebooks/tpe_3e/circulation/global_scale_circulation.html.

A. F. d. O. Falcao. Wave energy utilization: A review of the technologies. 2009.

A. F. d. O. Falcao. Wave energy utilization: A review of the technologies. *Journal of Offshore Mechanics and Arctic Engineering*, 14(3), 2010.

J. Falnes. Principles for capture of energy from ocean waves. phase control and optimum oscillation.

J. Falnes. Ocean waves and oscillating systems. *Department of Physics,NTNU*, 2002.

J. Falnes. Mechanical oscillator and its application for absorption of wave energy. *Hand wirtten lecture notes*, 2005. URL http://folk.ntnu.no/falnes/teach/wave/bylgjekraftboye.pdf.

J. Falnes. Conversation about: Wave absorption of a wec. February 2015.

J. Falnes and K. Budal. Wave-power conversion by point absorbers. norwegian maritime research. *Trondheim*, 1978.

J. Falnes and J.-H. Todalshaug. Heaving buoys, point absorbers and arrays. *NTNU*, 2012. URL http://rsta.royalsocietypublishing.org/content/roypta/370/1959/246.full.pdf.

O. M. Faltinsen. Sea loads on ships and offshore structures. 1999.

FPP. URL http://www.floatingpowerplant.com.

S. Frøyd, L.; Hauget. Analysis and design of wind turbine blades. 2010.

T. J. Gasch, R. Wind power plants. Berlin 2002.

D.-I. K.-U. Graw. Wellenenergie-eine hydrodynamische analyse. 1995.

A. Greenlee. Design of subsea energy storage chamber. June 2009. URL http://dspace.mit.edu/bitstream/handle/1721.1/54471/556005899-MIT.pdf?sequence=2.

GreenPower. Wind and its measurement in wind energy. 2015. URL http://green-power.com.pl/en/home/wiatr-i-jego-pomiar-w-energetyce-wiatrowej/.

J. Hals. Modelling an phase control of wave-eneergy converters. *Doctor theses*, 2010.

E. Hau. Wind turbines, fundamentals, technologies, applications, economics. 2nd ed, Germany 2006.

B.-S. M. W. Jonkman, J. and G. Scott. Definition of a 5-mw reference wind turbine for offshore system development. *National Renewable Energy Laboratory*, Technical Report No. NREL/Tp-500-3806, 2009.

M. Karimirad. Offshore energy structures, for wind power, wave energy and hybrid marine plattforms. 2014.

J. Layton. How wind power works. 2015. URL http://science.howstuffworks.com/environmental/green-science/wind-power2.htm.

Z. M. T. Li, Lin; Gao. Joint distribution of environmental condition at five european offshore sites for design of combined wind and wave energy devices. *Journal of Offshore Mechanics and Arctic Engineering*, Vol.137, June 2015.

J. Manwell. Understanding wind energy for water pumping. Second Edition, 1988. URL http://pdf.usaid.gov/pdf_docs/PNABC983.pdf.

J. . R. A. Manwell, J.F. Mcgowan. Wind energy explained. Second Edition, 2009.

J. F. Manwell, J. G. McGowan, and A. L. Rogers. Wind energy explained. Dec 2010. URL http://atibook.ir/dl/en/Siences/Natural%20sciences/Environment,%20Ecology,%20Forestry/9780470015001_wind_energy_explained.pdf.

MARINTEK. Sima-simulation and engineering analysis of marine operations and floating systems. 2014a. URL www.sintef.no.

MARINTEK. Riflex theory manual. 2014b.

M. Milnes. The mathematics of pumping water. AECOM Design Building, 2010.

M. J. Muliawan. Design and analysis of combined floating wave and wind power facilities. 2014.

G. B. J. Muljadi, E.; Nix. Analysis of the dynamics of a wind-turbine water-pumping system. July 2000.

B. Multon. Marine renewable energy handbook. 2012.

D. Myrhaug. Kompendium tmr4230 oceanography, wind waves. 2006.

D. Myrhaug. Tmr4180 marin dynamikk uregelmessig sj. 2007.

NEMOS. Technology. 2013. URL http://www.nemos.org/english/technology/.

K. Nielsen. On the experimental investigation of a wave power converter. July 1986.

norgesenergi. URL https://www.norgesenergi.no/.

NREL. New modeling tool analyzes floating platform concepts for offshore wind turbines. Feb 2011. URL http://www.nrel.gov/docs/fy11osti/50856.pdf.

S. P. L. B. Oerlemans, S. Location and quantification of noise sources on a wind turbine. 2006.

OpenEi. URL http://en.openei.org/wiki/Marine_and_Hydrokinetic_Technology_Glossary.

V. Quaschning. Regenerative energiesysteme. 8, 2013.

M. Ragheb. Optimal rotor tip speed ratio. November 2014.

R. Schramm. Underwater accumulator for storing preferably electrical energy. August 2013. URL http://worldwide.espacenet.com/publicationDetails/biblio?CC=WO&NR=2013117329A1&KC=A1&FT=D.

P. J. Schubel and R. J. Crossly. Wind turbine blade design. September 2012. URL www.mdpi.com/1996-1073/5/9/3425/pdf.

Shandong. Multistage split casing centrifugal pump. URL http://sdbspump.en.alibaba.com/product/60221862962-801179797/Multistage_split_casing_centrifugal_pump.html.

SIMA. Naca 64 geometry found at riflex-examples. 2015.

SINTEF. Nowitech. 2014. URL http://www.sintef.no/home/projects/sintef-energy-research/NOWITECH---Norwegian-Research-Centre-for-Offshore-Wind-Technology/.

M. Solutions. Hindcast data. 2015. URL http://www.metocean.co.nz/solutions/offshore-industry/hindcast-data-services/.

Statkraft. Vindkraft. 2015. URL http://www.statkraft.no/Energikilder/Vindkraft/.

Statoil. Sima-the new graphical interface for riflex and simo. Stavanger 2011.

SWECO. Potensialstudie av havenergi i norge. 2007.

theozonehole. Atmosphere. 2015. URL http://www.theozonehole.com/atmosphere.htm.

J. Todalshaug, Hals. Conversation about modeling the wave energy converte in sima. Mai 2015.

W. Treader. URL http://www.power-technology.com/projects/greenoceanenergywav/.

W2Power. URL http://www.pelagicpower.no/about.html.

A. L. Wanan Sheng. Assessment of wave energy extraction from seas: Numerical validation. 2012.

K. Wang. Modelling and dynamic analysis of semi-submersible floating vertical axis wind turbine. January 2015.

Wavebob. Presentation on wavebob to engineers ireland. 9 December 2008. URL https://www.engineersireland.ie/EngineersIreland/media/SiteMedia/groups/Divisions/new-energy/Wavebob-Development_of_a_Wave_Energy_Converter.pdf?ext=.pdf.

wavedragon. URL http://www.wavedragon.net/.

Wavestar. URL http://wavestarenergy.com/.

M. Welland. Wave base, moving sand - and the first underwater feature film on tts. October 18 2011. URL http://throughthesandglass.typepad.com/through_the_sandglass/2011/10/wave-base-moving-sand-and-the-first-underwater-feature-film-on-tts.html.

B. G. Ziter. Electric wind pumping for meeting off-grid community water demands. *Guelph Engineering Journal*, 2, 2009.

Appendix A

Wind Power

A.1 Blade Element Momentum Theory

The Blade Element Momentum (BEM) is most commonly used for analysis of wind turbine blades. The following derivation of the BEM theory is based on (Frøyd, 2010),(Quaschning, 2013) and (Gasch, 2002).

The blade element theory is two-dimensional for an infinity long wing. If we assume that this is also valid for a wing element of length dr, we can use two-dimensional aerodynamics on a finite blade by dividing it into finite number of blade elements. In Figure A.1 the idea behind the BEM theory is illustrated. In each ring there

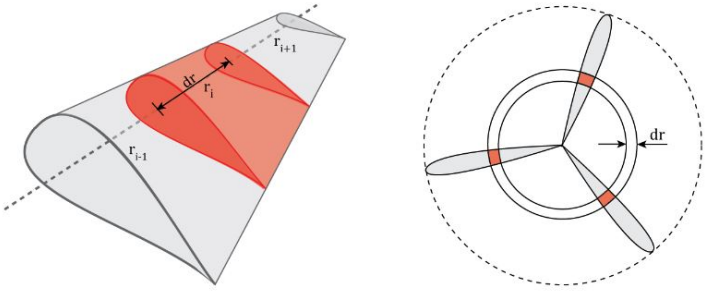

FIGURE A.1: Blade elements of a three-bladed turbine (Frøyd, 2010)

are Z blade elements of length dr, where Z is the number of blades assembling the wind turbine. By using the aerodynamic forces of lift and drag explained in Section 6.3.3, it is possible to describe the forces on each blade element. To find the thrust force T in the axial direction and the torque force M in the tangential direction, the lift and drag force have to be manipulated.

A.2 Forces on the Blade

If we combine F_L and F_D to a resultant force F_R we can decompose it into forces in any arbitrary direction, see Figure A.2. The relative velocity earlier expressed as U_{rel} is here appointed as W. Since we are interested in finding the forces in axial (T') and tangential (M') direction we decompose F_R along these axes. This can be done by using the flow angle φ. The flow angle is the angle between the relative flow velocity U_{rel} and the plane the blade rotates in.

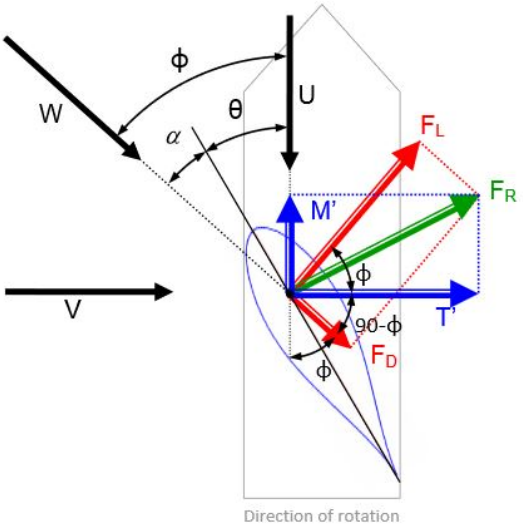

FIGURE A.2: Velocities and forces on a blade element (Frøyd, 2010)

Using the trigonometric relations in Figure A.2 we can express T' and M' as

$$T' = F_L \cdot cos\varphi + F_D \cdot sin\varphi \tag{A.1}$$

$$M' = F_L \cdot sin\varphi - F_D \cdot cos\varphi \tag{A.2}$$

To simplify the expression, two new coefficients are introduced. The axial force coefficient C_a and the rotational force coefficient C_r, which are defined as

$$C_a = C_L \cdot cos\varphi + C_D \cdot sin\varphi \tag{A.3}$$

$$C_r = C_L \cdot sin\varphi - C_D \cdot cos\varphi \tag{A.4}$$

With these new coefficients in place the forces on the blade element in the thrust direction T and the torque direction M can be determined as

$$dT' = C_a \cdot \frac{1}{2} \cdot \rho \cdot U_{rel}^2 \cdot L_C \cdot dr \tag{A.5}$$

$$dM' = C_r \cdot \frac{1}{2} \cdot \rho \cdot U_{rel}^2 \cdot L_C \cdot dr \tag{A.6}$$

By multiplying A.5 and A.6 with the number of blades Z the total force on the rotor can be found:

$$dT = C_a \cdot \frac{1}{2} \cdot \rho \cdot U_{rel}^2 \cdot L_C \cdot dr \cdot Z \tag{A.7}$$

$$dM = C_r \cdot \frac{1}{2} \cdot \rho \cdot U_{rel}^2 \cdot L_C \cdot dr \cdot Z \tag{A.8}$$

Note that the forces dT and dM are not the force on the whole blade, but the forces on an annulus of thickness dr, as shown in Figure A.1. In addition, dM is not to be confused with the moment contribution of the blade element, it is only the force on the blade element in the moment direction. The moment contribution would be calculated as $dM \cdot dr$.

A.2.1 Induction Factors

The next step of the method is to express the relative velocity with respect to the axial induction factors a, the rotational induction factor a' and the free stream velocity V_1. The goal is here to equate the change of momentum in the wake model with the forces on the element(Frøyd, 2010). BEM develops then expressions which include both theories to find the performance of the hole blade.
According to the Newtonian laws the airflow will experience an equal and opposite directed force, causing the flow to accelerate. The airflow will in other words experience acceleration in the opposite direction of the resultant force of the blade. The change of the direction induces a rotational velocity in the air in the opposite direction of the blade rotation. The induced velocity increases the velocity U_{rel} that the blade experiences. By using the blade-element and a wake model it is possible to express this velocity with respect to the axial a (section 6.2.1) and rotational $a^{'}$ induction factors to find the forces on each blade element, as shown in Figure A.4.

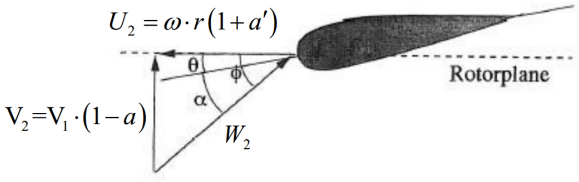

FIGURE A.3: Velocity Triangle (Quaschning, 2013)

From Figure A.4 the relative velocity can be expressed in two ways:

$$W = U_{rel} = \frac{V_1 \cdot (1-a)}{sin\varphi} \tag{A.9}$$

$$W = U_{rel} = \frac{\omega \cdot r \cdot (1+a')}{cos\varphi} \tag{A.10}$$

It can also be seen that the flow angle φ between the direction of the rotation and the resultant speed is changed because of the axial and rotational induction. From Figure A.4 the flow angle can be determined as

$$\varphi = tan^{-1}(\frac{(1-a_i)V_1}{(1+a_i')\omega r}) \tag{A.11}$$

We can now determine the twist angle,which is optimized for each blade element by the following equation.

$$\theta = \varphi - \alpha_{opt}, \tag{A.12}$$

where α_{opt} is the optimal angle of attack for the given airfoil. By choosing the same airfoil for each blade element, the optimal angle of attack will be theoretically constant for the whole blade. The optimal angle of attack was estimated to be where the ratio C_L/C_D is highest Frøyd (2010). This is found by identifying which angle of attack corresponds to the maximum C_L/C_D ratio, given by the airfoil information.

The new expressions for U_{rel} can now be replaced in Eq. (A.7) and Eq. (A.8). When Eq. (A.9) and Eq. (A.10) are equated with the expression for the rate of momentum in Section A.2, the expression for the axial direction will only contain a, while the one in the rotational direction will contain both a and a'. To shorten the mathematical derivation it was therefore decided to let the expression for T consist of $U_{rel} = f(a)$ and the expression for M consist of $U_{rel} = f(a, a')$:

$$dT = C_a \cdot \frac{1}{2} \cdot \rho \cdot \frac{V_1^2 \cdot (1-a)^2}{sin^2\varphi} \cdot L_C \cdot dr \cdot Z \tag{A.13}$$

$$dM = C_r \cdot \frac{1}{2} \cdot \rho \cdot \frac{V_1 \cdot (1-a)}{sin\varphi} \cdot \frac{\omega \cdot r \cdot (1+a')}{cos\varphi} \cdot L_C \cdot dr \cdot Z \tag{A.14}$$

As discussed in Section 6.1 the lift and drag coefficients are known for the airfoil at $Re = 10^7$, the variables ρ, ω, r, dr and Z are also fixed. The chord length Lc is also known at least for the initial blade, but has to be interpolated to find the maximum power output. The only three unknowns are a, a' and φ. To solve with respect to a, a' and φ the rate of change in the wake model is used to derive a set of equations to finally calculate the forces and the power output of the turbine.

A.2.2 Wake Momentum

The rate of change of momentum between the cross sections A_1 and A_2 is equal to the total force on the turbine blades. Since the blade is divided into elements, the cross sections have to be divided into elements as well. The cross sections are therefore divided into ring elements.

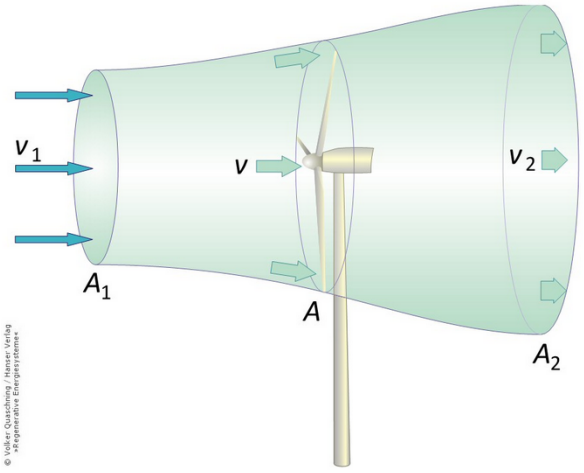

FIGURE A.4: Rate of change of momentum (Quaschning, 2013)

These ring elements will have an area dA equal to the circumference multiplied with the thickness dr of the ring element:

$$dA = 2 \cdot \pi \cdot r \cdot dr \tag{A.15}$$

This is a simplification, but for small values of dr it is a sufficiently accurate simplification. The rate of change of momentum in rotational and axial direction, dM_m and dT_m, is defined as the mass flow in the ring element multiplied with change of velocity. The mass flow in axial direction dT_m can be expressed as:

$$dT_m = d\dot{m} \cdot \Delta V = \rho \cdot V \cdot dA \cdot \Delta V \tag{A.16}$$

At the turbine cross section A, the rate of change of axial momentum can therefore be expressed as:

$$dT_m = \rho \cdot V \cdot dA \cdot (V_1 - V_2) \tag{A.17}$$

Using the axial induction factor the velocity at the turbine can be written as:

$$V = (1 - a) \cdot V_1 \tag{A.18}$$

By using Equation A.18 and the Bernoulli's equation the velocity V_2 can be expressed as:

$$V_2 = V \cdot (1 - 2 \cdot a) \tag{A.19}$$

Using Equation A.18, A.19 and A.15, Equation A.17 can be expressed as:

$$dT_m = 4 \cdot \pi \cdot r \cdot \rho \cdot V_1^2 \cdot (1 - a) \cdot a \cdot dr \tag{A.20}$$

Likewise for the rotational direction:

$$dM_m = 4 \cdot \pi \cdot r^2 \cdot \rho \cdot V_1 \cdot \omega \cdot (1 - a) \cdot a' \cdot dr \tag{A.21}$$

A.2.3 Completing the BEM method

The BEM method derived here is only valid for steady-state conditions. Due to conservation of momentum the blade momentum and thrust must be equal the wake momentum and thrust at all time. Because of this simplification, the complete blade element momentum method can finally be developed. This is done by equating Equation A.13 and A.20 in the thrust direction and A.21 A.14 in the torque direction. Solving the equations with respect to the induction factors a and

a' we get:

$$\frac{a}{(1-a)} = \frac{C_a \cdot L_C \cdot Z}{8 \cdot \pi \cdot r \cdot sin^2\varphi} \tag{A.22}$$

$$\frac{a'}{(1-a')} = \frac{C_a \cdot L_C \cdot Z}{8 \cdot \pi \cdot r \cdot sin\varphi \cdot cos\varphi} \tag{A.23}$$

These equations are implicit, since the flow angle φ is dependent on a an a'. The equations have to be solved by an iteration loop for each blade element. By combining the constants into one, this iteration should minimize the computational time. This is done by introducing the solidity factor σ:

$$\sigma = \frac{Z \cdot L_C}{2 \cdot \pi \cdot r} \tag{A.24}$$

which is the ratio of the area of the ring section that is covered by the bade. Equation A.22 and A.23 can now be expressed as:

$$a = \frac{1}{(\frac{4 \cdot sin^2\varphi}{\sigma \cdot C_a}) + 1} \tag{A.25}$$

$$a' = \frac{1}{(\frac{4 \cdot sin\varphi \cdot cos\varphi}{\sigma \cdot C_r}) - 1} \tag{A.26}$$

All equations required in order to calculate the forces on each blade element are now in place. There are, however, some corrections that must be done to improve the method.

A.2.3.1 Prandtl Corrections for Tip Loss

The BEM method assumes that the air flows straight across the wing, parallel to the airfoil. This is only true for the mid section, but the BEM theory is not valid near the root and at the tip of the blade. Here the air flow is no longer parallel, which means that the BEM theory overestimates the lift that is generated in these sections and consequently overestimates the blade performance. The root loss is neglected in this approach, since very little of the moment is created here. The tip loss, however, must be taken into consideration since the lift is reduced largely and power is lost. Additionally a vortex is created by the tip loss in the wake of the blade tip, which is the reason why a certain distance between wind turbines has to be accounted for. To correct for the tip loss the Prandtl tip loss factor was

used:

$$F = \frac{2}{\pi} \cdot cos^{-1}(e^{-(\frac{z}{2} \cdot \frac{R-r}{r \cdot sin\varphi})}) \tag{A.27}$$

This tip loss factor is used to correct Equation A.25 and A.26 when calculating the induction factors. In addition, Equation A.13 and A.14 have to be corrected when calculating the forces on each element. When inserting the tip loss factor A.27 in these equations we get:

$$a = \frac{1}{(\frac{4 \cdot F \cdot sin^2\varphi}{\sigma \cdot C_a}) + 1} \tag{A.28}$$

$$a' = \frac{1}{(\frac{4 \cdot F \cdot sin\varphi \cdot cos\varphi}{\sigma \cdot C_r}) - 1} \tag{A.29}$$

$$dT = F \cdot C_a \cdot \frac{1}{2} \cdot \rho \cdot \frac{V_1^2 \cdot (1-a)^2}{sin^2\varphi} \cdot L_C \cdot dr \cdot Z \tag{A.30}$$

$$dM = F \cdot C_r \cdot \frac{1}{2} \cdot \rho \cdot \frac{V_1 \cdot (1-a)}{sin\varphi} \cdot \frac{\omega \cdot r \cdot (1+a')}{cos\varphi} \cdot L_C \cdot dr \cdot Z \tag{A.31}$$

A.2.3.2 Glauert's Correction for Heavy Loads

From equation 6.11 it is clear that C_T will approach zero when the axial induction factor approaches 1. In reality the thrust force on the turbine would not approach zero but increase above 1. The thrust on a turbine can be higher than the static pressure in the wind. Glauert suggested a model to correct this based on empirical data. The model should only to be used for values above a certain level of a_c. Glauert suggested a_c to be 0.2. This model should be used instead of A.28 when the axial induction factor is higher than the critical limit. The new axial induction factor can then be expressed as:

$$a = \frac{1}{2} \cdot [2 + K \cdot (1 - 2 \cdot a_c - \sqrt{(K \cdot (1 - 2 \cdot a_c) + 2)^2 + 4 \cdot (K \cdot a_c^2 - 1)}] \tag{A.32}$$

$$K = \frac{4 \cdot F \cdot sin^2\varphi}{\sigma \cdot C_a} \tag{A.33}$$

A.2.4 Ideal Situation with no Drag

The BEM method derived above can be used to analyse the performance of a given blade design with given airfoil parameters (chord length, twist angle)(Frøyd, 2010). It is ,however, not intended for creating the blade design. When using BEM

method to analyse and correct the design, one needs a method of creating an initial blade design to use as a starting point . Glauert suggested a simplified method, to create a initial design by disregarding drag (Quaschning, 2013). Since the drag coefficient is only a tenth of the lift coefficient approximately, this simplification is justifiable. This assumption will, however, only be used to create the initial design of the blade and then use the fully developed blade element method to correct it. The power output for one blade element is defined as the torque contribution multiplied with rotational speed of the rotor as

$$dP = dM \cdot r \cdot \omega \tag{A.34}$$

if we now insert Eq. (A.21) we get

$$dP = (4 \cdot \pi \cdot r \cdot \rho \cdot V_1 \cdot \omega \cdot r \cdot (1 - a) \cdot a' \cdot dr) \cdot r \cdot \omega \tag{A.35}$$

If we define the ratio between the blade element velocity in the rotational direction and the far upstream wind speed we get

$$\lambda_r = \frac{\omega \cdot r}{V_1} \tag{A.36}$$

which is called the local speed ratio or at the tip of the blade the tip speed ratio TSR (Frøyd, 2010). By inserting Eq.(A.36) into Eq.(A.37) we get

$$dP = (4 \cdot \pi \cdot \rho \cdot V_1^3 \cdot \frac{V_1^2}{\omega^2} \cdot (1 - a) \cdot a' \cdot \lambda_r^3) \cdot d\lambda_r \tag{A.37}$$

Since we neglected the effect of drag, the only force affecting the blade and causing wake is the lift. The lift force is perpendicular to the relative wind speed, which means we get two geometrically similar triangles as can be seen from Figure A.5. This we can use to determine a relation between the sides of the triangles and get

$$tan\varphi = \frac{1 - a}{(1 + a') \cdot \lambda_r} \tag{A.38}$$

and

$$tan\varphi = \frac{a' \cdot \lambda_r}{a} \tag{A.39}$$

By combining these two equations we get a relation between the induction factors and the velocity ratio

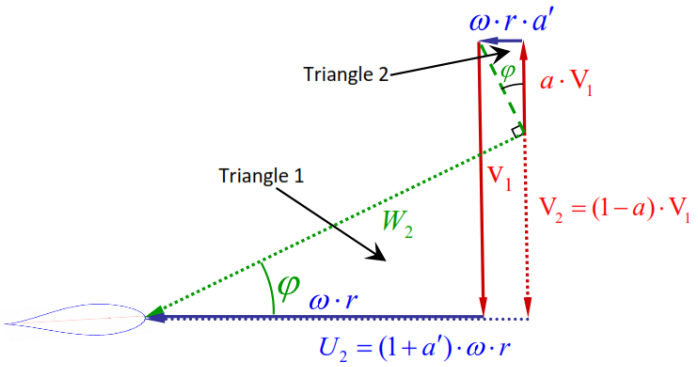

FIGURE A.5: Velocity triangles on a blade element(Frøyd, 2010)

$$a \cdot (1 - a) = a' \cdot (1 + a') \cdot \lambda_r^2 \tag{A.40}$$

From this it is possible to obtain the following relations:

$$a' = \frac{1 - 3 \cdot a}{4 \cdot a - 1} \tag{A.41}$$

$$\lambda_r = (4 \cdot a - 1) \cdot \sqrt{(\frac{1 - a}{1 - 3 \cdot a})} \tag{A.42}$$

To solve these two equations with three unknowns, we need at last one more equation in order to solve the equations explicitly. This is done by equating the force equations and the momentum equation.

A.2.5 Ideal BEM Theory

Since we neglected the effect of drag we can write Eq.(A.3) and Eq.(A.4) as

$$C_a = C_L \cdot cos\varphi \tag{A.43}$$

$$C_r = C_L \cdot sin\varphi \tag{A.44}$$

The new ideal expression for the blade element force (Eq.(A.13) and Eq.(A.14)) then becomes

$$dT = C_L \cdot cos\varphi \cdot \frac{1}{2} \cdot \rho \cdot \frac{V_1^2 \cdot (1-a)^2}{sin^2\varphi} \cdot L_C \cdot dr \cdot Z \tag{A.45}$$

$$dM = C_L \cdot \frac{1}{2} \cdot \rho \cdot \frac{V_1 \cdot (1-a)}{sin\varphi} \cdot \frac{\omega \cdot r \cdot (1+a')}{cos\varphi} \cdot L_C \cdot dr \cdot Z \tag{A.46}$$

By equating Eq.(A.20) and Eq.(A.45), and Eq.(A.21) and Eq.(A.46) respectively, we obtain

$$\frac{a}{1-a} = \frac{Z \cdot L_C \cdot C_L \cdot \varphi}{8 \cdot \pi \cdot r \cdot sin^2\varphi} \tag{A.47}$$

$$\frac{a'}{1-a'} = \frac{Z \cdot L_C \cdot C_L}{8 \cdot \pi \cdot r \cdot cos\varphi} \tag{A.48}$$

These two equations are implicit, and to solve them iteration has to be used. To simplify the Eq.(A.47) and Eq.(A.48) we gather the blade specific factors as

$$B_{EP} = \frac{Z \cdot L_C \cdot C_L \cdot \omega}{2 \cdot \pi V_1} \tag{A.49}$$

Substituting this blade element parameter to Eq.(A.47) we get

$$\frac{a}{a-1} = B_{EP} \cdot \frac{V_1}{\omega \cdot r} \cdot \frac{cos\varphi}{4^2\varphi} \tag{A.50}$$

The next step is to rearrange Eq.(A.11)as

$$\frac{V_1}{\omega \cdot r} = \frac{(1+a') \cdot sin\varphi}{(1-a) \cdot cos\varphi} \tag{A.51}$$

By inserting Eq.(A.50) we get an equation, which is still not explicit, as φ is a function of both induction factors, but the number of unknowns reduces to one, as

$$\frac{a}{1-a} = B_{EP} \cdot \frac{1+a'}{1-a} \cdot \frac{1}{4 \cdot sin\varphi} \tag{A.52}$$

Rearranging this equation we get

$$B_{EP} = \frac{a}{1+a'} \cdot 4 \cdot sin\varphi \tag{A.53}$$

It is now possible to create an ideal parameter table consisting of λ_r, a,a',φ and

B_{EP}, which will be used to create an initial design for the blade. The table is created by defining a vector of values of a that cover the relevant TSRs. By using Eq.(A.42) we can find the corresponding vector for $_r$, and by using Eq.(A.41) the corresponding vector a' can be found. The optimal values of B_{EP} are found by using Eq.(A.53). In Table A.1 the universal parameter table of induction factors, flow angle and B_{EP} is shown, which was obtained by MATLAB.

TABLE A.1: Universal parameter table of induction factors, flow angle and B_{EP} obtained from MATLAB

λ [-]	a [-]	a' [-]	φ [deg]	BEP [-]
0.25	0.28	1.364	50.6	0.366
0.5	0.298	0.543	42.3	0.521
0.75	0.31	0.294	35.4	0.555
1	0.317	0.183	30	0.536
1.25	0.322	0.124	25.8	0.497
1.5	0.325	0.089	22.5	0.455
1.75	0.327	0.067	19.8	0.415
2	0.328	0.052	17.7	0.379
2.5	0.33	0.034	14.5	0.32
3	0.331	0.024	12.3	0.275
3.5	0.331	0.018	10.6	0.24
4	0.332	0.014	9.4	0.213
4.5	0.332	0.011	8.4	0.191
5	0.332	0.008	7.5	0.173
6	0.33	0.007	6.3	0.145
7	0.33	0.007	5.4	0.125
8	0.33	0.006	4.7	0.109
9	0.33	0.005	4.2	0.097
10	0.33	0.005	3.8	0.088

A.2.6 Determining Twist angle φ and the Chord Length, L_C

The optimal flow angle is determined by Eq.(A.11) The chord length can be optimized for each blade element by the following equation.

$$L_C = B_{EP}\frac{2\pi V_1}{ZC_L\omega}, \tag{A.54}$$

The twist angle θ is found by subtracting the optimal angle of attack (C_L/C_D form airfoil data) from the flow angle

$$\theta = \varphi - \alpha_{opt} \tag{A.55}$$

TABLE A.2: Air Foil Data NACA0064 (SIMA)

Angel	Cd	Cl	Cm	Angel	Cd	Cl	Cm
-180	0.0198	0	0	0	0.0052	0.442	-0.1014
-175	0.0341	0.374	0.188	1	0.0052	0.556	-0.1076
-170	0.0955	0.749	0.377	2	0.0053	0.67	-0.1126
-160	0.2807	0.659	0.2747	3	0.0053	0.784	-0.1157
-155	0.3919	0.736	0.313	4	0.0054	0.898	-0.1199
-150	0.5086	0.783	0.3428	5	0.0058	1.011	-0.124
-145	0.6267	0.803	0.3654	6	0.0091	1.103	-0.1234
-140	0.7427	0.798	0.382	7	0.0113	1.181	-0.1184
-135	0.8537	0.771	0.3935	8	0.0124	1.257	-0.1163
-130	0.9574	0.724	0.4007	8.5	0.013	1.293	-0.1163
-125	1.0519	0.66	0.4042	9	0.0136	1.326	-0.116
-120	1.1355	0.581	0.4047	9.5	0.0143	1.356	-0.1154
-115	1.207	0.491	0.4025	10	0.015	1.382	-0.1149
-110	1.2656	0.39	0.3981	10.5	0.0267	1.4	-0.1145
-105	1.3104	0.282	0.3918	11	0.0383	1.415	-0.1143
-100	1.341	0.169	0.3838	11.5	0.0498	1.425	-0.1147
-95	1.3572	0.052	0.3743	12	0.0613	1.434	-0.1158
-90	1.3587	-0.067	0.3636	12.5	0.0727	1.443	-0.1165
-85	1.3456	-0.184	0.3517	13	0.0841	1.451	-0.1153
-80	1.3181	-0.299	0.3388	13.5	0.0954	1.453	-0.1131
-75	1.2765	-0.409	0.3248	14	0.1065	1.448	-0.1112
-70	1.2212	-0.512	0.3099	14.5	0.1176	1.444	-0.1101
-65	1.1532	-0.606	0.294	15	0.1287	1.445	-0.1103
-60	1.0731	-0.689	0.2772	15.5	0.1398	1.447	-0.1109
-55	0.9822	-0.759	0.2595	16	0.1509	1.448	-0.1114
-50	0.882	-0.814	0.2409	16.5	0.1619	1.444	-0.1111
-45	0.7742	-0.85	0.2212	17	0.1728	1.438	-0.1097
-40	0.661	-0.866	0.2006	17.5	0.1837	1.439	-0.1079
-35	0.5451	-0.86	0.1789	18	0.1947	1.448	-0.108
-30	0.4295	-0.829	0.1563	18.5	0.2057	1.452	-0.109
-25	0.3071	-0.853	0.1156	19	0.2165	1.448	-0.1086
-24	0.2814	-0.87	0.104	19.5	0.2272	1.438	-0.1077
-23	0.2556	-0.89	0.0916	20	0.2379	1.428	-0.1099
-22	0.2297	-0.911	0.0785	21	0.259	1.401	-0.1169
-21	0.204	-0.934	0.0649	22	0.2799	1.359	-0.119
-20	0.1785	-0.958	0.0508	23	0.3004	1.3	-0.1235
-19	0.1534	-0.982	0.0364	24	0.3204	1.22	-0.1393
-18	0.1288	-1.005	0.0218	25	0.3377	1.168	-0.144
-17	0.1037	-1.082	0.0129	26	0.3554	1.116	-0.1486
-16	0.0786	-1.113	-0.0028	28	0.3916	1.015	-0.1577
-15	0.0535	-1.105	-0.0251	30	0.4294	0.926	-0.1668
-14	0.0283	-1.078	-0.0419	32	0.469	0.855	-0.1759
-13.5	0.0158	-1.053	-0.0521	35	0.5324	0.8	-0.1897
-13	0.0151	-1.015	-0.061	40	0.6452	0.804	-0.2126
-12	0.0134	-0.904	-0.0707	45	0.7573	0.793	-0.2344
-11	0.0121	-0.807	-0.0722	50	0.8664	0.763	-0.2553
-10	0.0111	-0.711	-0.0734	55	0.9708	0.717	-0.2751
-9	0.0099	-0.595	-0.0772	60	1.0693	0.656	-0.2939
-8	0.0091	-0.478	-0.0807	65	1.1606	0.582	-0.3117
-7	0.0086	-0.375	-0.0825	70	1.2438	0.495	-0.3285
-6	0.0082	-0.264	-0.0832	75	1.3178	0.398	-0.3444
-5	0.0079	-0.151	-0.0841	80	1.3809	0.291	-0.3593
-4	0.0072	-0.017	-0.0869	85	1.4304	0.176	-0.3731
-3	0.0064	0.088	-0.0912	90	1.4565	0.053	-0.3858
-2	0.0054	0.213	-0.0946	95	1.4533	-0.074	-0.3973

Appendix B

Wave Power

	Infinite water depth
Velocity potential	$\varphi = \frac{g\zeta_a}{\omega} e^{kz} \cos(\omega t - kx)$
Connection between wave number k and circular frequency ω	$\frac{\omega^2}{g} = k$
Connection between wavelength λ and wave period T	$\lambda = \frac{g}{2\pi} T^2$
Wave profile	$\zeta = \zeta_a \sin(\omega t - kx)$
Dynamic pressure	$p_d = \rho g \zeta_a e^{kz} \sin(\omega t - kx)$
x-component of velocity	$v_x = \omega \zeta_a e^{kz} \sin(\omega t - kx)$
z-component of velocity	$v_z = \omega \zeta_a e^{kz} \cos(\omega t - kx)$
x-component of acceleration	$a_x = \omega^2 \zeta_a e^{kz} \cos(\omega t - kx)$
z-component of acceleration	$a_z = -\omega^2 \zeta_a e^{kz} \sin(\omega t - kx)$
$\omega = \frac{2\pi}{T}$, $k = \frac{2\pi}{\lambda}$, $T = Wave\ period$, $\lambda = Wavelength$, $\zeta_a = Wave\ amplitude$, $g = Acceleraiton\ of\ gravity$, $t = Time\ variable$, $x = Direction\ of\ wave\ propagation$, $z = Vertical\ coordinate\ positive\ upwards$, $z = 0\ mean\ water\ level$, $h = Average\ waterdepth$. $Total\ pressure\ in\ the\ fluid: p_d - \rho g z + p_o (p_o = atmospheric\ pressure)$	

FIGURE B.1: Potential flow theory Faltinsen (1999)

Hsp \ W	0.0-0.5	0.5 - 1.0	1.0-1.5	1.5-2.0	2.0-2.5	2.5-3.0	3.0-3.5	3.5-4.0	4.0-4.5	4.5-5.0	5.0-5.5	5.5-6.0	6.0-6.5	6.5-7.5	7.5-9.39	Marginal for W
1.0-2.0	753	1429	470	175	32	1	6	8	0	0	0	0	0	0	0	2874
2.0-3.0	1081	2067	779	209	33	12	5	2	3	0	0	0	0	0	0	4191
3.0-4.0	1123	2789	1083	266	49	6	4	2	2	1	0	0	0	0	0	5325
4.0-5.0	786	3724	1543	488	86	16	5	5	1	0	0	0	0	0	0	6654
5.0-6.0	232	4654	2435	774	187	46	9	3	1	0	0	0	0	0	0	8341
6.0-7.0	38	5004	4662	1356	328	91	26	10	4	2	0	0	0	0	0	11521
7.0-8.0	3	2080	4743	2025	560	137	48	18	4	1	1	0	0	0	0	9620
8.0-9.0	0	386	3803	2907	1039	299	63	26	9	2	0	0	0	0	0	8534
9.0-10-0	0	66	1682	3309	1726	541	167	56	16	5	1	0	0	0	0	7569
10.0-11.0	0	13	426	1980	2402	988	267	72	17	5	2	0	0	0	0	6172
11.0-12.0	0	4	91	689	1774	1463	581	166	41	20	4	1	1	2	0	4837
12.0-13.0	0	2	28	206	677	1276	831	355	132	39	9	6	2	0	0	3563
13-0-14.0	0	0	7	64	241	620	904	632	253	95	39	8	6	5	0	2874
14.0-15.0	0	0	1	9	55	210	536	693	335	146	66	28	8	10	0	2097
15.0-16.0	0	0	0	1	28	78	164	344	355	216	81	53	24	24	6	1374
16.0-17.0	0	0	0	1	4	22	55	150	218	226	107	56	20	22	4	885
17.0-18.0	0	0	0	0	4	6	16	56	97	152	103	60	20	24	3	541
18.0-20.0	0	0	0	0	1	3	10	30	43	113	138	100	36	38	29	541
20.0-25.895	0	0	0	0	0	1	1	6	10	14	14	25	16	21	27	135
Marginal for Hs	4016	22218	21753	14459	9226	5816	3698	2634	1541	1037	565	337	133	146	69	87648

FIGURE B.2: Scatter diagram for W and HSP from 10 years' hindcast data (site No. 15)(Li, 2015)

Hs[m] \ Tp[s]	0.0-1.0	1.0-2.0	2.0-3.0	3.0-4.0	4.0-5.0	5.0-6.0	6.0-7.0	7.0-8.0	8.0-9.0	9.0-10.0	10.0-11.0	11.0-12.0	12.0-13.0	13.0-14.0	14.0-15.0	15.0-16.0	16.0-17.0	Marginal for Hs	
0.0-0.5	0	3	96	996	1342	325	157	213	253	120	113	61	52	115	71	50	49	4016	>6%
0.5-1.0	0	0	118	1740	7665	5838	2731	824	816	936	748	269	184	177	78	34	60	22218	5-6%
1.0-1.5	0	0	0	76	3431	6884	4645	2548	1137	667	1111	595	352	183	90	20	14	21753	4-5%
1.5-2.0	0	0	0	0	282	4102	4645	2061	1244	592	400	416	346	272	77	17	5	14459	3-4%
2.0-2.5	0	0	0	0	3	834	4387	1888	869	518	209	146	151	186	20	4	11	9226	2-3%
2.5-3.0	0	0	0	0	0	40	2117	1995	791	322	221	56	67	169	28	7	3	5816	1-2%
3.0-3.5	0	0	0	0	0	2	402	2089	557	287	180	59	32	80	10	0	0	3698	0.5-1%
3.5-4.0	0	0	0	0	0	0	31	1386	628	279	156	58	26	57	10	0	3	2634	<0.5%
4.0-4.5	0	0	0	0	0	0	1	433	614	261	154	42	7	23	4	2	0	1541	
4.5-5.0	0	0	0	0	0	0	0	153	416	235	158	39	6	25	5	0	0	1037	
5.0-5.5	0	0	0	0	0	0	0	10	201	147	145	41	5	16	0	0	0	565	
5.5-6.0	0	0	0	0	0	0	0	0	71	91	115	45	3	11	1	0	0	337	
6.0-6.5	0	0	0	0	0	0	0	0	9	24	56	27	4	11	2	0	0	133	
6.5-7.0	0	0	0	0	0	0	0	0	3	9	26	19	14	10	1	0	0	82	
7.0-7.5	0	0	0	0	0	0	0	0	0	1	2	24	15	19	3	0	0	64	
7.5-8.0	0	0	0	0	0	0	0	0	0	5	0	10	18	15	0	0	0	48	
8.0-8.5	0	0	0	0	0	0	0	0	0	0	1	0	8	7	0	0	0	16	
8.5-9.0	0	0	0	0	0	0	0	0	0	0	0	0	1	1	0	0	0	2	
9.0-9.5	0	0	0	0	0	0	0	0	0	0	0	0	0	3	0	0	0	3	
Marginal for Tp	0	3	214	2812	12723	18025	19116	13600	7609	4494	3795	1907	1291	1380	400	134	145	87648	

FIGURE B.3: Scatter diagram (Li, 2015)

Condition		Site 1	Site 3	Site 5	Site 14	Site 15
Condition with maximum U_w	U_w (m/s)	23.7	28.3	27.5	33.6	27.2
	H_s (m)	8.0	8.8	11.4	13.4	8.1
	T_p (s)	12.2	11.9	13.5	13.1	10.0
Condition with maximum H_s	U_w (m/s)	21.4	24.3	25.1	31.2	25.3
	H_s (m)	10.2	12.1	14.0	15.6	9.5
	T_p (s)	13.8	13.8	15.11	14.5	12.3

FIGURE B.4: Environmental conditions on the 50-year contour surfaces with maximum U_w and maximum H_s (Li, 2015)

Hs[m] \ Tp[s]	0.0-1.0	1.0-2.0	2.0-3.0	3.0-4.0	4.0-5.0	5.0-6.0	6.0-7.0	7.0-8.0	8.0-9.0	9.0-10.0	10.0-11.0	11.0-12.0	12.0-13.0	13.0-14.0	14.0-15.0	15.0-16.0	16.0-17.0	Marginal for Hs
0.0-0.5	0,00000	0,00342	0,10953	1,13636	1,53112	0,37080	0,17913	0,24302	0,28865	0,13691	0,12892	0,06960	0,05933	0,13121	0,08101	0,05705	0,05591	4,5820
0.5-1.0	0,00000	0,00000	0,13463	1,98521	8,74521	6,66073	3,11587	0,94012	0,93100	1,06791	0,85341	0,30691	0,20993	0,20194	0,08899	0,03879	0,06846	25,3491
1.0-1.5	0,00000	0,00000	0,00000	0,08671	3,91452	7,85414	5,29961	2,90708	1,29723	0,76100	1,26757	0,67885	0,40161	0,20879	0,10268	0,02282	0,01597	24,8186
1.5-2.0	0,00000	0,00000	0,00000	0,00000	0,32174	4,68008	5,29961	2,35145	1,41931	0,67543	0,45637	0,47463	0,39476	0,31033	0,08785	0,01940	0,00570	16,4967
2.0-2.5	0,00000	0,00000	0,00000	0,00000	0,00342	0,95153	5,00525	2,15407	0,99147	0,59100	0,23845	0,16658	0,17228	0,21221	0,02282	0,00456	0,01255	10,5262
2.5-3.0	0,00000	0,00000	0,00000	0,00000	0,00000	0,04564	2,41534	2,27615	0,90247	0,36738	0,25214	0,06389	0,07644	0,19282	0,03195	0,00799	0,00342	6,6356
3.0-3.5	0,00000	0,00000	0,00000	0,00000	0,00000	0,00228	0,45865	2,38340	0,63550	0,32745	0,20537	0,06731	0,03651	0,09127	0,01141	0,00000	0,00000	4,2191
3.5-4.0	0,00000	0,00000	0,00000	0,00000	0,00000	0,00000	0,03537	1,58133	0,71650	0,31832	0,17798	0,06617	0,02966	0,06503	0,01141	0,00000	0,00342	3,0052
4.0-4.5	0,00000	0,00000	0,00000	0,00000	0,00000	0,00000	0,00114	0,49402	0,70053	0,29778	0,17570	0,04792	0,00799	0,02624	0,00456	0,00228	0,00000	1,7582
4.5-5.0	0,00000	0,00000	0,00000	0,00000	0,00000	0,00000	0,00000	0,17456	0,47463	0,26812	0,18027	0,04450	0,00685	0,02852	0,00570	0,00000	0,00000	1,1831
5.0-5.5	0,00000	0,00000	0,00000	0,00000	0,00000	0,00000	0,00000	0,01141	0,22933	0,16772	0,16543	0,04678	0,00570	0,01825	0,00000	0,00000	0,00000	0,6446
5.5-6.0	0,00000	0,00000	0,00000	0,00000	0,00000	0,00000	0,00000	0,00000	0,08101	0,10382	0,13121	0,05134	0,00342	0,01255	0,00114	0,00000	0,00000	0,3845
6.0-6.5	0,00000	0,00000	0,00000	0,00000	0,00000	0,00000	0,00000	0,00000	0,01027	0,02738	0,06389	0,03081	0,00456	0,01255	0,00228	0,00000	0,00000	0,1517
6.5-7.0	0,00000	0,00000	0,00000	0,00000	0,00000	0,00000	0,00000	0,00000	0,00342	0,01027	0,02966	0,02168	0,01597	0,01141	0,00114	0,00000	0,00000	0,0936
7.0-7.5	0,00000	0,00000	0,00000	0,00000	0,00000	0,00000	0,00000	0,00000	0,00000	0,00114	0,00228	0,02738	0,01711	0,02168	0,00342	0,00000	0,00000	0,0730
7.5-8.0	0,00000	0,00000	0,00000	0,00000	0,00000	0,00000	0,00000	0,00000	0,00000	0,00570	0,00000	0,01141	0,02054	0,01711	0,00000	0,00000	0,00000	0,0548
8.0-8.5	0,00000	0,00000	0,00000	0,00000	0,00000	0,00000	0,00000	0,00000	0,00000	0,00000	0,00114	0,00000	0,00913	0,00799	0,00000	0,00000	0,00000	0,0183
8.5-9.0	0,00000	0,00000	0,00000	0,00000	0,00000	0,00000	0,00000	0,00000	0,00000	0,00000	0,00000	0,00000	0,00114	0,00114	0,00000	0,00000	0,00000	0,0023
9.0-9.5	0,00000	0,00000	0,00000	0,00000	0,00000	0,00000	0,00000	0,00000	0,00000	0,00000	0,00000	0,00000	0,00000	0,00342	0,00000	0,00000	0,00000	0,0034
Marginal for Tp	0	0,00342278	0,24415845	3,2082877	14,5160186	20,5652154	21,8099671	15,5166119	8,68131617	5,12732749	4,32981928	2,17574845	1,4729372	1,57447974	0,45637094	0,15288426	0,16543447	100,0000

>6%
5-6%
4-5%
3-4%
2-3%
1-2%
0.5-1%
<0.5%

FIGURE B.5: Wave probability distribution [%]

Hs[m] \ Tp[s]	0.0-1.0	1.0-2.0	2.0-3.0	3.0-4.0	4.0-5.0	5.0-6.0	6.0-7.0	7.0-8.0	8.0-9.0	9.0-10.0	10.0-11.0	11.0-12.0	12.0-13.0	13.0-14.0	14.0-15.0	15.0-16.0	16.0-17.0
0.0-0.5	0	40100	38709	49914	50290	42727	36848	29985	24574	21732	19109	16732	15069	13533	12446	11860	10752
0.5-1.0	0	0	91887	117900	96882	83871	66020	58915	50038	43339	37280	34608	28846	26557	24110	22659	21804
1.0-1.5	0	0	0	190250	170530	128040	110980	88083	75017	64795	56828	48789	43122	39197	36967	33851	32631
1.5-2.0	0	0	0	0	238950	181920	139030	117430	100400	86609	77389	67594	60053	52140	49021	42398	43335
2.0-2.5	0	0	0	0	269870	235530	180260	149550	122820	131110	109940	92234	82107	70545	67764	60258	55235
2.5-3.0	0	0	0	0	0	273560	216090	172650	149000	129920	116450	103470	100830	87563	81611	75132	66513
3.0-3.5	0	0	0	0	0	322800	259670	205950	178660	155880	136230	113700	101520	93540	84882	0	0
3.5-4.0	0	0	0	0	0	0	284730	235540	198010	173500	147180	128020	117570	109110	100170	0	84191
4.0-4.5	0	0	0	0	0	0	329600	279490	246430	227530	199930	175680	155790	138930	122110	109570	0
4.5-5.0	0	0	0	0	0	0	0	287350	266890	234050	222220	196370	176310	148700	132990	0	0
5.0-5.5	0	0	0	0	0	0	0	322500	278520	257930	243140	218290	190680	169860	0	0	0
5.5-6.0	0	0	0	0	0	0	0	0	304480	270810	255910	235000	205310	181360	156140	0	0
6.0-6.5	0	0	0	0	0	0	0	0	329090	292980	265310	240990	231750	196990	176540	0	0
6.5-7.0	0	0	0	0	0	0	0	0	344730	298850	273520	262210	241040	213340	191720	0	0
7.0-7.5	0	0	0	0	0	0	0	0	0	322600	299340	273850	250490	227130	201990	0	0
7.5-8.0	0	0	0	0	0	0	0	0	0	337340	0	281780	264170	245550	0	0	0
8.0-8.5	0	0	0	0	0	0	0	0	0	0	322270	0	272360	249520	0	0	0
8.5-9.0	0	0	0	0	0	0	0	0	0	0	0	0	279420	258470	0	0	0
9.0-9.5	0	0	0	0	0	0	0	0	0	0	0	0	0	263450	0	0	0

>6%
5-6%
4-5%
3-4%
2-3%
1-2%
0.5-1%
<0.5%

FIGURE B.6: MATLAB results for average captured wave power [W]

Hs[m] \ Tp[s]	0.0-1.0	1.0-2.0	2.0-3.0	3.0-4.0	4.0-5.0	5.0-6.0	6.0-7.0	7.0-8.0	8.0-9.0	9.0-10.0	10.0-11.0	11.0-12.0	12.0-13.0	13.0-14.0	14.0-15.0	15.0-16.0	16.0-17.0	>6%
0.0-0.5	0	12023	371403	4968712	6745222	1387867	578197	638331	621382	260641	215813	102009	78316	155544	88318	59268	52656	5-6%
0.5-1.0	0	0	1083673	20503365	74219385	48937075	18020188	4851937	4080865	4054309	2787017	930445	530476	469801	187955	76998	130752	4-5%
1.0-1.5	0	0	0	1445108	58476801	88094465	51521979	22431257	8524762	4319460	6310133	2901356	1517063	716912	332521	67665	45658	3-4%
1.5-2.0	0	0	0	0	6734700	74582717	64544068	24189069	12482920	5124445	3093865	2810370	2076696	1417431	377255	72037	21656	2-3%
2.0-2.5	0	0	0	0	80917	19632444	79036754	28219577	10667213	6787779	2296488	1345879	1239137	1311418	135454	24090	60725	1-2%
2.5-3.0	0	0	0	0	0	1093641	45721200	34424812	11779446	4181133	2572136	579115	675191	1479004	228386	52564	19943	0.5-1%
3.0-3.5	0	0	0	0	0	64525	10433017	42999394	9945912	4471306	2450797	670463	324686	747910	84836	0	0	<0.5%
3.5-4.0	0	0	0	0	0	0	882180	32627966	12428218	4837999	2294751	742109	305515	621586	100115	0	25243	
4.0-4.5	0	0	0	0	0	0	32942	12095289	15122516	5935281	3077236	737452	108993	319364	48817	21902	0	
4.5-5.0	0	0	0	0	0	0	0	4394047	11096544	5497163	3509153	765424	105728	371546	66459	0	0	
5.0-5.5	0	0	0	0	0	0	0	322323	5595186	3789495	3523599	894499	95288	271627	0	0	0	
5.5-6.0	0	0	0	0	0	0	0	0	2160624	2463021	2941353	1056921	61559	199387	15605	0	0	
6.0-6.5	0	0	0	0	0	0	0	0	296019	702767	1484922	650317	92649	216570	35289	0	0	
6.5-7.0	0	0	0	0	0	0	0	0	103362	268818	710763	497926	337271	213223	19162	0	0	
7.0-7.5	0	0	0	0	0	0	0	0	0	32242	59835	656880	375529	431311	60564	0	0	
7.5-8.0	0	0	0	0	0	0	0	0	0	168578	0	281626	475246	368123	0	0	0	
8.0-8.5	0	0	0	0	0	0	0	0	0	0	32209	0	217769	174568	0	0	0	
8.5-9.0	0	0	0	0	0	0	0	0	0	0	0	0	27927	25833	0	0	0	
9.0-9.5	0	0	0	0	0	0	0	0	0	0	0	0	0	78992	0	0	0	

FIGURE B.7: MATLAB results for average energy produced over one year [Wh/year]

Hs[m] \ Tp[s]	0.0-1.0	1.0-2.0	2.0-3.0	3.0-4.0	4.0-5.0	5.0-6.0	6.0-7.0	7.0-8.0	8.0-9.0	9.0-10.0	10.0-11.0	11.0-12.0	12.0-13.0	13.0-14.0	14.0-15.0	15.0-16.0	16.0-17.0
0.0-0.5	0,00000	0,11001	0,10620	0,13694	0,13797	0,11722	0,10109	0,08226	0,06742	0,05962	0,05242	0,04590	0,04134	0,03713	0,03415	0,03254	0,02950
0.5-1.0	0,00000	0,00000	0,25209	0,32345	0,26579	0,23010	0,18112	0,16163	0,13728	0,11890	0,10228	0,09495	0,07914	0,07286	0,06614	0,06216	0,05982
1.0-1.5	0,00000	0,00000	0,00000	0,52194	0,46784	0,35127	0,30447	0,24165	0,20581	0,17776	0,15591	0,13385	0,11830	0,10754	0,10142	0,09287	0,08952
1.5-2.0	0,00000	0,00000	0,00000	0,00000	0,65555	0,49909	0,38142	0,32216	0,27544	0,23761	0,21231	0,18544	0,16475	0,14304	0,13449	0,11632	0,11889
2.0-2.5	0,00000	0,00000	0,00000	0,00000	0,74038	0,64617	0,49454	0,41028	0,33695	0,35970	0,30162	0,25304	0,22526	0,19354	0,18591	0,16532	0,15154
2.5-3.0	0,00000	0,00000	0,00000	0,00000	0,00000	0,75050	0,59283	0,47366	0,40878	0,35643	0,31948	0,28387	0,27662	0,24023	0,22390	0,20612	0,18248
3.0-3.5	0,00000	0,00000	0,00000	0,00000	0,00000	0,88559	0,71240	0,56502	0,49015	0,42765	0,37374	0,31193	0,27852	0,25662	0,23287	0,00000	0,00000
3.5-4.0	0,00000	0,00000	0,00000	0,00000	0,00000	0,00000	0,78115	0,64620	0,54323	0,47599	0,40378	0,35122	0,32255	0,29934	0,27481	0,00000	0,23097
4.0-4.5	0,00000	0,00000	0,00000	0,00000	0,00000	0,00000	0,90425	0,76677	0,67607	0,62422	0,54850	0,48197	0,42740	0,38115	0,33500	0,30060	0,00000
4.5-5.0	0,00000	0,00000	0,00000	0,00000	0,00000	0,00000	0,00000	0,78833	0,73220	0,64211	0,60965	0,53873	0,48370	0,40795	0,36485	0,00000	0,00000
5.0-5.5	0,00000	0,00000	0,00000	0,00000	0,00000	0,00000	0,00000	0,88477	0,76411	0,70762	0,66705	0,59887	0,52312	0,46600	0,00000	0,00000	0,00000
5.5-6.0	0,00000	0,00000	0,00000	0,00000	0,00000	0,00000	0,00000	0,00000	0,83533	0,74296	0,70208	0,64471	0,56326	0,49755	0,42836	0,00000	0,00000
6.0-6.5	0,00000	0,00000	0,00000	0,00000	0,00000	0,00000	0,00000	0,00000	0,90285	0,80378	0,72787	0,66115	0,63580	0,54043	0,48433	0,00000	0,00000
6.5-7.0	0,00000	0,00000	0,00000	0,00000	0,00000	0,00000	0,00000	0,00000	0,94575	0,81988	0,75039	0,71936	0,66128	0,58529	0,52598	0,00000	0,00000
7.0-7.5	0,00000	0,00000	0,00000	0,00000	0,00000	0,00000	0,00000	0,00000	0,00000	0,88504	0,82123	0,75130	0,68721	0,62312	0,55415	0,00000	0,00000
7.5-8.0	0,00000	0,00000	0,00000	0,00000	0,00000	0,00000	0,00000	0,00000	0,00000	0,92548	0,00000	0,77305	0,72474	0,67366	0,00000	0,00000	0,00000
8.0-8.5	0,00000	0,00000	0,00000	0,00000	0,00000	0,00000	0,00000	0,00000	0,00000	0,00000	0,88414	0,00000	0,74721	0,68455	0,00000	0,00000	0,00000
8.5-9.0	0,00000	0,00000	0,00000	0,00000	0,00000	0,00000	0,00000	0,00000	0,00000	0,00000	0,00000	0,00000	0,76658	0,70910	0,00000	0,00000	0,00000
9.0-9.5	0,00000	0,00000	0,00000	0,00000	0,00000	0,00000	0,00000	0,00000	0,00000	0,00000	0,00000	0,00000	0,00000	0,72277	0,00000	0,00000	0,00000

>6%
5-6%
4-5%
3-4%
2-3%
1-2%
0.5-1%
<0.5%

FIGURE B.8: MATLAB results for average pump rare per sec $[m^3/s]$

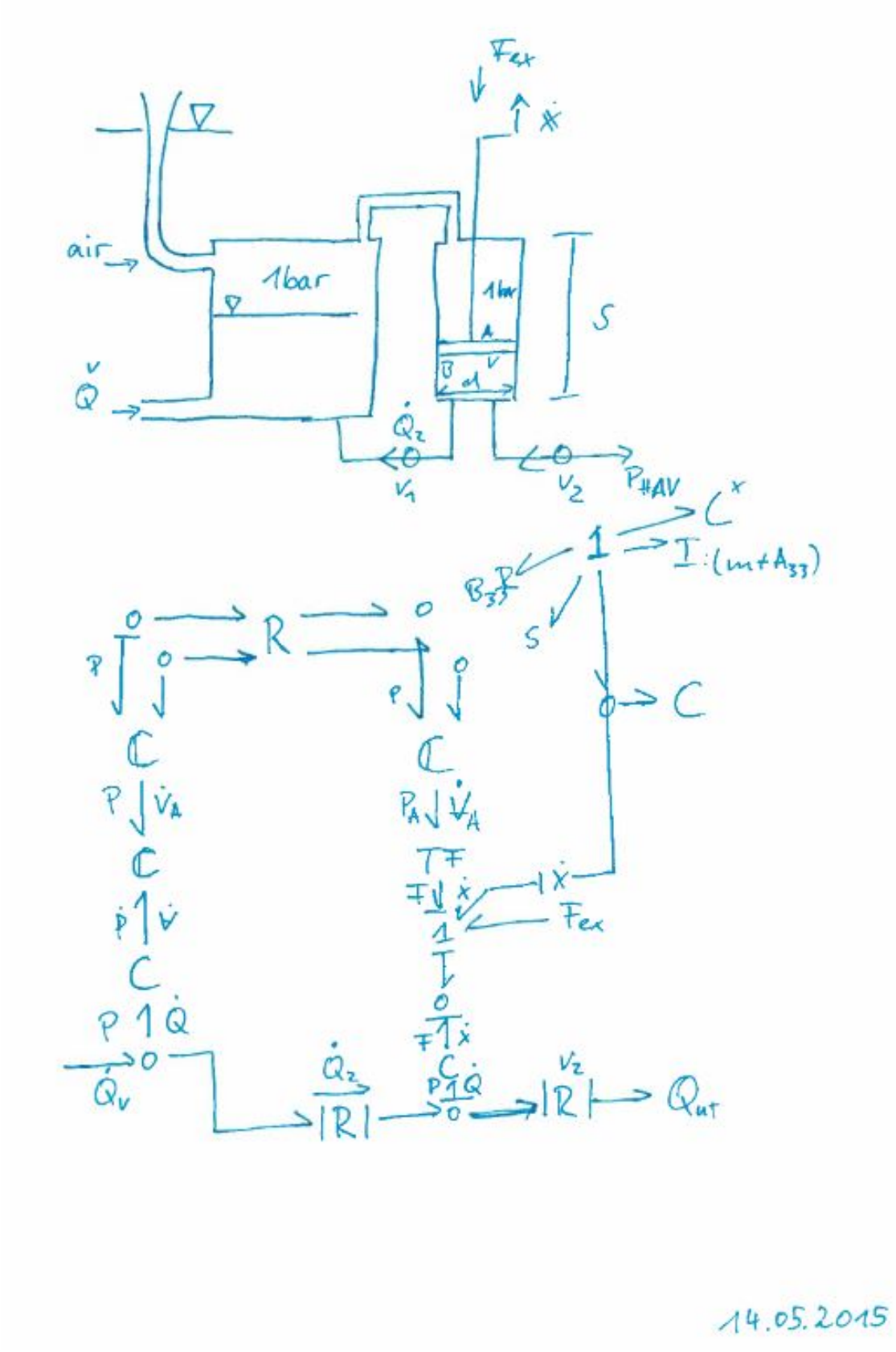

FIGURE B.9: Bond graph sketch of wave driven piston pump

Appendix C

Underwater Storage Tank

TABLE C.1: Volume required per unit of energy as a function of depth

	Volum/kWh
400.00	0.873341258
380.00	0.9181343
360.00	0.967770552
340.00	1.02308041
320.00	1.085095609
300.00	1.155114188
280.00	1.234792332
260.00	1.326277048
240.00	1.432402537
220.00	1.556989043
200.00	1.705312522
180.00	1.88487103
160.00	2.106692259
140.00	2.387687492
120.00	2.755179355
100.00	3.256371407
80.00	3.98045156
60.00	5.118616836
40.00	7.168316043
30.00	8.962860148
29.00	9.193001317
20.00	11.95596221
19.00	12.36901939
18.00	12.81163866
17.00	13.28711141
16.00	13.79923644
15.00	14.35242172
14.00	14.95181156
13.00	15.60344706
12.00	16.31447048
11.00	17.09338806
10.00	17.95041199
9.00	18.8979106
8.00	19.95100919
7.00	21.12840347
6.00	22.4534792
5.00	23.95588125
4.00	25.67375785
3.00	27.65704496
2.00	29.97240041
1.00	32.71084296
0.00	36